STUDY OF TRAPPING EFFECTS IN ALGAN/GAN MOSHEMTS

PANNIRSELVAM S/O SOMASUNTHARAM

(B.ENG.(HONS)),

NANYANG TECHNOLOGICAL UNIVERSITY

A THESIS SUBMITTED

FOR THE DEGREE OF DOCTOR OF PHILOSOPHY

DEPARTMENT OF ELECTRICAL AND COMPUTER ENGINEERING

NATIONAL UNIVERSITY OF SINGAPORE

2015

Declaration

I hereby declare that this thesis is my original work and it has been written by me in its entirety. I have duly acknowledged all the sources of information which have been used in the thesis.

This thesis has also not been submitted for any degree in any university previously.

Pannirselvam S/O Somasuntharam

23rd July 2015

Acknowledgements

First and foremost, I would like to express my greatest appreciation to my supervisor, Associate Professor Tan Leng Seow, for his continuous support and invaluable guidance during my Ph.D. candidature at National University of Singapore. His undying encouragement, outstanding work ethics and expert knowledge in the field of semiconductor devices are truly inspiring. I believe that the knowledge gained from him will be beneficial to me in my life and career.

I would also like to thank Professor Yeo Yee Chia for his guidance and support during my candidature. I am truly grateful for the knowledge imparted to me during group discussions and for providing me with financial support. I am deeply impressed with his dedication to research and excellent work ethics.

I would also like to thank Dr. Tan Swee Tiam, Dr. Ye Jiandong and Dr. Yang Yi for inspiring and motivating me towards pursuing higher education.

I would like to thank my friends and colleagues for all their help, insightful discussions and fun times. They are Dr. Liu Xinke, Dr. Ashvini, Dr. Zhou Qian, Dr. Gong Xiao, Dr. Sandipan, Dr. Liu Zhihong, Dr. Eugene Kong, Dr. Sujith, Dr. Tong Yi, Dr. Vijay, Dr. Phyllis Lim, Dr. Guo Pengfei, Dr. Xingui, Dr. Liu Bin, Dr. Ivana, Dr. Samuel Owen, Zhan Chunlei Low Kain Lu, Goh Kian Hui, Guo Cheng, Edwin Low, Kien Mun, Dong Yuan, Xu Xin, Lei Dian, Sachin and many others.

I would like to thank the Laboratory Technologists, Mr. O Yan and Mr. Patrick Tang, for their efforts in ensuring that the equipment are operational, and keeping the cleanrooms and laboratory safe places to work. I would also like to say thanks to the Emergency Response Team for working hard in keeping the cleanrooms safe.

I cannot express enough thanks to my parents, wife, siblings and children for their love, extremely strong support, encouragement and sacrifices during my pursuit for higher education. They are my pillars of support not only during my candidature but my entire life. This journey would not have been possible without them. Thank you very, very, very much.

Table of Content

Abstract

Study of Trapping Effects in AlGaN/GaN MOSHEMTs

by

Pannirselvam S/O Somasuntharam

Doctor of Philosophy – Electrical and Computer Engineering

National University of Singapore

AlGaN/GaN metal oxide semiconductor high electron mobility transistors (MOSHEMTs) are very attractive for high power and high frequency and high temperature applications, with low gate leakage current. However, it is believed that charge trapping at the insulator/AlGaN interface limits the performance of AlGaN/GaN MOSHEMTs. This thesis work involved fabrication of $Al_{0.25}Ga_{0.75}N$/GaN MOSHEMTs on Si(111) substrates and the trapping effects of the devices were investigated using electrical measurements, and TCAD device simulation fittings.

To have a better understanding of the effects of SiH_4 passivation on the HfAlO/AlGaN/GaN MOSHEMTs, TCAD device simulation was adopted to fit the experiment data presented by Liu *et al*. SiH_4 passivation on AlGaN/GaN MOSHEMTs were reported to show vast enhancements in device performance. Good simulation fittings to the measured I_D-V_{GS}, log(I_D)-V_{GS} and g_m-V_{GS} plots of the passivated and unpassivated devices were obtained. To achieve the good fitting, the donor-like trap densities in the unpassivated and passivated devices were set as 2.96×10^{13} cm^{-2}. Also, the simulation fittings showed that the

unpassivated device had 6.0×10^{12} cm^{-2} of acceptor-like traps less compared to the passivated device.

In order to investigate the characteristics (eg. trap energy and time constant) of traps under the gate electrode in $Al_2O_3/Al_{0.25}Ga_{0.75}N/GaN$ MOSHEMTs gate stress-induced transient drain current method was utilised. Trapping of electrons at regions under and near the gate electrode was induced by applying a gate stress V_{GS} = -20 V at V_{DS} = 0 V for 50 s, immediately followed by detrapping transient I_D measurement in the linear regime (V_{GS} = 1 V and V_{DS} = 0.5 V) at T = 340 K – 370 K. The temperature-dependent time constant spectra showed two dominant detrapping processes (E1 and E2). The activation energies of E1 and E2 were 0.32 eV and 0.46 eV respectively. TCAD fitting using SILVACO ATLAS showed that E1 and E2 were donor-like traps, located at the Al_2O_3/AlGaN interface, with densities of 1.43×10^{13} cm^{-2} and 1.07×10^{13} cm^{-2} respectively, at T = 370 K.

The pulsed I-V method was used to investigate the trap behavior under and near the gate electrode of $Al_{0.25}Ga_{0.75}N/GaN$ MOSHEMTs. The pulsed I_D-V_{GS} and I_D-V_{DS} measurements comprised of ($V_{GS,Q}$, $V_{DS,Q}$) = (-15 V, 0 V), (0 V, 0 V), (0.5 V, 0 V), (1.0 V, 0 V) and (1.5 V, 0 V). The impact of the electron trapping on the threshold voltage (V_{th}), two-dimensional electron gas density (n_s), electron mobility and density of ionized donor-like traps, at the Al_2O_3/AlGaN interface were also analyzed using TCAD device simulations and fittings. It was observed that ($V_{GS,Q}$, $V_{DS,Q}$) = (-15 V, 0 V) caused the V_{th} to decrease from –6.17 V to -6.27 V and mobility to decrease from 1627 $cm^2V^{-1}s^{-1}$ to 1599 $cm^2V^{-1}s^{-1}$. While ($V_{GS,Q}$,

$V_{DS,Q}$) = (1.5 V, 0 V) caused the V_{th} to increase from -6.17 V to -5.77 V and mobility to increase from 1627 $cm^2V^{-1}s^{-1}$ to 1735 $cm^2V^{-1}s^{-1}$. The impact of the electron trapping on the electrical characteristics obtained through this pulsed *I-V* study provided evidence that the active traps had donor-like characteristic.

List of Tables

List of Figures

List of Symbols

Symbol	Description	Unit
E_G	Bandgap	eV
ε_r	Dielectric constant	
ξ_{br}	Breakdown field	MV/cm
v_p	High-field peak electron velocity	cm/s
μ_n	Electron mobility	$cm^2/V.s$
K	Thermal conductivity	$WK^{-1}cm^{-1}$
P_{PE}	Piezoelectric polarization charge	C/m^2
P_{SP}	Spontaneous polarization charge	C/m^2
σ	Polarization-induced sheet charge density	C/m^2
e_{31}, e_{33}	Piezoelectric constant	C/m^2
C_{13}, C_{33}	Elastic constant	GPa
n_s	Two-dimensional electron gas sheet charge density	cm^{-2}
a	Lattice constant	Å
d	Thickness of AlGaN barrier layer	nm
q	Electronic charge	C
E_{FN}	Electron quasi Fermi energy	eV
ΔE_C	Conduction band offset	eV
V_{BR}	Breakdown voltage	V
R_{ON}	Specific on-state resistance	$\Omega.cm^2$
L_{GS}	Gate-to-source separation	µm
L_{GD}	Gate-to-drain separation	µm
L_G	Gate Length	µm
W	Gate Width	µm
I_G	Gate leakage current	mA/mm
D_{it}	Interface state density	cm^{-2}
V_{th}	Threshold voltage	V
SS	Sub-threshold swing	mV/decade

Ec	Conduction band edge energy	eV
E_V	Valance band edge energy	eV
E_T	Trap energy	eV
E_D	Energy of donor-like trap	eV
E_A	Energy of acceptor-like trap	eV
T	Temperature	K
k	Boltzmann constant	eV/K
v_{th}	Thermal velocity	Cm/s
g_m	Measured extrinsic transconductance (per unit width)	S/mm
R_C	Contact resistance	Ω.mm
ρ_C	Specific contact resistivity	Ω.cm^2
V_{GS}	Gate-to-source voltage	V
V_{DS}	Gate-to-drain voltage	V
$\sigma_{Surface}$	Sheet charge at AlGaN surface	cm^{-2}
τ_e	Emission time constant	s
t_{CR}	Critical AlGaN barrier thickness	nm
$TP1$	Trapping process 1	
$TP2$	Trapping process 2	
$DP1$	Detrapping process 1	
$DP2$	Detrapping process 2	

List of Abbreviations

Abbreviation	Description
2DEG	Two-dimensional electron gas
ALD	Atomic Layer Deposition
BFOM	Baliga’a figure of merit
DC	Direct Current
HEMT	High electron mobility transistor
ICP-RIE	Inductively Coupled Plasma Reactive Ion Etching
MOCVD	Metalorganic chemical vapour deposition
MOSHEMT	Metal oxide semiconductor high electron mobility transistor
RF	Radio Frequency
RTA	Rapid Thermal Anneal
TCAD	Technology Computer Aided Design

Chapter 1: Introduction to GaN

This chapter firstly discusses the major milestones that paved the advancement of GaN device technology. Followed by, a discussion of the attractive features of the GaN and AlGaN/GaN heterostructure that sets them apart from other competing materials. Next, the polarization in GaN and AlGaN is discussed in detail.

1.1 A Brief History of GaN Technology

The initial works on fabricating GaN devices began more than four decades ago. The first GaN-based light emitting diode was reported by Pankove *et al*. in 1971 [1]. One major obstacle that early researchers in GaN devices faced was the absence of suitable technology for producing GaN substrates. GaN films were grown on highly lattice-mismatched substrates, which led to poor surface morphology and high defect density. This caused high intrinsic n-type background doping and acceptors with deep activation energies, which resulted in problems with achieving p-type conductivity in GaN films [2].

In the mid-1980s, major contributions by Isamu Akasaki at Nagoya and Meijo Universities and Shuji Nakamura at Nichia Chemical Company in Japan led to the breakthrough in fabricating high quality GaN films on sapphire substrates by metalorganic chemical vapor deposition (MOCVD) using AlN [3] or GaN nucleation layers [4]. In 1989, p-type conductivity in GaN was first realized with Mg-doped GaN by low-energy electron-beam irradiation (LEEBI) treatment by Amano *et al*. [5].

In 1991, the presence of two-dimensional electron gas (2DEG) was discovered by Khan *et al*. when 50 nm of $Al_{0.09}Ga_{0.91}N$ was deposited on 0.3 µm GaN. The electron mobility in the heterostructure was reported to have increased to $1600 cm^2/Vs$ at 77 K, while the mobility in the GaN bulk was $19 cm^2/Vs$ at 77 K [6]. In 1992, Nakamura *et al*. achieved low resistivity p-type GaN films. It was shown that annealing Mg-doped GaN at temperatures above 700 °C in N_2 ambient led to reduction in resistivity from 1×10^6 Ω.mm to 2 Ω.mm [7]. The first AlGaN/n-GaN high electron mobility transistor (HEMT) was demonstrated by Khan *et al*. in 1993 [8]. In 1994, the development of candela-class high-brightness InGaN/GaN double-heterostructure (DH) blue light emitting diodes (LEDs) with the luminous intensity over 1 cd by Nakamura *et al*. was yet another breakthrough [9]. This led Nakamura *et al*. to develop the first InGaN multiple quantum well (MQW) structure laser diode with light output at 417 nm in room temperature [10]. This paved the way for rapid improvement in GaN-based optoelectronic technology. Currently, GaN optoelectronics have reached technology maturity and are already at the stage of commercialization.

GaN power devices are also currently commercially available. Panasonic has developed GaN power devices with high on-current and low on-resistance, and low thermal generation for different applications such as servo motor drive, power supplies, photovoltaic inverter, automotive, etc [11]. Figure 1.1 shows a few applications of GaN power devices fabricated by Panasonic, is suitable for operation at 600 V [11]. However, the full potential of AlGaN/GaN MOSHEMT devices is not fully realized and more knowledge can be gained by studying the trapping effects in the GaN devices.

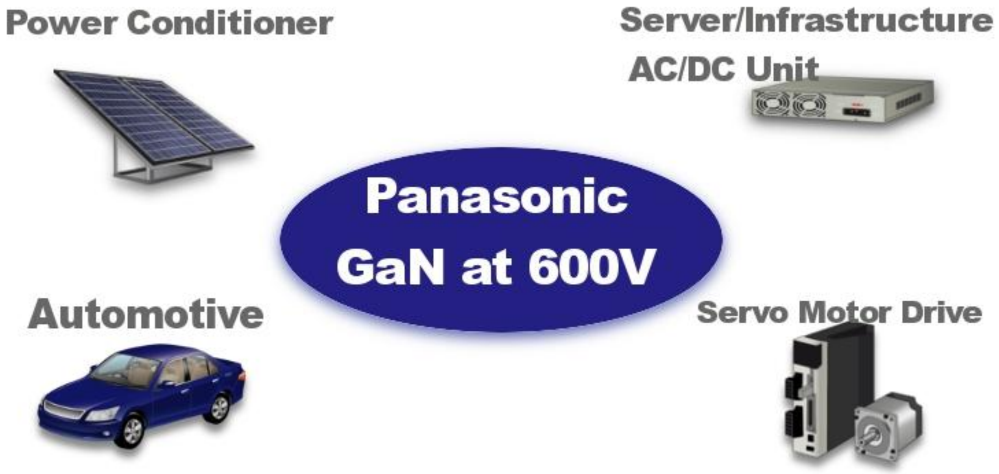

Figure 1.1: GaN power devices fabricated by Panasonic for various applications, which is suitable for application at 600 V [11].

1.2 Superior Material Properties of GaN and AlGaN/GaN

GaN is an excellent material for power transistors. Due to its wide bandgap [12] and high electron saturation velocity [13], GaN devices are able to operate at high voltage and speeds, respectively. Its high thermal conductivity [14], which is essential for high power devices, allows the devices to efficiently dissipate heat easily. Table 1.1 compares the material properties of GaN to competing materials such as GaAs, 4H-SiC and Si. Baliga's Figure of Merit (BFOM) is normalized to Si for the different materials.

Table 1.1: Properties of GaN compared with other semiconductors. Baliga's figure of merit (BFOM) for power transistor performance ($\mu.\varepsilon.E_g^3$) with respect to Si [15]- [16].

Material	Si	GaAs	4H-SiC	GaN
Mobility μ ($cm^2V^{-1}s^{-1}$)	1300	5000	260	1500
Dielectric Constant ε_r	11.9	12.5	10	9.5
Bandgap E_g (eV)	1.12	1.42	3.2	3.4
Breakdown field E_b ($\times 10^6$V/cm)	0.3	0.4	3.5	>2
BFOM Ratio	1.0	9.6	3.1	24.6

One of the features of AlGaN/GaN heterostructure that makes it favorable for high power applications is the high electron density at the AlGaN/GaN interface. GaN-based epitaxial layers grown in the wurtzite crystal system, gives rise to unique material properties such as built-in electric fields due to spontaneous and piezoelectric polarizations, which are absent in other compound semiconductors such as InP and GaAs. This polarization field enables very high electron densities (~ 1 – 2 $\times 10^{13}$ cm^{-2}) to form in the AlGaN/GaN interface [17]. The polarization in GaN and the polarization induced charge density will be further explained in the next section. (See section 1.3)

Another property is the high electron mobility in the AlGaN/GaN heterostructure. Tokuda *et al*. recently reported electron mobility of over 3000 $cm^2V^{-1}s^{-1}$ in AlGaN/GaN heterostructure at room temperature [18]. Monte Carlo calculation predicts that the peak steady-state drift velocity can reach up to 3.3×10^7 cm/s at T = 77 K [19]. Also, the breakdown voltage of over 2200 V was reported by Srivastava *et al*. [20] for AlGaN/GaN double-heterostructure field effect transistor.

1.3 Polarization in GaN and AlGaN/GaN heterostructure

III-Nitride materials have significant advantage over *III-V* materials. Among group *V* elements, nitrogen is the smallest and most electronegative. Therefore, metal-nitrogen bond has a greater degree of ionic characteristic compared to other *III-V* covalent bonds. Also, wurtzite *III-Nitride* materials do not have inversion symmetry along the [0001] direction. The combinations of these features result in the orientation of a large polarization field along the c-axis. Figure 1.2 shows the atomic layer sequences of wurtzite GaN crystal grown along [0001] and $[000\bar{1}]$, commonly known as Ga- and N-face, respectively. GaN crystals are more commonly grown normal to the {0001} basal plane [21].

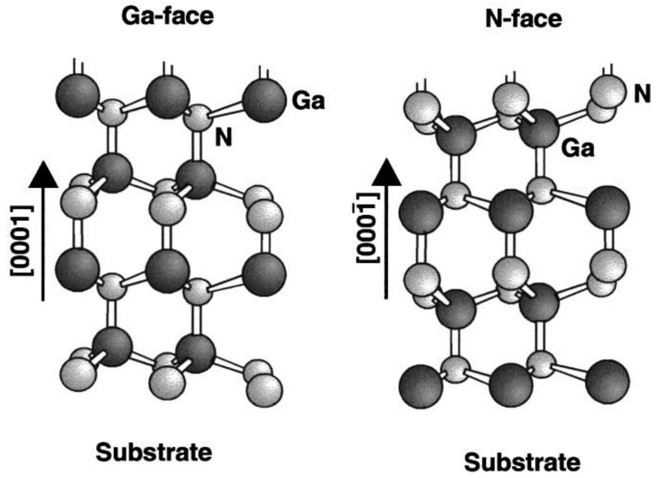

Figure 1.2: Atomic layer sequences of Ga-face and N-face wurtzite GaN crystals [22].

1.3.1 Spontaneous Polarization (P_{SP})

The spontaneous polarization of relaxed alloys for a given composition depends linearly on the average cell-internal parameter *u*. Parameter *u* is defined as the anion-cation bond length along the [0001] direction, in units of c [23]. Figure 1.3 shows the representation of parameter *u* in a wurtzite structure.

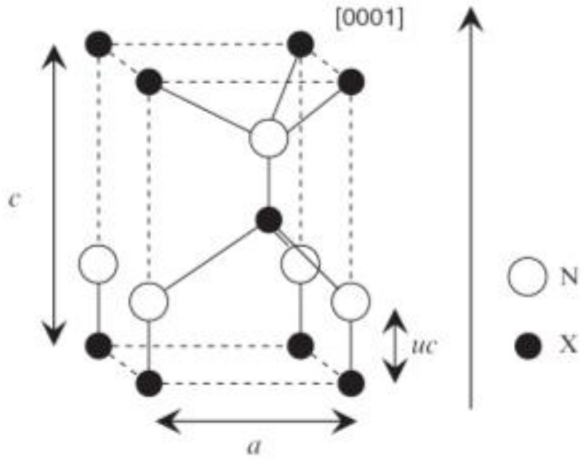

Figure 1.3: Unit cell of wurtzite structure showing lattice constants and parameter *u* [23].

As the composition of the alloy varies, the average cation-anion bond lengths will also vary. Thus, the changes in the spontaneous polarization due to the changes in alloy composition is said to be mainly due to the change in the cation-anion bond length along the c-axis [24].

For binary compounds such as GaN, the relative displacement of cation and anion sub lattices in the [0001] direction has a strong impact on the spontaneous polarization [21]. Furthermore, theoretical studies from Ashcroft *et al*. [25] shows that binary compound with wurtzite crystal structure presents a strong indication of linear dependence between the u parameter and the spontaneous polarization [25] .

However, it is expected that for ternary compounds, the change in alloy composition will lead to a non-linear behavior of the spontaneous polarization. This non-linear behavior is explained by Bernardini *et al*. [21] to be caused by the difference in electronegativity among the cations. The spontaneous polarization of an arbitrary group III-Nitride alloy (ABN) can be described with the following equation:

$$P_{ABN}^{SP}(x) = P_{AN}^{SP}x + P_{BN}^{SP}(1-x) + bx(1-x) \tag{1.1}$$

In Equation 1.1, the first two terms are the linear interpolations of the binary compounds. The third term represents the non-linear behavior in the ternary compounds. b is a bowing parameter and x is the mole composition of an element A [25].

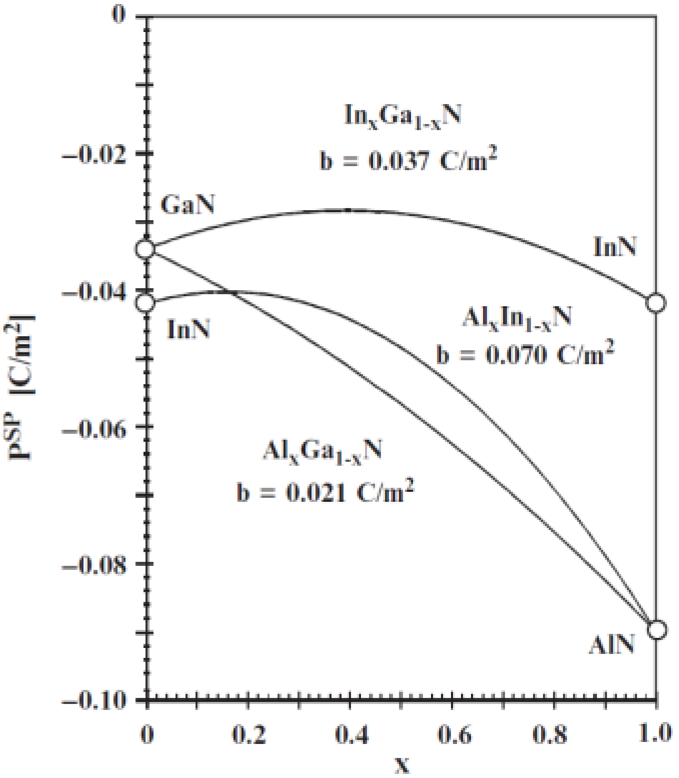

Figure 1.4: Calculated P_{SP} for AlN, GaN, InN and its ternary alloys verses composition [25].

Figure 1.4 illustrates the relationship of composition dependent P_{SP} for *III-V* ternary alloys. GaN-based epilayers, heterostructure and nanostructures are usually grown pseudomorphically on substrates made by other elements or compounds. These substrates can have a different lattice constant and thermal expansion coefficient compared to GaN. Therefore, the GaN layer can experience strain due to lattice mismatch and difference in thermal expansion coefficient. Thus, it is important to note that for wurtzite group *III-Nitride* compounds, polarization depends on both spontaneous and piezoelectric polarizations [25].

1.3.2 Piezoelectric Polarization (P_{PE})

The piezoelectric polarization has three independent components ($\epsilon_x, \epsilon_y \ and \ \epsilon_z$). The piezoelectric polarization (P_{PE}) along the c-axis is measured using two of the components. The relationships between piezoelectric polarization and the components in the linear regime are as follows:

$$P_{PE} = e_{33}\epsilon_z + e_{31}(\epsilon_x + \epsilon_y) \tag{1.2}$$

$$\epsilon_z = \frac{(c-c_0)}{c_0} \tag{1.3}$$

$$\epsilon_x = \epsilon_y = \frac{(a-a_0)}{a_0} \tag{1.4}$$

where ϵ_z refers to the strain along the c-axis. ϵ_x and ϵ_y refer to the in-plane biaxial strain and are assumed to be uniform. e_{31} and e_{33} are piezoelectric constants, and a and c are the lattice constants of the strained layer [26]. Equation 1.5 shows the relationship between the lattice constants in the wurtzite AlGaN, where C_{13} and C_{33} are elastic constants.

$$\frac{c-c_0}{c_0} = -2\frac{C_{13}}{C_{33}}\frac{a-a_0}{a_0} \tag{1.5}$$

$$P_{PE} = 2\frac{a-a_0}{a_0}\left(e_{31} - e_{33}\frac{C_{13}}{C_{33}}\right) \tag{1.6}$$

The values of the piezoelectric polarization of a strained layer can be calculated using Equation 1.6. Since the Equation 1.2 is described to be in the linear regime, we can infer that the piezoelectric polarization will also vary linearly with the lattice parameters (*a* and *c*) [26].

In other words, if a group *III-Nitride* layer is subjected to a strain that is parallel or perpendicular to the c-axis, there will be a displacement of the metal atom with respect to the nitrogen atom (or vice versa). Thus, the piezoelectric polarization experienced is the result of the sum of the displacement of the atoms in the layer, due to the strain. The directions of the spontaneous and piezoelectric polarizations of *III-Nitride* are defined with the assumption that the positive direction starts from the metal and ends at the nitrogen atom. Therefore, the signs of the spontaneous and piezoelectric polarizations are negative [26].

$$\left(e_{31} - e_{33}\frac{C_{13}}{C_{33}}\right) < 0. \tag{1.7}$$

Using Equation 1.6 and 1.7, it can be understood that for tensile or compressively strained layers, the piezoelectric polarization is in the negative or positive directions respectively. Therefore, for tensile or compressive strain, the piezoelectric polarization is parallel or anti-parallel respectively, to the direction of the spontaneous polarization. For the case of thin AlGaN layer grown on bulk GaN layer, the AlGaN layer is believed to be under tensile strain due to the lattice mismatch between the AlGaN and GaN layers. Therefore, the directions of the spontaneous and piezoelectric polarizations of the AlGaN layer are the same, and the sum of their magnitudes contributes to the total polarization (*P*) [26]

$$P = P_{SP} + P_{PE}. \tag{1.8}$$

1.3.3 Formation of Polarization Induced Sheet Charge at AlGaN/GaN Interface

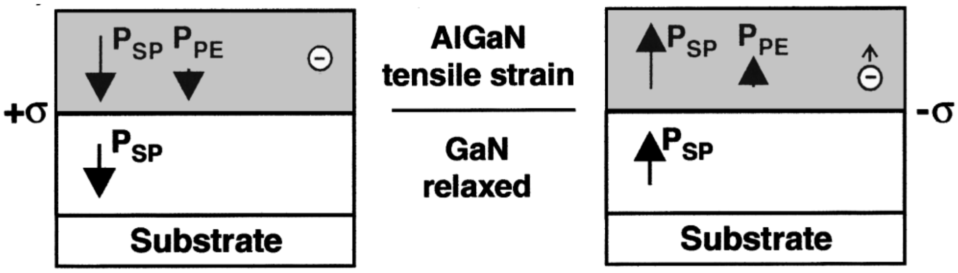

Figure 1.5: Spontaneous and piezoelectric polarization in AlGaN/GaN heterostructure for Ga-face (left) and N-face (right) [22]

Figure 1.5 shows the spontaneous and piezoelectric polarization in Ga-face (left) and N-face AlGaN/GaN heterostructures. For Ga–face AlGaN/GaN heterostructure, the polarization points from the top surface towards the substrate. On the other hand, for N-face AlGaN/GaN heterostructure, the polarization points from the substrate towards the top surface. In addition, an abrupt AlGaN/GaN interface will cause an abrupt change in the magnitude of the polarization. This change in the polarization gradient leads to the formation of polarization induced charge density (ρ_p) [26]

$$\rho_p = -\nabla P. \tag{1.9}$$

The following method (Equation 1.10) can be used to calculate the fixed polarization charge density at the AlGaN/GaN interface, assuming that the interfaces of the heterostructure are abrupt.

$$|\sigma(P_{SP} + P_{PE})| = |P(bottom) - P(top)|$$

$$= |\{P_{SP}(bottom) + P_{PE}(bottom)\} - \{P_{SP}(top) + P_{PE}(top)\}| \tag{1.10}$$

The fixed polarization charge density will be compensated by charges of the opposite polarity. For example, positive polarization charge density will be compensated by free electrons and negative polarization charge density will be compensated by free holes [26].

1.3.4 Calculation of Polarization Induced Sheet Charge

The polarization induced sheet charge density at the pseudomorphically grown AlGaN on GaN layer was determined with the assumption that the piezoelectric constants and other physical parameters of $Al_xGa_{1-x}N$ can be interpolated linearly. Equations 1.11 – 1.17 can be used to estimate the lattice constants, elastic constants, piezoelectric constants and spontaneous polarization constants of $Al_xGa_{1-x}N$, where x is the mole fraction of Al [26]- [27]. The magnitude of the polarization induced sheet charge at the AlGaN/GaN interface can be calculated using Equations 1.18 and 1.19 [26].

Lattice Constants:

$$a_0(x) = (-0.077x + 3.189) \times 10^{-10}\, m\,, \tag{1.11}$$

$$c_0(x) = (-0.203x + 5.189) \times 10^{-10}\, m\,. \tag{1.12}$$

Elastic Constants:

$$C_{13}(x) = (5x + 103)\, GPa\,, \tag{1.13}$$

$$C_{33}(x) = (-32x + 405)\ GPa\ . \tag{1.14}$$

Piezoelectric Constants:

$$e_{13}(x) = (-0.11x - 0.49)\ \frac{C}{m^2}\ , \tag{1.15}$$

$$e_{33}(x) = (0.73x + 0.73)\ \frac{C}{m^2}\ . \tag{1.16}$$

Spontaneous Polarization:

$$P_{SP}(x) = (-0.052x - 0.029)\ \frac{C}{m^2}\ , \tag{1.17}$$

$$|\sigma(x)| = |P_{PE}(Al_xGa_{1-x}N) + P_{SP}(Al_xGa_{1-x}N) - P_{SP}(GaN)|\ , \tag{1.18}$$

$$|\sigma(x)| = \left|2\,\frac{a(0)-a(x)}{a(x)}\left\{e_{31}(x) - e_{33}(x)\,\frac{C_{13}(x)}{C_{33}(x)}\right\} + P_{SP}(x) - P_{SP}(0)\right|\ . \tag{1.19}$$

1.3.5 Sheet Carrier Concentrations (n_s) of Two-Dimensional Electron Gas (2DEG)

For undoped Ga-face AlGaN/GaN heterostructures, the sheet electron concentration can be calculated using Equation 1.20 [28]

$$n_s(x) = \frac{\sigma(x)}{e}\left(\frac{\epsilon_0\epsilon(x)}{d_{AlGaN}e^2}\right)[e\varphi_b(x) + E_F(x) - \Delta E_C(x)]\ . \tag{1.20}$$

Table 1.2: Parameters of Equation (1.20) [26]

Parameters	Definition
$\epsilon(x)$	Relative Dielectric Constant of $Al_xGa_{1-x}N$
d_{AlGaN}	Thickness of AlGaN layer
$\varphi_b(x)$	Schottky Barrier Height of gate contact on top of AlGaN
$E_F(x)$	Fermi level w.r.t the conduction band energy level
$\Delta E_C(x)$	Conduction band offset at the AlGaN/GaN interface
e	Electronic charge

Equation 1.20 assumes that the background carrier concentration is negligible ($N_d < 10^{16}$ cm^{-3}). It is understood that the sheet carrier concentration is mainly controlled by the total polarization induced sheet charge, which can be controlled by varying the alloy composition in the AlGaN layer. Equation 1.20 also shows that the sheet carrier concentration can be increased if the AlGaN layer thickness is reduced and/or the Schottky barrier height is increased [26].The following approximations can be used in Equation 1.20 to calculate the sheet carrier concentration of the 2DEG at the AlGaN/GaN interface with varying Al mole composition in the AlGaN layer *(x)* [22].

Dielectric Constant:

$$\epsilon(x) = -0.5x + 9.5, \tag{1.21}$$

Schottky Barrier:

$$e\varphi_b = (1.3x + 0.84)\ eV, \tag{1.22}$$

Fermi Energy:

$$E_F(x) = E_0(x) + \frac{\pi\hbar^2}{m^*(x)} n_s(x), \tag{1.23}$$

where $E_0(x)$ is the ground state subband level of the 2DEG.

$$E_0(x) = \left\{\frac{9\pi\hbar e^2}{8\epsilon_0\sqrt{8m^*(x)}}\frac{n_s(x)}{\epsilon(x)}\right\}^{\frac{2}{3}}, \tag{1.24}$$

where the effective electron mass, $m^*(x) \approx 0.22m_e$.

Band Offset:

$$\Delta E_C = 0.7\left[E_g(x) - E_g(0)\right]. \tag{1.25}$$

1.4 Objectives of Research

The objectives of this research work were to fabricate AlGaN/GaN MOSHEMTs and characterize the traps in the devices. Electron trapping in the surface or interface states of the MOSHEMT can degrade the performance and reliability, and are thought to be responsible for drain current collapse [29]- [30]. The electron trapping can also lead to threshold voltage (V_{th}) instability [31] and mobility degradation [32]. In this thesis, various methods were utilized to study the trap characteristics in the AlGaN/GaN MOSHEMTs.

The effects of SiH_4 treatment on the trap states in AlGaN/GaN MOSHEMT were investigated using TCAD device simulation. The TCAD simulation allowed the investigation of trap characteristics such as trap density at the Al_2O_3/AlGaN interface and impact of the trap occupancy on the electron mobility and energy band, which may be difficult to obtain using device measurements only.

In order to have a deeper understanding of the trap characteristics, trap activation energy, trap time constants, nature of traps (i.e., donor-like or acceptor-like) and trap densities were studied using drain current methodology together with TCAD device simulation. The current transient method was used to study the transient response of the traps after a trap filling pulse. This method investigated the drain current collapse in the device, which is believed to be a recoverable and transient reduction in drain current associated with AlGaN surface traps that respond to external voltage applied to the device [33].

Pulsed current-voltage (*I-V*) measurement together with TCAD device simulation was another method utilized to study the behavior of the traps in the AlGaN/GaN MOSHEMT. Several quiescent bias points were used to induce electron trapping/detrapping at the Al_2O_3/AlGaN interface. The impacts of the trapping/detrapping on the pulsed I-V characteristics were analyzed. The pulsed *I-V* measurements with small duty cycle can avoid the negative effects faced in direct current (DC) measurements such as joule heating and transient effect of trapped traps.

1.5 Thesis Organization

Chapter 2 presents the literature review on the basic concepts of the origin of the 2DEG, formation and effects of virtual gate and current transient methodology. These concepts and techniques are applied in the other chapters.

Chapter 3 discusses the TCAD device simulation used to investigate the effects of SiH_4 treatment on AlGaN/GaN MOSHEMT. The device simulations were used to fit measured data presented in the literature. Details of the simulation process such as mesh design and models used are documented in this Chapter. Simulation results revealed that the SiH_4 treatment reduced the acceptor-like trap states located at the Al_2O_3/AlGaN interface by 6.0×10^{12} cm^{-2}.

Chapter 4 investigates the trap characteristics using drain current transient methodology. The trap characteristics were investigated using V_{DS} = 0 V state detrapping method. The device was biased at V_{GS}=-20 V and V_{DS} = 0 V for 50 s, immediately followed by recovery drain current transient measurements at V_{GS} = 1 V and V_{DS} = 0.5 V, at different temperatures. A fitting function was used to mathematically fit the measured drain current transients. The time constant spectra were constructed using fitting parameter and pre-defined time constants. The temperature-dependent time constant spectra showed two dominant detrapping processes which were sensitive to temperature. TCAD simulation was used to fit the measured data plot in order to evaluate the densities of the traps.

Chapter 5 studies the behavior of the AlGaN surface traps using pulsed *I-V* measurements. The measurements showed significant shifts in the V_{th} at different gate-to-source quiescent biases. With the aid of TCAD simulation fittings, the changes in the V_{th}, lateral electron mobility, two-dimension electron gas sheet charge density, due to the changes in the ionized donor-like trap density at the Al_2O_3/AlGaN interface are discussed here. The active traps at the Al_2O_3/AlGaN interface were concluded to display donor-like characteristics instead of acceptor-like characteristics.

Chapter 6 contains the summary of the major contributions presented in this thesis, followed by suggestions for future work.

Chapter 2: Literature Review

This Chapter discusses work presented in the literature, so as to provide a basic understanding of the AlGaN/GaN MOSHEMT study related to this thesis research. Section 2.1 discusses the origin of the two-dimensional electron gas (2DEG) at the AlGaN/GaN interface reported by Ibbetson *et al.* [34]. Section 2.2 describes the work presented by Vetury *et al*. [29] on the concept of the virtual gate mechanism. The current transient methodology to extract the time constants and trap energies in the AlGaN/GaN HEMT device is presented in Section 2.3 [35].

2.1 Two-Dimensional Electron Gas in AlGaN/GaN

The origin of the 2DEG in the AlGaN/GaN heterostructure field effect transistor (HFET) was discussed by Ibbetson *et al*. [34]. Figure 2.1 shows the various charge components in the conduction band of AlGaN/GaN HFET. The charges in the AlGaN/GaN HFET are described below [34]:

- Negative charge at the AlGaN/GaN interface due to 2DEG sheet charge density (n_s).
- Polarization-induced sheet charge density at the AlGaN surface and AlGaN/GaN interface (-σ_{PZ} and $+\sigma_{PZ}$ respectively).
- Integrated sheet charge due to ionized donors in the AlGaN ($+\sigma_{AlGaN}$).
- Ionized states at the AlGaN surface ($\sigma_{Surface}$).

- Buffer charge (σ_{Buffer}) in the GaN buffer.

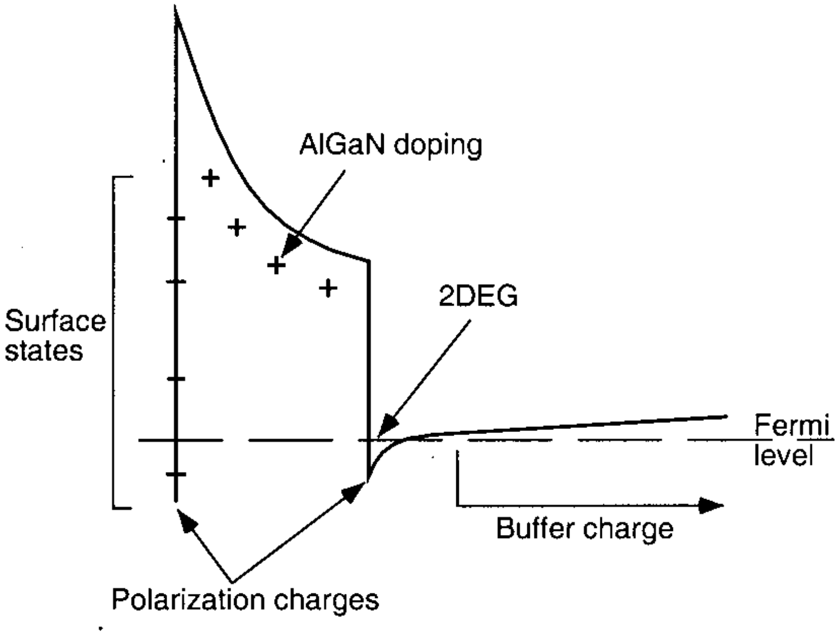

Figure 2.1: Schematic of AlGaN/GaN HFET conduction band showing various charge components [34].

Ibbetson *et al.* described the following assumptions in his study on the origin of the 2DEG in AlGaN/GaN HFETs [34]:

- In order to maintain charge neutrality in the absence of externally applied electric field, the sum of the charges in the AlGaN/GaN HFET must be zero.
- The contribution of the dipole due to the polarization-induced charges is exactly zero.
- In order for the 2DEG to be confined at the AlGaN/GaN interface, σ_{Buffer} must be negative. Also, the formation of the 2DEG cannot be due to thermal

generation of electrons from the buffer as it will leave behind positive space charges. For a high quality buffer layer, σ_{Buffer} is expected to be very small, therefore, it is set as zero.

$$\sigma_{Surface} + \sigma_{AlGaN} - qn_s = 0 \tag{2.1}$$

Similar to how doping the AlGaN barrier layer with donor impurity atoms increases $+\sigma_{AlGaN}$, it is believed that the positive surface charge ($+\sigma_{Surface}$) originates from electron transfer from donor-like surface states into empty states of lower energy. On the other hand, negative surface charge ($-\sigma_{Surface}$) is due to transfer of electrons into acceptor-like surface states. If the AlGaN barrier layer is undoped, the density of the 2DEG is solely due to the net positive surface states ($\sigma_{Surface} = qn_s$) [34].

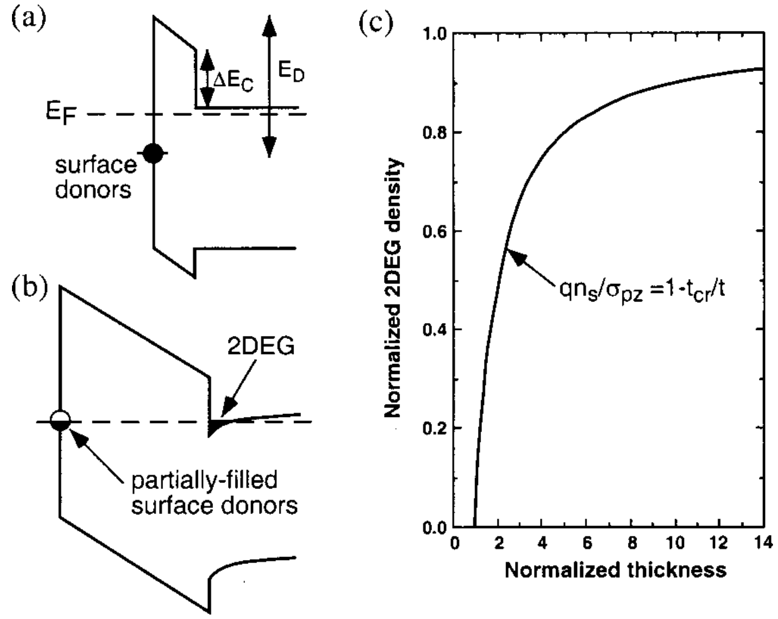

Figure 2.2: (a) Schematic of AlGaN/GaN energy band showing absence of 2DEG density at AlGaN/GaN interface when surface donor state energy E_D is below E_F. (b) Schematic of

AlGaN/GaN energy band (thick AlGaN barrier layer) showing E_F pinning at the surface donor state and presence of 2DEG at the AlGaN/GaN interface. (c) 2DEG dependence on the thickness of the AlGaN barrier layer [34].

Figure 2.2(a) shows the bandgap diagram of AlGaN/GaN HFET with undoped AlGaN layer. The donor-like surface state is located at energy E_D below the conduction band edge (E_C). It is assumed that the trap state is donor-like, which has neutral charge when occupied and positive charge when empty. If this donor state lies at an energy level sufficiently deep below the Fermi energy level, E_F, there is no 2DEG at the AlGaN/GaN interface. From Equation 2.1, since $\sigma_{Surface}$ = 0, n_s is also zero. However, there exists an electric field in the AlGaN layer due to the unscreened polarization charges at the AlGaN surface and AlGaN/GaN interface. With increasing AlGaN layer thickness, the energy separation between E_F and E_D decreases. At a critical AlGaN thickness, the donor state energy is at E_F (Figure 2.2(b)). Then, electrons from the occupied surface states are able to transfer into empty conduction band states at the interface, thus, creating positive charges at the AlGaN surface and 2DEG at the AlGaN/GaN interface. The E_F will remain essentially at E_D until all the surface states are empty. However, as the AlGaN barrier layer thickness increases, the transfer of electrons from the donor states also increases. The critical AlGaN barrier thickness can be expressed as

$$t_{CR} = (E_D - \Delta E_C)\epsilon / q\sigma_{PZ} \tag{2.2}$$

where ϵ is the relative dielectric constant of AlGaN and ΔE_C is the conduction band offset at the AlGaN/GaN interface. The 2DEG as a function of the AlGaN barrier thickness, t, (for $t > t_{CR}$) can be expressed as

$$qn_S = \sigma_{PZ}(1 - t_{CR}/t). \quad (2.3)$$

Figure 2.2(c) shows that when the thickness of the AlGaN barrier layer exceeds the critical thickness, the 2DEG density increases rapidly. For $t \gg t_{CR}$, the 2DEG density approaches σ_{PZ}/q [34].

In the case where surface states are absent on the AlGaN, the origin of the 2DEG is then dependent on the occupied states in the AlGaN valance band. If the AlGaN barrier layer is thick enough for the valance band to reach E_F, electrons can transfer from the AlGaN valance band to the GaN conduction band. Thus, forming a 2DEG in the AlGaN/GaN interface and surface hole gas on the AlGaN layer [34].

2.2 Virtual Gate Mechanism

In order to develop AlGaN/GaN-based high power devices, it is vital to improve the structural quality of AlGaN and GaN layers [36]. Despite the vast improvement in structural quality, the surface trapping effects have significant impact on the current collapse phenomenon. The strong polarization fields in the AlGaN/GaN materials are thought to be a reason behind the presence of surface states [34],[39]-[40]. Work presented by Vetury *et al*. [29] studied the impact of surface states on electrical performance in AlGaN/GaN HFETs.

2.2.1 Concept of Virtual Gate Formation

Figure 2.3 shows that if there is negative charge on the AlGaN surface, the potential of the AlGaN surface becomes negative. This negative potential depletes the channel electrons at the AlGaN/GaN interface. This extends the depletion region under the gate to regions outside the gate metal. Therefore, the gate metal and the negative surface potential act as two gates between the source and the drain contacts (Figure 2.4). The applied gate bias controls the potential of the metal gate while the total amount of trapped charge in the gate-to-drain access region controls the potential on the second gate. This second gate is known as the 'virtual gate'. Therefore, in addition to the applied gate bias, the output drain current is controlled by the charging and discharging of the virtual gate [29].

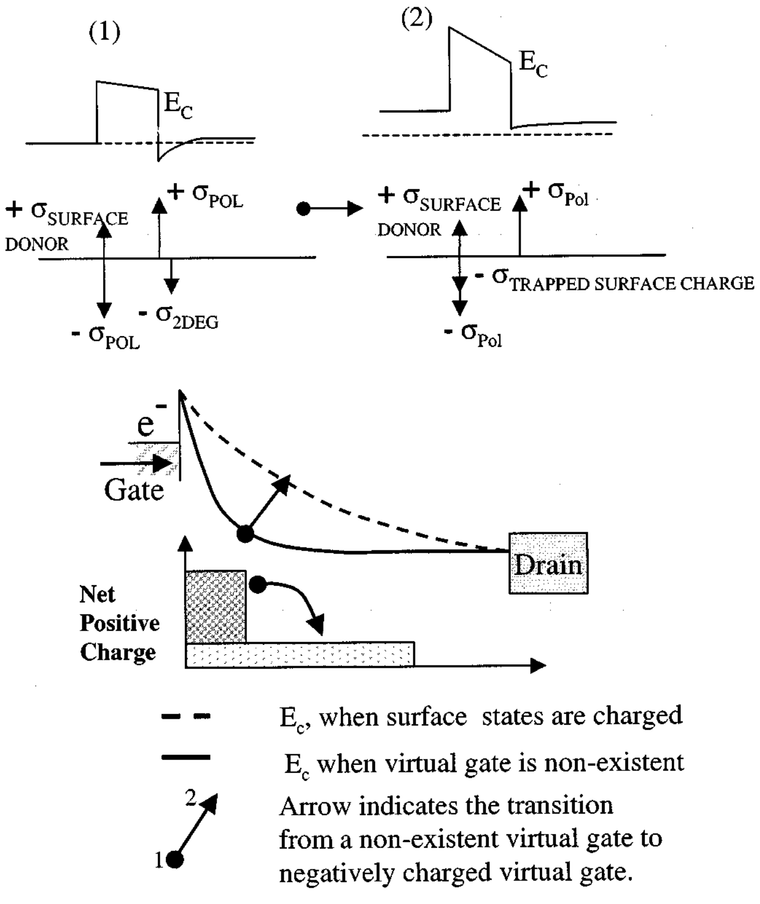

Figure 2.3: (1) Schematic of AlGaN/GaN conduction band showing the presence of 2DEG density at the AlGaN/GaN interface. (2) Shows the absence of 2DEG density at the AlGaN/GaN interface due to the presence of negative surface charge at the AlGaN surface.

The trapping of electrons at the gate-to-drain spacing reduces the net positive charge and leads to an extension of the depletion region [29].

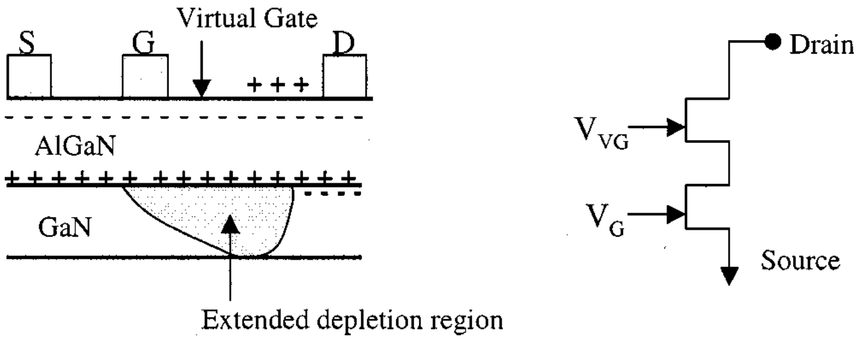

(a) (b)

Figure 2.4: (a) Cross-sectional schematic of AlGaN/GaN HEMT showing the formation of virtual gate at the region near the gate edge at the drain side. The presence of the virtual gate extends the depletion region under the gate. (b) A simplified model describing that the virtual gate acts as a second gate between the source and drain [29].

2.2.2 Mechanism of Current Collapse due to Formation of Virtual Gate

The mechanism of current collapse due to the formation of virtual gate is explained by Vetury *et al.* as follows [29]:

- Net positive charge exists on the as-grown AlGaN surface of AlGaN/GaN heterostructure [29].
- The trapping of electrons in the donor-like surface states in the AlGaN leads to the formation of the virtual gate by reducing the density of the net positive charge on the AlGaN surface. Now, the potential on the virtual gate also determines the drain current of the device [29].

- In the absence of light, the current collapse is dependent on how fast the reverse bias on the virtual gate increases. If the electrons that fill up the empty states are from the gate metal, then the supply of electrons being trapped is dependent on the gate electric field, gate leakage current and surface mobility of the electrons [29].
- There is a strong dependence of trapping transient on the drain bias. The trapping process is strongly dependent on the electric field between the gate and the drain. As the trapping in the surface states increases, the depletion region extends due to the formation of the virtual gate. This in turn, causes the electric field at the gate edge to reduce. Thus, rate of electron trapping at the surface states decreases [29].

2.2.3 Recovery of Current Collapse due to neutralization of virtual gate

- When the gate metal is forward biased with respect to source and drain, the electrons trapped at the surface states can be removed [29].
- Illumination using photon energy greater than the GaN bandgap leads to the formation of electron-hole pairs in the GaN channel. The holes are pulled towards the surface of the AlGaN due to the electric field. The accumulation of holes at the AlGaN surface causes the surface to become forward biased. Thus, the virtual gate is eliminated [29].
- Using UV light ($hv> E_g$), incident photons can knock electrons out of the surface traps [29].

2.2.4 Effect of Surface Passivation Using Si_3N_4

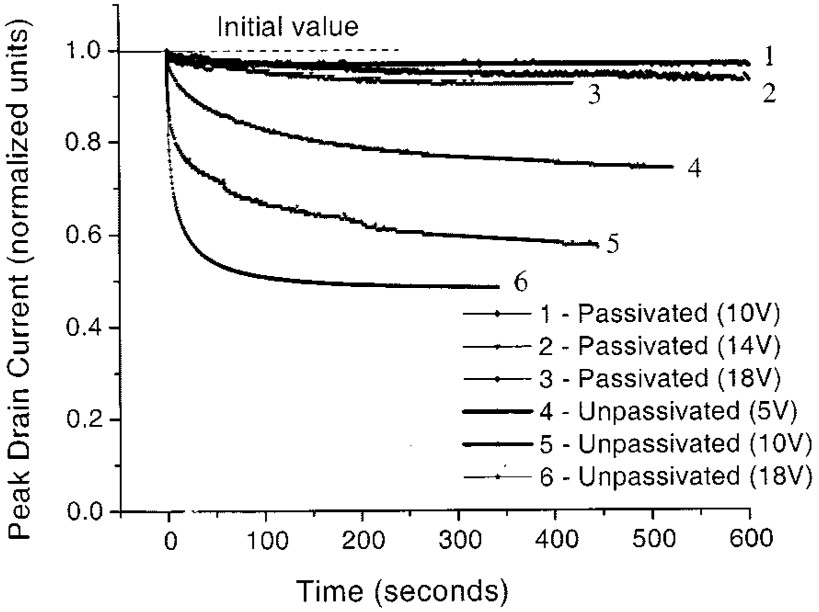

Figure 2.5: The trapping transients of passivated and unpassivated devices. The passivated devices show lower current collapse compared to unpassivated devices [29].

Figure 2.5 shows the trapping transients of unpassivated and Si_3N_4 passivated AlGaN/GaN HEMT devices. The passivated devices show smaller current collapse and reduced current collapse dependence on the drain bias. Thus, the formation of the virtual gate in the gate-to-drain region is prevented by the surface passivation. Possible mechanisms related to the prevention of the virtual gate due to surface passivation are discussed below [29].

- If the virtual gate is formed by ionic adsorbates from the ambient, then the passivation shields those ionic adsorbates from the AlGaN surface. Thus, the formation of virtual gate can be prevented [29]. However, this is unlikely since experiments involving other dielectrics and experiments in vacuum did not suppress the current collapse [29].

- The passivation makes the surface donor states inaccessible to the electrons leaking from the gate metal [29].
- During the Si_3N_4 passivation process, Si is incorporated as shallow donors at the AlGaN surface in adequately large quantities so as to replace the surface donor [29].

However, if the Si_3N_4/AlGaN interface or the bulk Si_3N_4 layer contains defect states, then electrons can get trapped at the defect states during high power operation. These trapped electrons can similarly lead to the formation of a negatively charged virtual gate, which can have a negative impact on the reliability and long term stability of the device characteristics and performance [29].

2.3 Current Transient Methodology For Trap Analysis

Trapping effects are one of the most detrimental mechanisms that restrict the performance and reliability in GaN HEMTs [37]. Current collapse, which arises due to the trapping effects during high voltage application, is a temporary recoverable reduction in drain current. In GaN HEMTs, the trapping effects are reported to have a slow nature. Generally, the recovery time from current collapse is greater than 100 s [29], [38]-[44] . Therefore, the performance of GaN HEMTs in RF systems and power electronics will be critically affected. Also, the slow nature of the traps in AlGaN/GaN devices plays a critical role in reliability. For example, when the device is subjected to high voltage, the electrons become trapped at various locations, degrading the performance of the device. In addition, the degradation of the device increases the trapping effects, which further reduces the performance of the device, thus, degrading the reliability [30],[37],[45]-[49].

The current transient methodology presented by Joh *et al*. [35] aids in analyzing trapping and detrapping behaviour in GaN HEMTs. This method can also be used in long-term stress experiments. Using this technique, the trapping/detrapping time constant and energy level of dominant traps in the device can be studied. It consists of trapping and detrapping transient current measurements, mathematical fitting and analysis of data from time constant spectra. For this method to be true, it is assumed that the changes in current are due to the changes in trapping status in the measured device [35].

For trapping experiments, a voltage bias is applied on the device and the drain and/or gate currents are measured in time scale to monitor the carrier trapping. Different modes of trapping and at different locations in the device can be induced using different biases to the gate and/or drain contacts. For detrapping experiments, carrier trapping is first induced by applying a trapping pulse to the gate and/or drain contacts. Immediately after removing the trapping pulse, the recovery transient current is monitored over a period of time. The dominant time constants associated with the measured transient data, $I_{\text{data}}(t)$, from the trapping and/or detrapping data are extracted using a mathematical technique [35].

2.3.1 Mathematical Fitting Function

The mathematical technique involves fitting $I_{\text{data}}(t)$ to a sum of pure exponentials in a least-mean-square manner. It is assumed that $I_{\text{data}}(t)$ involves several independent trapping and detrapping processes, each decaying exponentially in time. Joh *et al*. explains that this assumption is justified for detrapping processes since the process of recovery from a state of non-equilibrium has an exponential decay rate that is proportional to the population of the state. Joh *et al*. further explains that the exponential decay is also justified for trapping processes if the carriers have to overcome an energy barrier as rate of carrier transport through the barrier is proportional to the carrier population. Equation 2.4 shows the fitting function used to extract the dominant time constants involved in the trapping and/or detrapping processes [35].

$$I_{fitted} = \sum_{i=1}^{n} a_i exp(-t/\tau_i) + I_{\infty} \tag{2.4}$$

The fitting method involves minimizing the sum of $|I_{\text{data}} - I_{\text{fitted}}|^2$ at measured points. The a_i's refer to fitting parameters to be evaluated, which is the magnitude of trapping/detrapping of predefined time constant τ_i. The evaluated values of a_i are then plotted as a function of τ_i to construct the time constant spectrum. Positive and negative values of a_i refer to trapping and detrapping processes, respectively [35].

2.3.2 ON-state Trapping Measurement and Trap Analysis

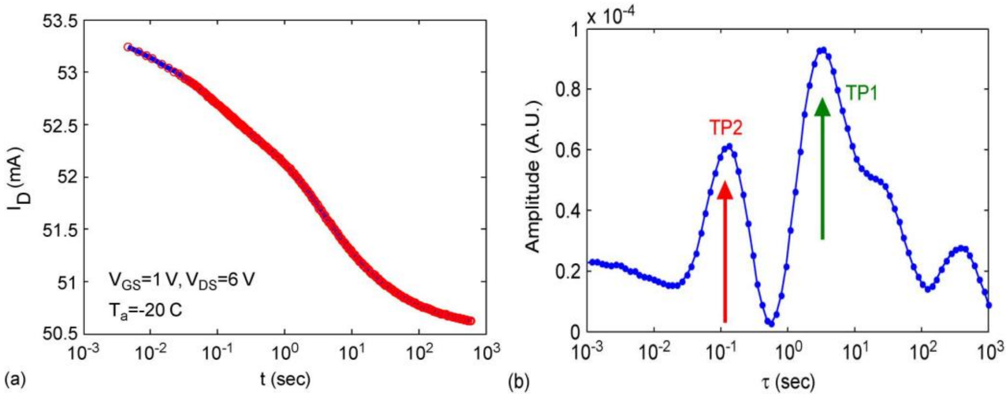

Figure 2.6: (a) Drain current transient measurement (red circles) and fitting (blue line) during ON-state (V_{GS} = 1 V, V_{DS} = 6 V) at T = 30 °C. (b) Time constant spectrum extracted using the fitting function shows two dominant trapping processes (TP1 and TP2) [35].

The trapping behavior of the device was first studied in the ON-state. The AlGaN/GaN HEMT was measured at V_{GS} = 1 V and V_{DS} = 6 V at temperatures from 0 °C to 40 °C. Figure 2.6(a) shows an example of the measured drain transient current (red circles) and fitting (blue line) using the fitting function described in Equation 2.4 at T = 30 °C. The corresponding time constant spectrum (Figure 2.6(b)) shows two dominant trapping processes labelled as TP1 and TP2. The time constant of TP1 and TP2, at T = 30 °C are 3 s and 0.1 s, respectively [35].

Figure 2.7 shows the temperature dependent time constant spectra. It can be seen that TP1 shows temperature dependence, while TP2 is insensitive to temperature. It is explained that in the trapping process of TP1, the electrons will have to overcome an energy barrier before getting trapped. During the ON-state measurement, the device temperature can increase considerably due to the power dissipation. In order to overcome this drawback, similar trapping transient was measured at V_{DS} = 0 V, thus, making self-heating negligible [35].

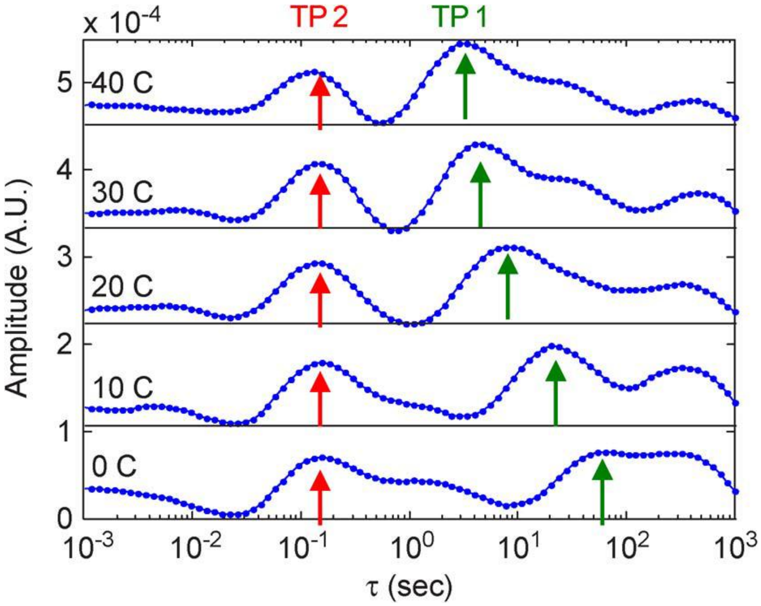

Figure 2.7: Temperature-dependent time constant spectra at *T* = 0 °C – 40 °C. TP1 process is temperature dependent while TP2 process is insensitive to temperature [35].

2.3.3 V_{DS} = 0 V State Trapping Measurement and Trap Analysis

The V_{DS} = 0 state trapping measurement involved biasing the device at V_{DS} = 0 V and V_{GS} = -5 V and the gate current (I_G) is monitored. Since V_{DS} = 0 V, the channel current is zero. Figure 2.7 shows a time constant spectra at *T* = 70 °C to 110 °C. Similar to TP1 from the ON-state trapping time constant spectra, a dominant trapping process peak was seen in the V_{DS} = 0 state trapping time constant spectra [35].

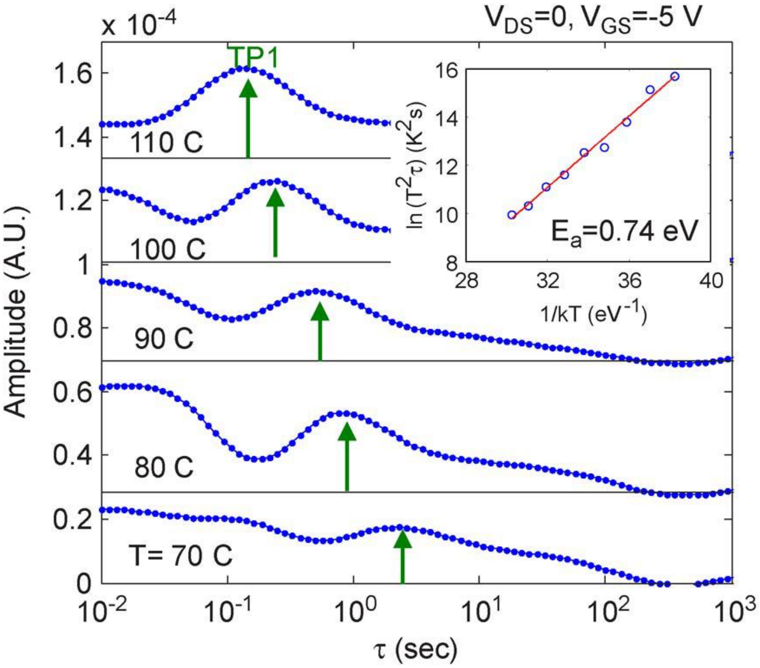

Figure 2.8: Temperature-dependent time constant spectra for V_{DS} = 0 V trapping transient (V_{GS} = -5 V and V_{DS} = 0 V) at T = 70 °C – 110 °C. Activation energy of trap extracted from Arrhenius plot fitting is 0.74 eV [35].

Unlike the ON-state measurement, at V_{DS} = 0 V state the temperature independent process like TP2 is not observed. It can be concluded that TP1 is related to injection of electrons from the gate, into the AlGaN barrier or surface close to the gate since V_{DS} = 0 V. Conversely, TP2 should be associated with trapping of channel electrons since TP2 only appears when the channel current is present. Since TP2 is observed at low V_{DG} suggests that it is unlikely to be a hot–electron trapping process inside or at the surface of the AlGaN. It is believed that the TP2 process occurs in the channel or in the buffer region [35].

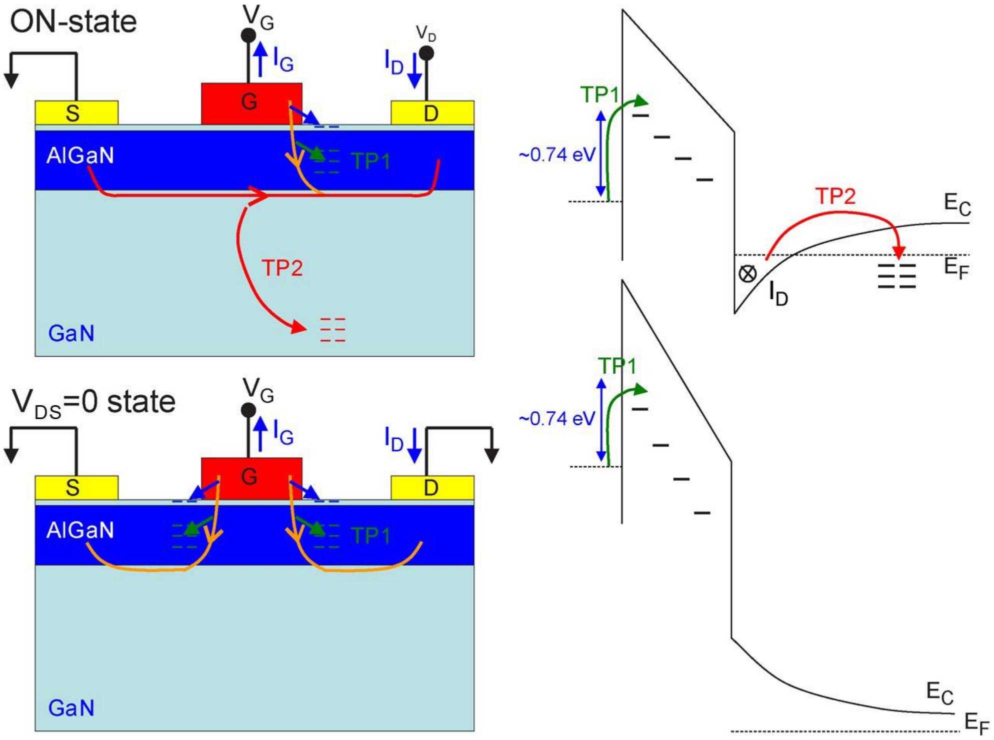

Figure 2.9: Schematic and energy band diagrams showing the flow of electron during the ON-state and V_{DS} = 0 V state trapping measurement [35].

Trapping processes of TP1 and TP2 are shown in Figure 2.9 for ON-state and V_{DS}=0 V state trapping. During the ON-state and V_{DS} = 0 V state trapping measurement, the electrons from the gate are injected into the AlGaN bulk layer and AlGaN surface. This trapping process from preceding discussions is attributed to TP1. During the ON-state trapping measurement, the capture of electrons in the buffer or channel is related to TP2. Only for V_{DS} = 0 V state trapping measurement, the TP1 occurs on both sides of the gate metal [35].

2.3.4 ON-state Detrapping Transient Measurement and Trap Analysis

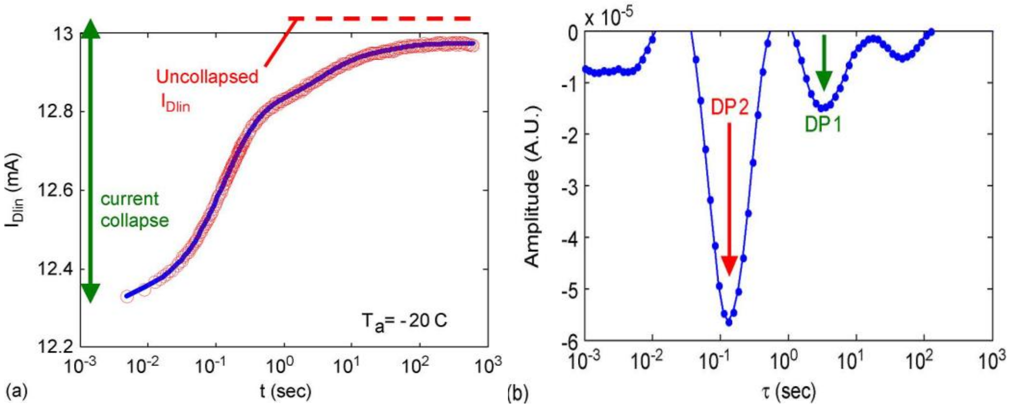

Figure 2.10: (a) Detrapping recovery transient measurement (red circles) after ON-state trapping pulse (V_{GS} = 0 V, V_{DS} = 10 V for 1 s) at T = -20 °C and fitting (blue line) using the fitting function. (b) Time constant spectrum shows two dominant detrapping processes (DP1 and DP2) [35].

ON-state detrapping involves measuring the recovery transient (in linear regime) after an ON-state pulse. The trapping pulse was V_{GS} = 0 V, V_{DS} = 10 V for 1 s. Due to the high drain-to-source trapping pulse bias, it is expected that the trapping occurs inside the AlGaN or the surface close to the gate edge or in the buffer. Figure 2.10(a) shows the measured recovery transient (red circles) and the fitting (blue line) using the fitting function in Equation 2.4. The time constant spectra in Figure 2.10(b) show two distinct time constants (DP1 and DP2). Figure 2.11 shows the cross-sectional diagram and energy band during the recovery transient measurement. The arrows indicate the flow of electrons during the recovery transient [35].

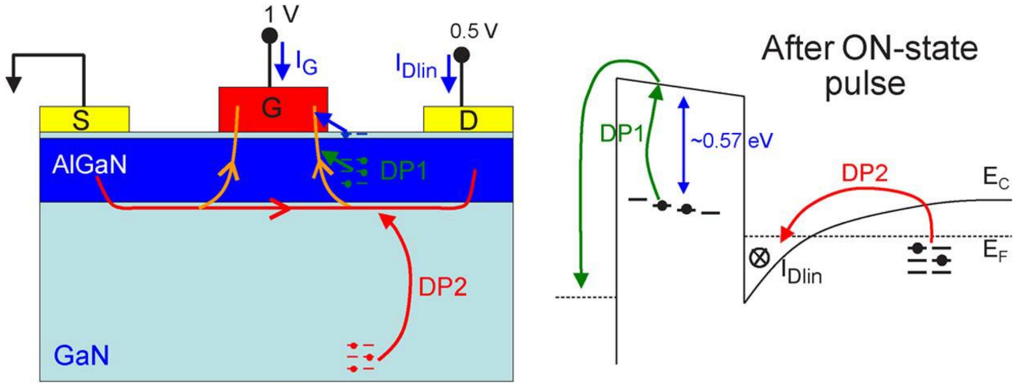

Figure 2.11: Schematic diagram showing the detrapping behaviour after ON-state trapping pulse. The energy band diagram shows the detrapping process during the recovery phase. The arrows indicate the flow of electrons [35].

2.3.5 V_{DS} = 0 V State Detrapping Transient Measurement

The V_{DS} = 0 V state detrapping measurement involves a trapping pulse at V_{DS} = 0 V, followed by recovery transient drain current in the linear regime. An example of the trapping pulse is V_{GS} = -10 V and V_{DS} = 0 V for 1s. This method is further discussed in Chapter 4 of this thesis. In this thesis, this current transient method was applied to study the trap characteristics in the Al_2O_3/AlGaN/GaN MOSHEMT. The presence of Al_2O_3 layer between the gate metal and AlGaN layer, can allow the trapping of electrons at the Al_2O_3/AlGaN interface states. The trapping of electrons at the Al_2O_3/AlGaN interface can affect the V_{th}, mobility and can be responsible for the drain current collapse [34],[50].

2.4 Summary

In Section 2.1, the origin of the 2DEG in the AlGaN/GaN HEMT device was discussed. If the thickness of the AlGaN layer is greater than the critical thickness, the 2DEG at the AlGaN/GaN interface is dependent on the net positive charge at the AlGaN surface. In Section 2.2, the concept of virtual gate mechanism was discussed. The formation of negative potential at the AlGaN surface due to trapping of electrons at the AlGaN surface extends the depletion region under the gate to regions outside the gate metal. This negative potential on the AlGaN surface acts as a second gate, which is also known as virtual gate, and controls the output drain current. Analysis of trap characteristics using current transient methodology was discussed in Section 2.3. This method includes ON-state trapping, V_{DS} = 0 V state trapping, ON-state detrapping and V_{DS} = 0 V detrapping measurements. Using this method, the trap time constant and activation energy of temperature-dependent trapping/detrapping processes can be studied.

Chapter 3: Study of Surface Passivation of AlGaN/GaN MOS-HEMT using TCAD simulation

3.1 Introduction

Gallium Nitride (GaN) based materials with their superior properties such as large bandgap [39], high electron mobility [40], high breakdown voltage [41] are attractive for high power [42], high temperature [43] and high frequency [44] device applications.

The large spontaneous and piezoelectric polarizations in the AlGaN/GaN HEMT (discussed in Chapter 1) form the polarization induced charges at the AlGaN surface, AlGaN/GaN interface and GaN/substrate interfaces. The polarity of the charges at the AlGaN surface and AlGaN/GaN interface are opposite. Ibbetson *et al*. reported that the presence of these polarization induced charges alone is insufficient to form the two-dimensional electron gas (*2DEG*) at the AlGaN/GaN interface. Therefore, it is necessary that a positive sheet charge exists at the AlGaN surface so that *2DEG* can be formed at the AlGaN/GaN interface [34].

However, one of the major obstacles that limits the development of reliable high power AlGaN/GaN devices is the drain current collapse due to surface states in the AlGaN layer. Vetury *et al*. [29] reported on the formation of a second (virtual) gate which was formed due to the charging of the AlGaN surface, in the gate-to-drain region. It was explained that the surface states near the gate became negatively charged due to electron trapping. Therefore, the maximum drain current is limited by discharging of the trapped electrons in the virtual gate. Thus, this virtual gate phenomenon leads to drain current collapse in AlGaN/GaN HEMTs [29].

Several methods of AlGaN surface passivation have been shown to improve the performance of AlGaN/GaN HEMTs. AlGaN surface passivation using 10 nm of MgO, deposited at 100 °C using plasma-enhanced molecular beam epitaxy, was demonstrated by Luo *et al*. [45]. It was reported that the passivation using MgO led to a 20 % increase in drain current. This increase in drain current was suggested to be attributed to the increase in effective sheet carrier density in the AlGaN/GaN interface due to increase in positive charge at the MgO/AlGaN interface [46].

Lu *et al*. reported the use of 250 nm of Si_3N_4 layer, deposited by plasma enhanced chemical vapour deposition, as surface passivation of AlGaN/GaN HEMTs. The passivated devices displayed lower gate leakage current and improved pinch-off characteristics. Also, it was shown that the passivation increased the drain current from 791 mA/mm to 812.2 mA/mm and peak extrinsic transconductance from 207.2 mS/mm to 220.9 mS/mm. An increase in positive charges at the Si_3N_4/AlGaN was attributed to the improvement in the device performance [47].

This Chapter reports the use of device simulation to give a deeper understanding of the effects of SiH_4 passivation of AlGaN/GaN MOSHEMTs, by Liu *et al*. [48]. It was reported that the SiH_4 passivation had a great impact on the electrical characteristics of the AlGaN/GaN MOSHEMTs. Some of the reported enhancements due to the passivation in device performances were 53 % increase in drain saturation current, increase of peak extrinsic transconductance from 66 mS/mm to 93 mS/mm and increase in 2DEG density from 0.86×10^{13} cm^{-2} to 1.04×10^{13} cm^{-2} [48].

3.2 Summary of Results from Experiment [48]

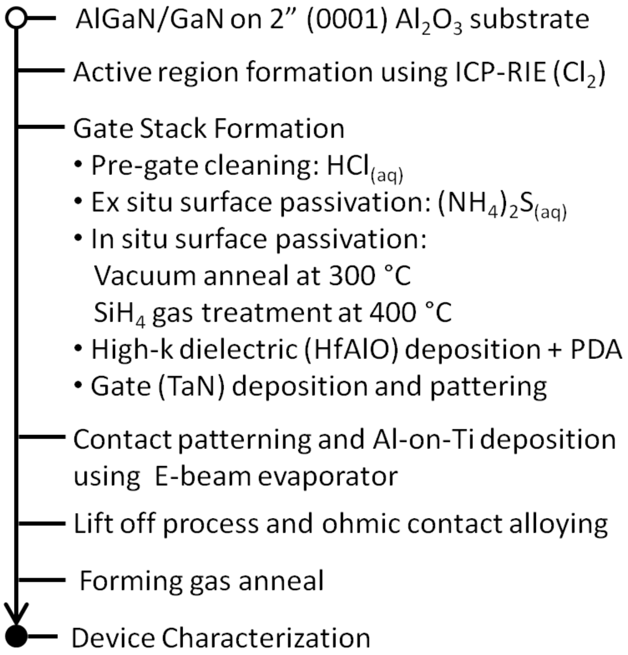

Figure 3.1: Process flow of the fabricated AlGaN/GaN MOS-HEMTs [48].

Figure 3.1 shows the process flow of the main steps taken during the fabrication of the AlGaN/GaN MOS-HEMTs as described in Ref. [48]. The *in situ* passivation steps, which consist of vacuum annealing and SiH_4 gas, are the key steps in that work. It was reported that the unpassivated and passivated devices showed significant difference in the device characteristics.

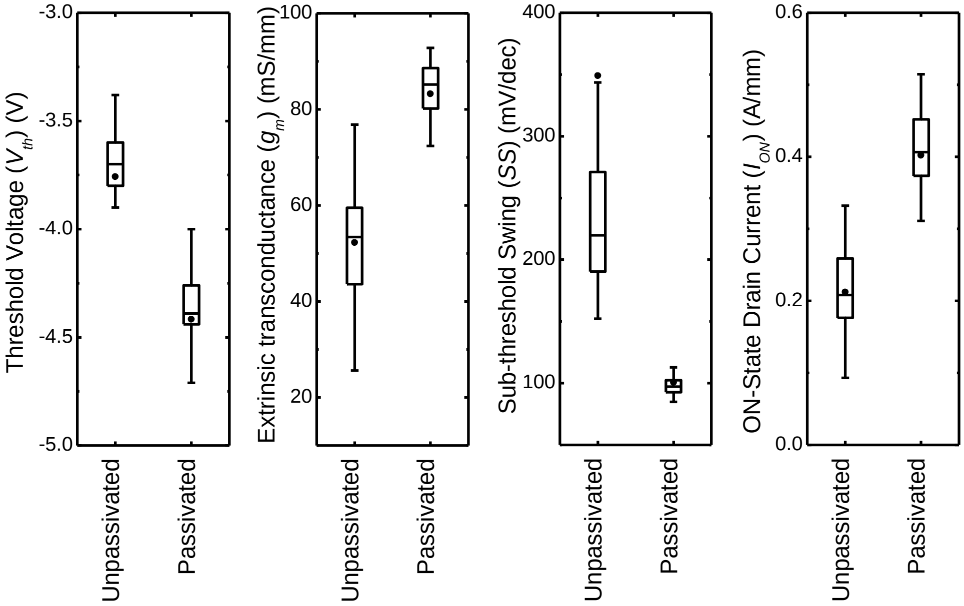

Figure 3.2: Summary of results from *in situ* passivation of AlGaN/GaN MOSHEMT reported by Liu *et al*. [48]

Figure 3.2 shows the summary of results from the *in situ* surface passivation of AlGaN/GaN MOSHEMT. The results show that the passivation causes an increase in the threshold voltage (V_{th}) in the negative direction, increase in the extrinsic transconductance (g_m), decrease in sub-threshold swing (SS) and increase in ON-state drain current (I_{ON}).

3.3 TCAD Simulation

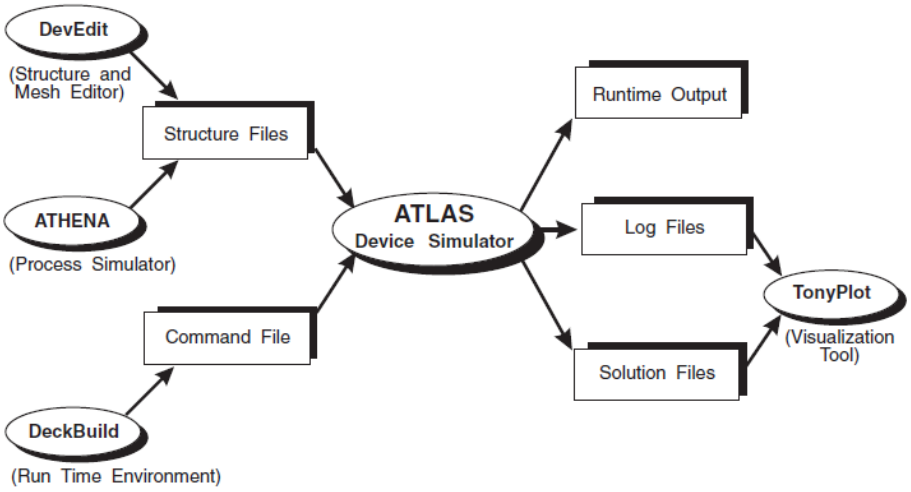

Figure 3.3: Flowchart for device simulation using SILVACO ATLAS TCAD [49].

Figure 3.3 shows the flowchart of the device simulation using SILVACO ATLAS. The first step in this simulation work is the construction of the device structure that is similar to the fabricated device. In SILVACO ATLAS TCAD, there are three ways to construct the device structure. These methods are DevEdit, ATHENA and DeckBuild. DevEdit uses a Graphical User Interface (GUI) to build the device structure. ATHENA is used in simulating fabrication process of devices. Since this method focuses on the device fabrication simulation instead of simulating the device characteristics, ATHENA is not a suitable method for this study. DeckBuild method involves building the device structure purely using codes. This was the selected method in this simulation work. The three methods can be used to construct one-dimensional (1D), two-dimensional (2D) and three-dimensional (3D) structures. Since this work is on the study of AlGaN/GaN planar device, 2D simulation was sufficient.

3.4 Simulated Device Structure

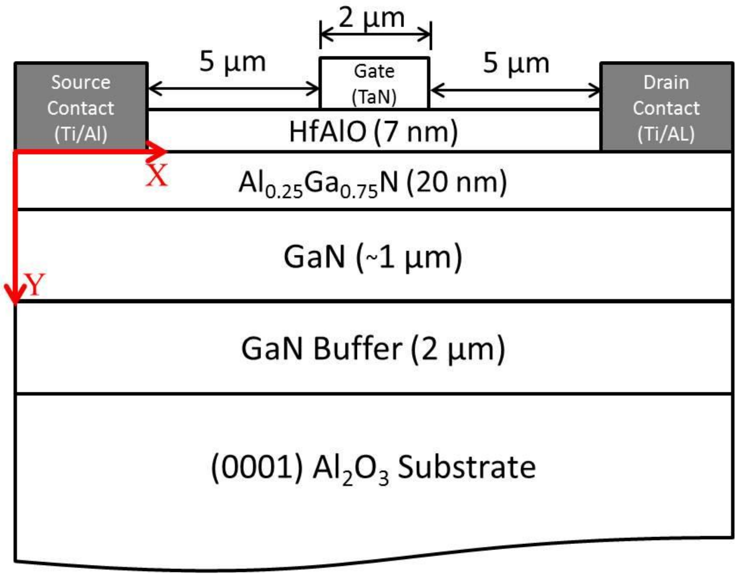

Figure 3.4: Cross-sectional schematic of the simulated AlGaN/GaN MOSHEMT using SILVACO ATLAS TCAD.

Figure 3.4 shows the cross-sectional schematic of the AlGaN/GaN MOSHEMT designed using SILVACO ATLAS TCAD. When constructing the device structure using the TCAD, it is necessary that the simulated device has similar structure as the real (fabricated) device. Therefore, the device in the simulation was designed with close reference to the actual device. The X-Y axes shown in Figure 3 are related to the coordinates used during the simulation process (units in microns). X = 0 refers to the left-edge of the device and Y = 0 refers to the AlGaN surface.

3.4.1 Source and Drain Contacts

Although it is necessary to replicate the exact device structure in the simulation, certain factors need to be taken into consideration in order to optimise and simplify the simulation and yet preserve the accuracy of the simulation results.

The lengths of the source and drain contacts in the real device were 94 µm. However, it would not be practical to simulate a 200 µm device (total length of device) because simulation of such a large device structure will be too time consuming. In order to optimise the simulation time, without compromising the accuracy of the simulation results, the simulated source and drain lengths were reduced to 1 µm. It was observed that the lengths of source and drain greater than 1 µm did not have significant impact on the simulation results, as most of the current flows into or out of the first 1 µm of the contacts.

For the real device, the source and drain Ohmic contacts were deposited on the AlGaN surface during the device fabrication process. However, for the simulation, the Ohmic contacts were designed to be in contact with the 2DEG at the AlGaN/GaN interface. This was another simplification used in the device structure for the simulation. Fontserè *et al*. [50] proposed a direct electron path mechanism for the Ohmic contacts in AlGaN/GaN HEMT. This mechanism is also known as spike contact. It was explained that during the Ohmic contact annealing process, TiN (formed due to reaction between Ti and nitrogen in AlGaN) penetrates through the dislocations in the AlGaN layer. This 'spiking' of the Ohmic contact establishes a direct contact between the 2DEG electrons in the AlGaN/GaN interface and the metal [50].

3.4.2 Gate Electrode

The gate lengths (L_G) of the real and simulated devices are 2 µm. Tantalum Nitride (TaN) was deposited, using RF sputter system, as the gate electrode during the device fabrication process. Therefore, in order to simulate TaN as the gate electrode, the work function of TaN (4.8 eV) [51] was incorporated in the simulation.

3.4.3 AlGaN Layer

The energy band gap of GaN used in the simulation was 3.4 eV [39]. The energy band gap of $Al_{0.25}Ga_{0.75}N$ was calculated to be 3.9 eV using the equation 3.1 [26],[64].

$$E_g(x) = xE_g(AlN) + (1-x)E_g(GaN) - x(1-x)1.0\ eV \tag{3.1}$$

3.4.4 Gate Dielectric

Hafnium aluminum oxide (HfAlO) was used as the gate dielectric during the fabrication process. The important parameters such as the dielectric thickness, permittivity, bandgap and electron affinity that were used to simulate the HfAlO dielectric were 7 nm, 19, 6.4 eV and 2.1 eV respectively [52] [53].

3.4.5 Mesh Design

Once the device structure was constructed in the simulation, the next important step was to design the mesh. The nodes of SILVACO ATLAS mesh contain primary solution variables such as carrier concentration, potential, carrier temperature and lattice temperature [49].

Figure 3.5: Mesh design of simulated AlGaN/GaN MOSHEMT showing different mesh densities at different regions.

Figure 3.5 shows the mesh design of the AlGaN/GaN MOSHEMT in the simulation. In order to optimise the speed and accuracy of the simulation, regions of interest such as the HfAlO/AlGaN and AlGaN/GaN interfaces, and GaN channel region were designed to have higher mesh density. On the other hand, regions such as GaN bulk and substrate had lower mesh density.

3.5 Mathematical model and Mobility models

The mathematical model consists of fundamental equations, which link together the electrostatic potentials and carrier densities in the simulation. The equations consist of Poisson's Equation, carrier continuity equations and transport equations, which were derived from Maxwell's laws [49].

3.5.1 Poisson's Equation

Poisson's equation relates the electrostatic potential to the space charge density using equation 3.2:

$$div(\varepsilon \nabla \Psi) = -\rho \tag{3.2}$$

where ε is the permittivity, Ψ is the electrostatic potential and ρ is the space charge density. The space charge density is the sum of contributions from all fixed and mobile charges, including electrons, holes and ionized impurities. Equation 3.3 shows the electric field obtained from the gradient of the potential [49].

$$\vec{E} = -\nabla \Psi \ . \tag{3.3}$$

3.5.2 Carrier Continuity Equation

$$\frac{dn}{dt} = \frac{1}{q} \nabla \overrightarrow{J_n} + G_n - R_n \ . \tag{3.4}$$

$$\frac{dp}{dt} = \frac{1}{q} \nabla \overrightarrow{J_p} + G_p - R_p \ . \tag{3.5}$$

The continuity equations for electrons and holes are defined by equations 3.4 and 3.5, respectively, where n and p are the electron and hole concentration, $\overrightarrow{J_n}$ and $\overrightarrow{J_p}$ are the current densities for electrons and holes, G_n and G_p are the electron and holes generation rates, R_n and R_p are electrons and holes recombination rates, respectively. q is the magnitude of electron charge. By default, equations 3.4 and 3.5 are included in ATLAS [49].

3.5.3 Drift-Diffusion Transport Model

Drift-diffusion model is the simplest charge transport model that approximates the current densities in the carrier continuity equations. The current densities for electrons and holes are given in equations 3.6 and 3.7 respectively [49].

$$\overrightarrow{J_n} = -nq\mu_n \nabla \Phi_n \ , \tag{3.6}$$

$$\overrightarrow{J_p} = -pq\mu_p \nabla \Phi_p \ , \tag{3.7}$$

where μ_n and μ_p are the mobilities of electrons and holes, Φ_n and Φ_p are electron and hole quasi-Fermi potentials, respectively. The carrier concentrations and potentials are related to the quasi-Fermi levels through the Boltzmann approximations in equations 3.8 and 3.9 [49].

$$n = n_{ie} exp \left[\frac{q(\Psi - \Phi_n)}{kT_L} \right] , \tag{3.8}$$

$$p = n_{ie} exp \left[\frac{q(\Psi - \Phi_p)}{kT_L} \right] , \tag{3.9}$$

where n_{ie} and T_L are the effective intrinsic carrier concentration and the lattice temperature, respectively.

In this simulation, three different kinds of mobility models were used. These include low-field, high-field and perpendicular field mobility.

3.5.4 Low-Field Mobility

The low-field mobility was simulated using the mobility model reported by Albrecht *et al.* [54]. The mobility model is dependent on the ambient temperature, donor concentration and compensation ratio. Equation 3.10 shows the low-field mobility model [54].

$$\frac{1}{\mu} = a\left(\frac{N_I}{10^{17}cm^{-3}}\right) ln(1+\beta_{cw}^2)\left(\frac{T}{300\ K}\right)^{-1.5} + b\left(\frac{T}{300\ K}\right)^{1.5} + \frac{c}{exp\left(\frac{\theta}{T}\right)-1} \tag{3.10}$$

where

$$\theta = \frac{\hbar\omega_{LO}}{k_B} = 1065\ K,$$

$$\beta_{cw}^2 = 3.00\left(\frac{T}{300\ K}\right)^2\left(\frac{N_I}{10^{17}cm^{-3}}\right)^{-2/3},$$

$$N_I = (1+k_c)N_D.$$

Parameters (a, b and c) are the fitting parameters obtained from the Monte Carlo calculation results. N_D is the ionized donor concentration (cm^{-3}), T is the ambient temperature (K) and k_c is the compensation ratio (N_A/N_D). The peak electron drift velocity in GaN can be calculated using Equation 3.11. In the simulation, values of a, b and c (fitting parameters) were 3×10^{-3} Vs cm^{-2}, 3×10^{-4} Vs cm^{-2} and (2 – 3.6)×10^{-2} Vs cm^{-2} respectively. The υ_{peak} used in the simulation was 3×10^{7} cm/s.

$$\upsilon_{peak} \approx \left[3.70 - 0.65\left(\frac{T}{300K}\right)\right](10^7\ cm/s) \tag{3.11}$$

3.5.5 High-field Mobility

The high-field mobility was simulated using the mobility model developed by Farahmand *et al*. [55]. It was reported that this high-field mobility model has excellent agreement with the Monte Carlo calculations. It was also reported that the Monte Carlo model includes all of the important scattering mechanisms. Equation 3.12 shows the high field mobility model

$$\mu = \frac{\mu_0(T,N) + \upsilon^{sat}\frac{E^{n_1-1}}{E_C^{n_1}}}{1 + a\left(\frac{E}{E_C}\right)^{n_2} + \left(\frac{E}{E_C}\right)^{n_1}} \tag{3.12}$$

where, μ_0 is the low-field mobility. υ^{sat}, E_c, a, n_1 and n_2 are parameters that were determined from the least square fitting to the Monte Carlo simulation. The values of υ^{sat}, E_c, a, n_1 and n_2 used in the simulation are about 1.12×10^{7} cm/s, 3.66×10^{5} V/cm, 3.23, 5.32 and 1.04 respectively [55].

3.5.6 Perpendicular Field Mobility Model

In the literature, the perpendicular field mobility model is not available for GaN. Hence, the mobility degradation effects due to the perpendicular field were accounted for using a simple perpendicular field dependent mobility model in Equation 3.13 [49]

$$\mu_n = GSURFN \frac{\mu_{0n}}{\sqrt{1+\frac{E_\perp}{ECN.MU}}} . \tag{3.13}$$

In the simulation, the values of GSURFN and ECN.MU were 1.0 and 6.48×10^4 V/cm respectively.

3.6 Fowler-Nordheim (*FN*) Tunnelling Model

FN tunnelling is defined as the tunnelling of electrons from metal (or semiconductor) Fermi energy into the insulator conduction band, if the electric field across the insulator is sufficiently high [49] [56] [57]. The off state drain current was simulated using *FN* tunnelling model in the simulation. The FN tunnelling is described using Equation 3.14.

$$J = \frac{q^3E^2}{8\pi h\Phi} exp\left[-\frac{4(2m)^{1/2}\Phi^{3/2}}{3\bar{h}qE}\right] \tag{3.14}$$

where q is the electronic charge, E is the electric field, h is the Plank's constant, Φ is the barrier height and m in the mass of free electron.

3.7 Results and Discussion

3.7.1 Polarization Charge Density Modelling

In the simulation, the polarization charge densities were modelled as fixed interface charge densities. Table 3.1 lists the spontaneous and piezoelectric polarization charges of AlGaN and GaN layers that were calculated using equations 1.11 – 1.19 in Chapter 1. Table 3.2 shows the calculated polarization charge densities at the HfAlO/AlGaN, AlGaN/GaN and GaN/substrate interfaces. Please see Appendix A and B for the simulation codes used for unpassivated and passivated devices, respectively.

Table 3.1: Calculated spontaneous and piezoelectric charges calculated using equation 1.11 – 1.19.

Polarization	Sheet Density (cm^{-2})
P_{SP}(GaN)	-1.81004×10^{13}
P_{SP}(AlGaN)	-2.62143×10^{13}
P_{PE}(AlGaN)	-4.12225×10^{12}

Table 3.2: Theoretical and adjusted polarization charges at the HfAlO/AlGaN, AlGaN/GaN and GaN/substrate interfaces.

Interface	Polarization Sheet Charge Density (cm^{-2})	
	Calculated Values	Adjusted Values
HfAlO/AlGaN	-3.0337×10^{13}	-2.57861×10^{13}
AlGaN/GaN	1.2236×10^{13}	1.04008×10^{13}
GaN/Substrate	1.81×10^{13}	1.53853×10^{13}

3.7.2 Discrepancy in theoretical and experimental values

When the calculated values were incorporated into the simulation, the results showed a significant offset between simulated and experimental V_{th}. In order, to fit the simulated and experimental V_{th} the polarization charge densities at the HfAlO/AlGaN, AlGaN/GaN and GaN/substrate interfaces were reduced by 15%. The adjusted values used in the simulation are listed in Table 3.2. This discrepancy between the calculated values and real values are believed to be due to uncertainties in the physical parameters used in the simulation, possible partial relaxation of the strained AlGaN layer, partial screening of the polarization field by residual doping in the GaN layer and interface roughness [58]-[72]. One of the smallest discrepancies between the calculated and real values was reported to be 15 % [59] and thus the results obtained are not unreasonable.

3.7.3 Charge Trapping Defect States

In this simulation, both donor-like and acceptor-like states are considered to be present at the HfAlO/AlGaN interface. It was reported that nitrogen vacancy (V_N) and gallium vacancy (V_{Ga}) sites act as deep donor [60] and deep acceptor traps [61], respectively. In the simulation, these discrete traps were placed at the HfAlO/AlGaN interface, within the AlGaN bandgap. The relative energy levels of the donor-like traps ($E_{T,donor}$) [60] and acceptor-like traps ($E_{T,acceptor}$) [62] are stated in the equations 3.15 and 3.16 .

$$E_{T,donor} = E_c - 0.37\ eV \tag{3.15}$$

$$E_{T,acceptor} = E_V + 1.0\ eV \tag{3.16}$$

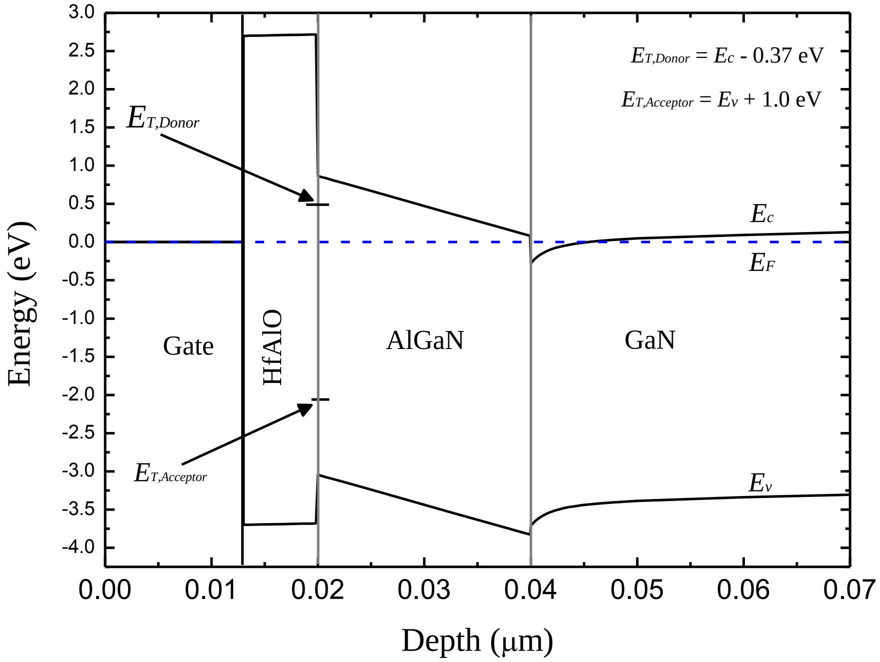

Figure 3.6: Band diagram of AlGaN/GaN MOSHEMT showing the trap energies of the donor-like and acceptor-like traps at the HfAlO/AlGaN interface.

Figure 3.6 shows band diagram of the unpassivated AlGaN/GaN MOSHEMT structure under the gate electrode at zero gate bias. The band diagram shows the positions of $E_{T,donor}$ and $E_{T,acceptor}$ at the HfAlO/AlGaN interface. The acceptor-like trap energy is located far below the E_F is completely filled and ionized. On the other hand, the donor-like trap energy, located above E_F, is completely empty and ionized. In order to achieve good fitting to the measured electrical data, the density of the donor-like trap was set as 2.96×10^{13} cm^{-2} for the passivated devices. The unpassivated device required an additional acceptor-like trap with density of 6.0×10^{12} cm^{-2} at the HfAlO/AlGaN interface.

3.7.4 Simulation Sensitivity Studies

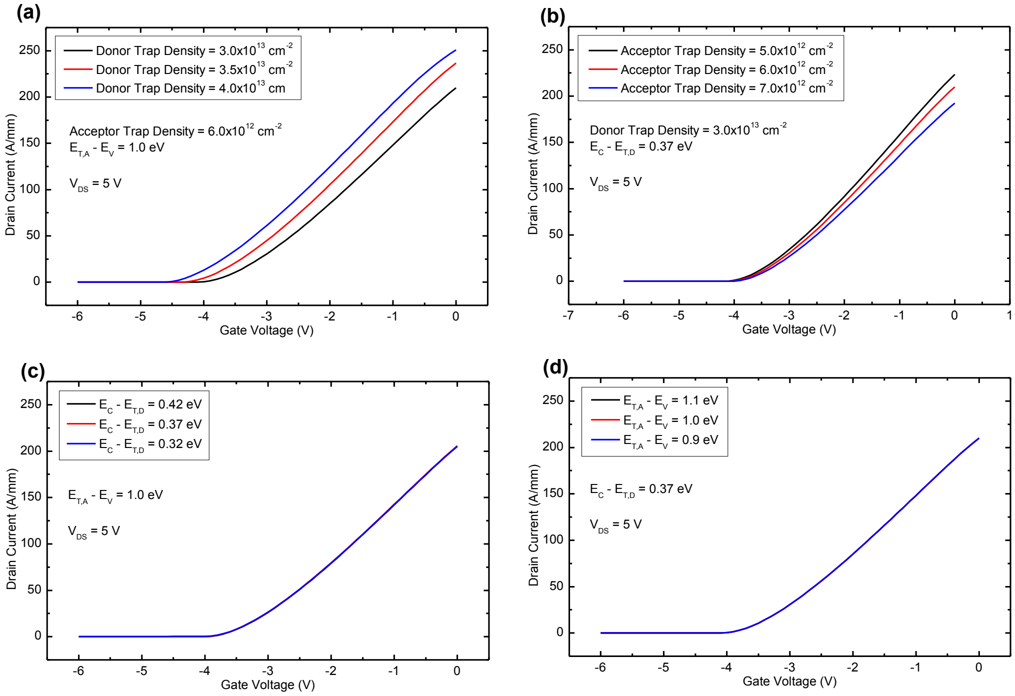

Figure 3.7: Simulated I_D-V_{GS} plots with varying (a) donor-like trap density, (b) acceptor-like trap density, (c) donor-like trap energy and (d) acceptor-like trap energy.

Simulation sensitivity studies were performed by simulating I_D-V_{GS} plots with varying the trap parameters such as trap type (ie., donor-like or acceptor-like), trap density and trap energy, in order to learn which parameters have the most influence on the *I*-*V* characteristics of the AlGaN/GaN MOSHEMTs

Figure 3.7(a) show I_D-V_{GS} plots simulated at V_{DS} = 5 V with varying donor-like trap density while the acceptor-like trap density was fixed at 6.0×10^{12} cm^{-2}. Simulation results show that both the acceptor-like and donor-like trap states are fully ionized. Increasing the donor-like trap density from 3.5×10^{13} cm^{-2} to 4.0×10^{13} cm^{-2} caused the net positive charge density (Ionized donor-like trap density – Acceptor-like trap density) at the Al_2O_3/AlGaN interface to increase. Therefore, the 2DEG density at the AlGaN/GaN interface increased from 9.03×10^{12} cm^{-2} to 9.30×10^{12} cm^{-2} and the V_{th} decreased from -4.38 V to -4.67 V. On the other hand, decreasing the donor-like trap density from 3.5×10^{13} cm^{-2} to 3.0×10^{13} cm^{-2} caused the net positive charge density at the Al_2O_3/AlGaN interface to decrease from 2.9×10^{13} cm^{-2} to 2.4×10^{13} cm^{-2}. Simulation results show that this caused the 2DEG density at the AlGaN/GaN interface to decrease from 9.03×10^{12} cm^{-2} to 8.37×10^{12}, causing the V_{th} to increase from -4.38 V to -4.12 V.

Figure 3.7(b) show I_D-V_{GS} plots simulated at V_{DS} = 5 V with varying acceptor-like trap density while the donor-like trap density was fixed at 3.0×10^{13} cm^{-2}. As mentioned earlier, since the donor-like trap states are fully ionized, increasing the acceptor-like trap density from 6.0×10^{12} cm^{-2} to 7.0×10^{12} cm^{-2}, caused the net positive charge density at the Al_2O_3/AlGaN interface to decrease from 2.4×10^{13} cm^{-2} to 2.3×10^{13} cm^{-2}. Thus, the 2DEG density at the AlGaN/GaN interface decreased from 8.37×10^{12} cm^{-2} to 8.24×10^{12} cm^{-2}, and the V_{th} increased from -4.11 V to -4.07 V. Conversely, decreasing the acceptor-like trap density from 6.0×10^{12} cm^{-2} to 5.0×10^{12} cm^{-2} at the Al_2O_3/AlGaN interface, caused the net positive charge density at the AlGaN surface to increase from 2.4×10^{13} cm^{-2} to 2.5×10^{13} cm^{-2}. Simulation results show that the 2DEG density at the AlGaN/GaN interface increased from 8.37×10^{12} cm^{-2} to 8.50×10^{12} cm^{-2}. Therefore, the V_{th} decreased from -4.11 V to -4.18 V.

Figure 3.7(c) show I_D-V_{GS} plots simulated at V_{DS} = 5 V with varying donor-like trap energy ($E_C - E_{T,D}$) while the acceptor-like trap energy ($E_{T,A} - E_V$) was fixed at 1.0 eV. Simulation results show that varying the donor-like trap energy from 0.32 eV to 0.42 eV does not show any significant change in the I_D-V_{GS} plots. This is because the donor-like trap states are fully ionized at energies of 0.31 eV – 0.42 eV. Similarly, varying the acceptor-like trap energy does not show significant change in the I_D-V_{GS} plots (Figure

3.7(d)). This is because both the donor-like and acceptor-like traps are fully ionized, thus no change in the I_D-V_{GS} plots was observed. Therefore, it can be concluded that the *I*-*V* characteristics of the AlGaN/GaN MOSHEMT is highly influenced by the effective positive charge density at the Al_2O_3/AlGaN interface.

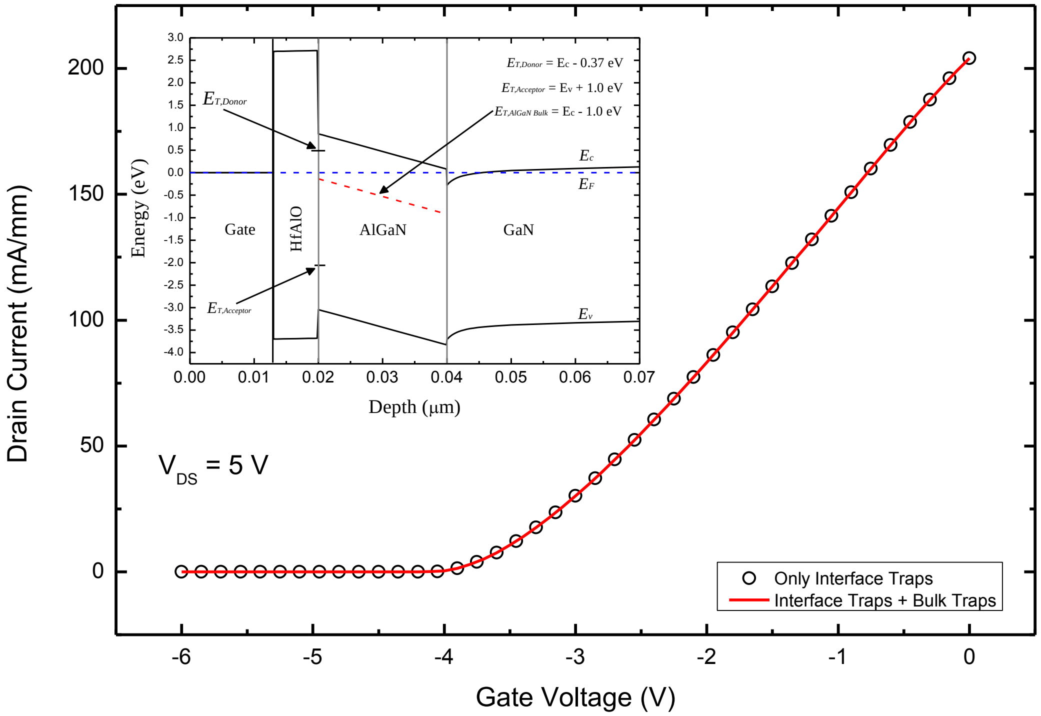

Figure 3.8: Simulated I_D-V_{GS} plots with Black Circles: Al_2O_3/AlGaN interface traps; Red Line: Both AlGaN bulk traps and interface traps. Band diagram of AlGaN/GaN MOSHEMT with interface and AlGaN bulk traps (inset).

Besides Al_2O_3/AlGaN interface traps, the AlGaN bulk traps might also affect the DC characteristics of the AlGaN/GaN MOSHEMTs. From literature AlGaN bulk trap density of 7.71×10^{16} cm^{-3} at E_C-E_T = 1.0 eV was reported by Kaushik *et al.* using experimentally observed inverse temperature dependence of reverse gate leakage current and trap-assisted tunnelling model [63]. In the simulation, the Al_2O_3/AlGaN interface traps consisted of donor-like traps (density

= 2.96×10^{13} cm^{-2}, $E_C - E_T = 0.37$ eV) and acceptor-like traps (6.0×10^{12} cm^{-2}, $E_T - E_V = 1.0$ eV). Simulated I_D-V_{GS} plots using Al_2O_3/AlGaN interface traps + AlGaN bulk traps shows insignificant change with respect to I_D-V_{GS} plot with only Al_2O_3/AlGaN interface traps. The band diagram (Figure 3.8(inset) shows that the AlGaN bulk traps are located below E_F and are completely filled. Therefore, the AlGaN bulk traps do not significantly affect the DC characteristics of the AlGaN/GaN MOSHEMT.

3.7.5 Simulation Fittings

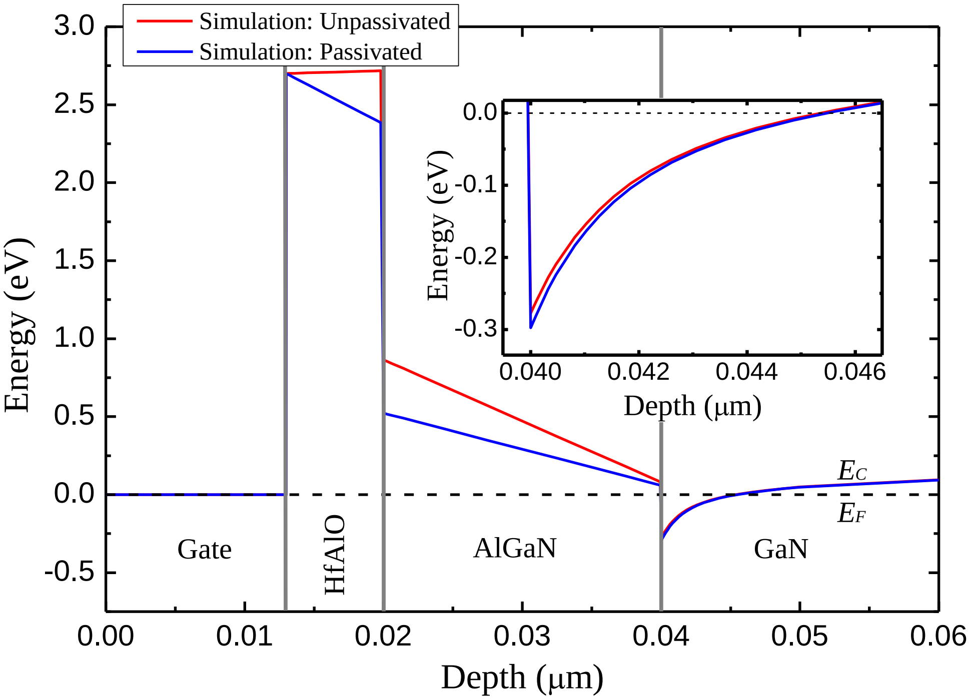

Figure 3.9: Simulated conduction band of AlGaN/GaN MOSHEMT under the gate electrode. Inset shows the triangular quantum well at the AlGaN/GaN interface.

Figure 3.9 shows the conduction bands in the AlGaN/GaN MOSHEMT under the gate electrode at zero gate bias, for the unpassivated and passivated devices. It can be seen that reduction in the acceptor-like density has caused the conduction band alignment at the HfAlO/AlGaN interface to experience a sharp drop in energy. In the previous section, it was mentioned that for the unpassivated device both the donor-like and acceptor like density are fully ionized. However, for the passivated device, simulation shows a very slight decrease (8.1×10^{10} cm^{-2}) in the density of the ionized donor-like traps. It can be explained that the close proximity of the Fermi energy level (E_F) to the donor-like trap energy level has partially filled the donor-like traps. The inset in Figure 3.9 shows the triangular quantum well at the AlGaN/GaN interface. The conduction band profile at the AlGaN/GaN interface only shows a small difference between the unpassivated and passivated samples.

From the simulations, the 2DEG density at the AlGaN/GaN interface for the unpassivated and passivated devices are 7.32×10^{12} cm^{-2} and 8.73×10^{12} cm^{-2} respectively. These values are about 15% smaller that the experimental measurements using room-temperature Hall measurement. It is reported in the literature that the sheet carrier concentration between experimental measurement and theoretical calculation can differ by ±20%. Therefore, the *2DEG* densities from the simulations can be said to agree reasonably well with the experimental values [26],[77].

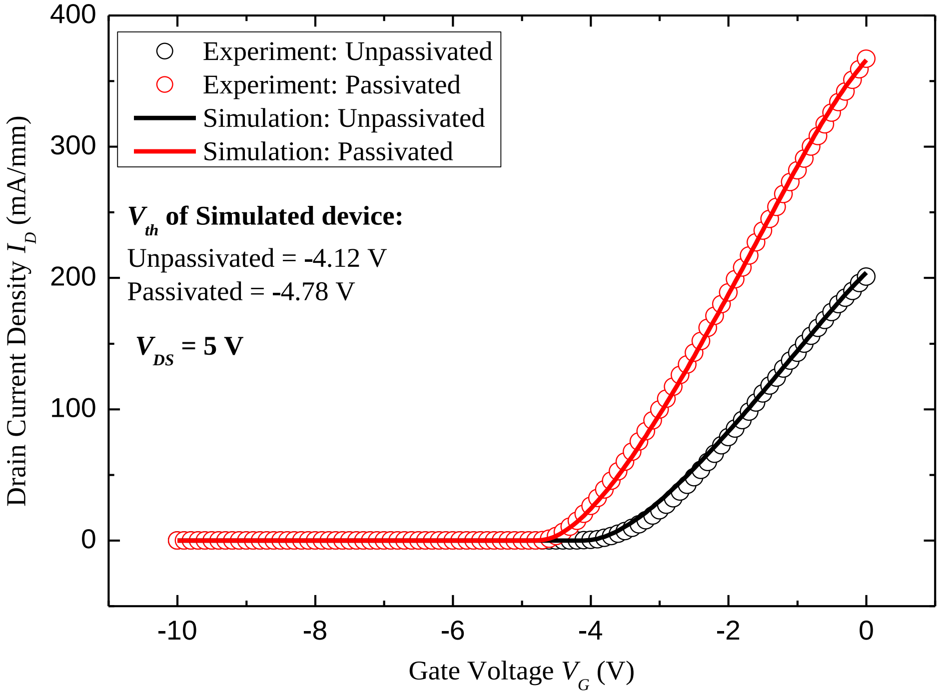

Figure 3.10: I_D-V_{GS} plot for simulation and experiment [48] at V_{DS} = 5 V.

Figure 3.10 shows the I_D-V_{GS} linear plot at V_{DS} = 5 V for the unpassivated and passivated samples. The experimental data from Ref. [48] and the simulated data are superimposed in Figure 3.8. The superimposed plots show a very close fit for both the unpassivated and passivated devices. The extracted V_{th} from the simulation are -4.12 and -4.78 V for the unpassivated and passivated devices respectively. Also, it is noticeable that the gradients of ON-state drain current (I_{ON}) for the passivated device is higher than the unpassivated device. Also, for the same gate overdrive, the passivated device shows higher I_{ON} compared to the unpassivated device. It is notable that in order to fit the unpassivated and passivated devices to the experimental data, the low-field mobility fitting parameter *c* had to be different for the two devices. This resulted in the difference in the lateral mobility in the two devices. The mobilities of the unpassivated and passivated devices from the simulation are 661 cm^2/V.s and 983 cm^2/V.s, respectively. Since the fitting parameters are from Monte Carlos calculations and are said to include most of the scattering mechanism, it is safe to say that the increase in mobility could be due to reduction in carrier scattering.

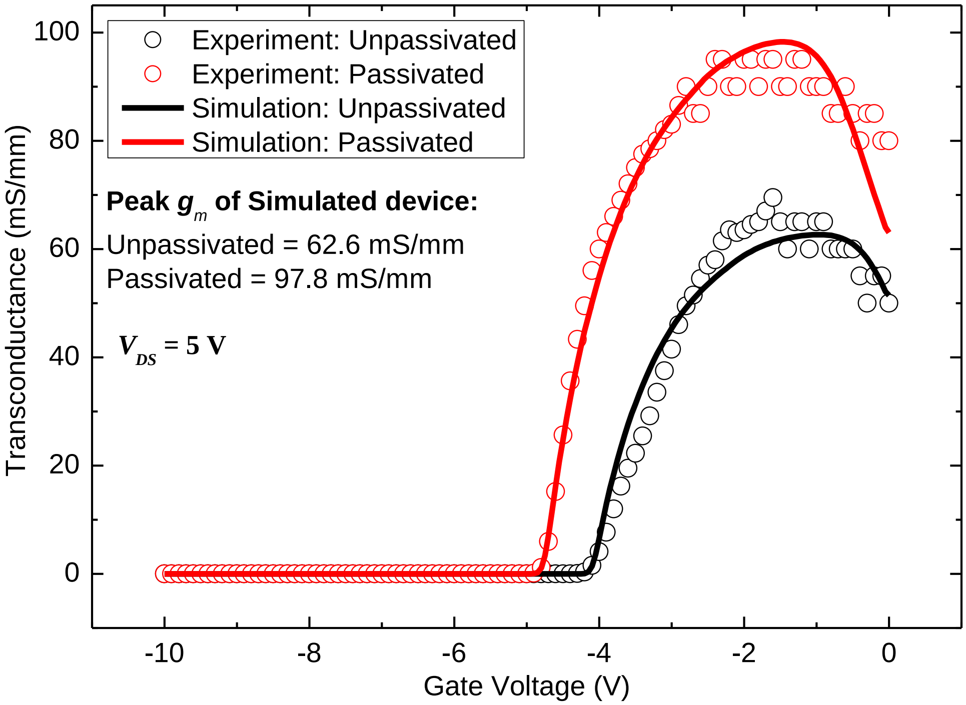

Figure 3.11: Extrinsic g_m-V_{GS} transfer characteristics of AlGaN/GaN MOS-HEMT devices for simulation and experimental [48] devices at V_{DS} = 5 V.

Figure 3.11 shows the extrinsic g_m-V_{GS} transfer characteristics of the AlGaN/GaN MOSHEMT devices for the unpassivated and passivated devices. Again, the superimposition of the simulation and experimental [48] data show close fit. The peak g_m values from the simulation are 62.6 and 97.8 mS/mm for the unpassivated and passivated device respectively. As discussed earlier, this increase in g_m also indicates the *in situ* passivation increased the mobility of the

AlGaN/GaN MOS-HEMT devices, which is believed to be due to reduction in carrier scattering.

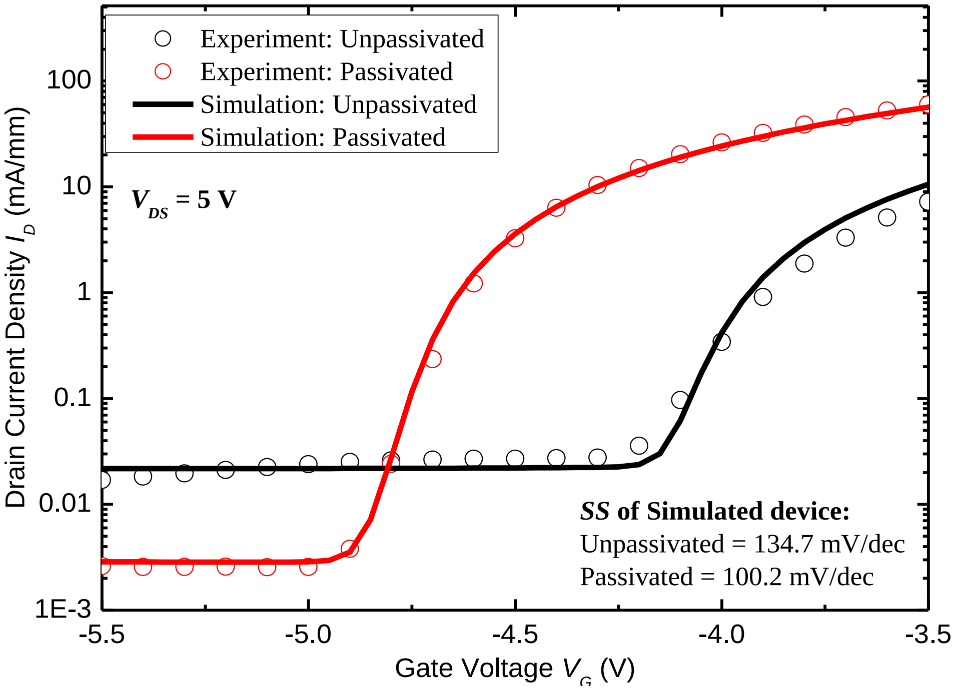

Figure 3.12: Log(I_D)-V_{GS} plot for AlGaN/GaN MOS-HEMT for simulated and experimental [48] devices.

Figure 3.12 shows the log(I_D)-V_{GS} plot for the unpassivated and passivated devices near the sub-threshold region. Again, the overlay between the experimental data and simulation data shows a good fitting. The extracted sub-threshold swings (SS) from the simulated devices are 134.7 and 100.2 mV/dec for the unpassivated and passivated devices.

$$D_{it} = \frac{C_{ox}}{q^2}\left(\frac{q(SS)}{ln(10)kT} - 1\right) - \frac{C_b}{q^2} \tag{3.17}$$

The decrease in *SS* can be related to reduction in interface state density using Equation 3.17. This is consistent with the simulation work which shows the reduction of 6.0×10^{12} cm^{-2} of acceptor-like trap density resulted in the decrease in *SS*.

Table 3.3: Comparison of V_{th}, n_s, peak g_m and *SS* for the unpassivated experimental [48] and simulated devices.

	Experiment	Simulation	Offset (%)
Threshold Voltage (V_{th}) (V)	-4.14	-4.12	~0.5
2DEG Sheet Carrier Concentration (n_s) (cm^{-2})	0.86×10^{13}	0.73×10^{13}	~15.1
Peak Transconductance (g_m) (mS/mm)	65	62.6	~3.7
Sub-threshold Swing (*SS*) (mV/dec)	> 150	134.7	10.4

Tables 3.3 compares the values of V_{th}, n_s, peak g_m and *SS* extracted from the unpassivated device in the experiment and simulation. The values of the V_{th} from the experiment and simulation are very close. The difference in the 2DEG n_s is around 15%, which is within the acceptable limit. The difference in the peak g_m is also small. The difference in the SS between the experiment and simulation is close to 10 %.

Table 3.4: Comparison of V_{th}, n_s, peak g_m and *SS* for the passivated experimental [48] and simulated devices.

	Experiment	Simulation	Offset (%)
Threshold Voltage (V_{th}) (V)	-4.77	-4.78	~0.2
2DEG Sheet Carrier Concentration (n_s) (cm^{-2})	1.04×10^{13}	0.87×10^{13}	~16.3
Peak Transconductance (g_m) (mS/mm)	95	97.8	~2.9
Sub-threshold Swing (*SS*) (mV/dec)	< 100	100.2	0.2

Tables 3.4 compares the values of V_{th}, n_s, peak g_m and SS extracted from the passivated device in the experiment and simulation. The difference in the V_{th} for the passivated devices is very small. As explained earlier, the difference in the 2DEG n_s is close to 15 % for the passivated devices as well. The peak g_m and SS show very close values to the experiment.

3.8 Conclusion

TCAD simulations were performed to fit with the experimental results to better understand the effect of surface passivation for AlGaN/GaN MOSHEMTs. The simulations results provided good fit for the experimental data. The simulation gave a plausible explanation that a decrease of 6×10^{12} cm^{-2} of acceptor-like trap density led to the V_{th} becoming more negative, an increase in I_{ON}, increase in g_m and decrease in SS.

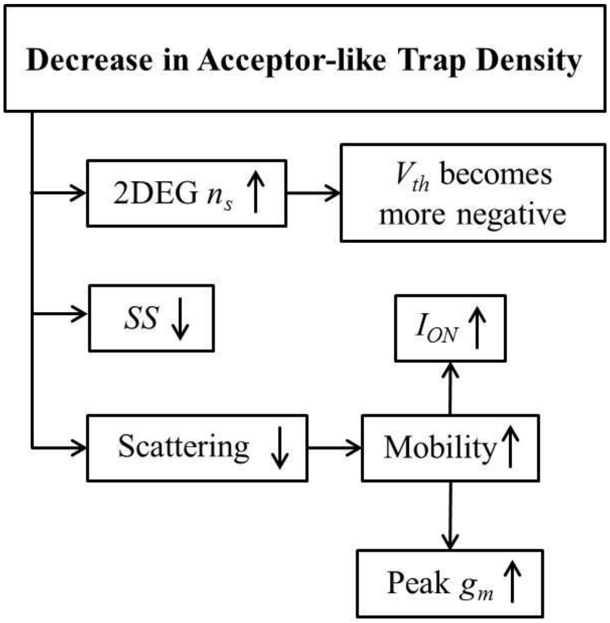

Figure 3.13: Flow chart of the effects observed in the simulation.

Figure 3.13 shows a flowchart summarizing the observations made during the simulation study. The decrease in the ionized acceptor-like trap density led to an increase in *2DEG* n_s. Thus, a larger negative gate bias is required to turn OFF the device. Thus, the V_{th} has become more negative. The decrease in *SS* is directly related to the reduction of the acceptor-like trap density. It is also believed that the decrease in the acceptor-like traps decreases carrier scattering. Thus, the mobility of the passivated device increased which led to the increase in g_m and an increase in I_{ON} for the same gate overdrive, compared to the unpassivated device.

Chapter 4: Trap Analysis of AlGaN/GaN MOSHEMTs using Gate Stress Induced Current Transient Methodology and TCAD Simulation

4.1 Introduction

AlGaN/GaN high electron mobility transistors (HEMTs) are very attractive for high power [42], high temperature [64], and high frequency [44] applications. By inserting a high quality dielectric between the gate electrode and the AlGaN layer, thus converting the device into a metal-oxide semiconductor high electron mobility transistor (MOSHEMT), the gate leakage current can be significantly reduced [65]. One of the factors that degrade the performance and reliability of GaN-based MOSHEMTs is electron trapping in the surface or interface states of the device, which is thought to be responsible for current collapse [29]-[32].

Drain current transient measurements are useful in studying the effects of carrier trapping due to its sensitivity to the entire region between the source and drain [37]. This method is in contrast to capacitance-based methods that only allow analysis mainly under the gate metal [66]. The two main transient measurement techniques are gate-lag and drain-lag measurements. The former and the latter analyse the drain current with respect to gate and drain voltage stresses, respectively. The drain-lag technique studies the impact of the substrate and buffer carrier trapping [67]-[85] and the gate-lag technique studies the impact of surface traps [68]-[88] on the drain current. In order to realize the full potential of the device, it is important to understand the nature and properties of these traps by directly studying the transient behavior of the traps.

In this Chapter, the AlGaN/GaN MOSHEMT was fabricated and we report a study of the properties of the Al_2O_3/AlGaN interface states using a combination of electrical measurements and numerical simulations. The current transient methodology was introduced by Joh *et al*. [35] for AlGaN/GaN HEMTs. This method was applied, for the first time, on a MOSHEMT, to obtain the detrapping time constants and energies of the trap states at the Al_2O_3/AlGaN interface using gate-stress induced transient current measurements. Device simulation and curve fitting were used to determine the type of interface states (i.e., donor or acceptor-like traps) and their densities. In this way, a more complete characterization of the traps at the Al_2O_3/AlGaN interface was achieved.

4.2 Experiment Details

4.2.1 Device Fabrication

The MOSHEMT devices were fabricated on $Al_{0.25}Ga_{0.75}N$(25 nm)/GaN on Si(111) substrate. The AlGaN/GaN heterostructure of Si substrate was purchased from NTT-AT (Japan). The active region was defined using Cl_2 chemistry based (BCl_3 = 20 sccm and Cl_2 = 10 sccm) inductive coupled plasma reactive ion etching (ICP-RIE). The power settings of ICP and RIE, during the etching, were

400 W and 200 W, respectively, with chamber pressure of 10 mTorr. Dilute hydrochloric acid (HCl) ($HCl:H_2O$ = 1:1) was used to remove the native oxide on the AlGaN surface prior to the dielectric deposition. 10 nm of Al_2O_3 layer was deposited as gate dielectric at 250 °C by atomic layer deposition (ALD) using $Al(CH_3)_3$ and H_2O precursors. This was followed by post deposition anneal (PDA) at 500 °C for 1 min. in N_2 ambient. Gate metal consisting of TaN (100 nm) was deposited using reactive sputtering with DC power of 450 W, RF power of 12 W, chamber pressure of 3 mTorr and N_2 flow rate of 5 sccm. The gate electrodes were patterned using Cl_2-based plasma etching using 450 W RF power, 200 W bias power, 100 sccm Cl_2 flow rate and chamber pressure of 10 Torr. Source and drain contact openings were etched through the Al_2O_3 layer using dilute hydrofluoric acid (HF) solution ($HF:H_2O$ = 1:100). Metal stacks consisting of Al(75 nm)-on-Ti(25 nm) were then deposited using electron beam evaporation, and annealed at 650 °C for 30 s in N_2 ambient to form the source and drain contacts. The device used in this study had a gate width of 500 μm and a gate length (L_G) of 10 μm. Gate-to-source (L_{GS}) and gate-to-drain (L_{GD}) distances were 9 μm each. Figure 4.1 shows the cross-sectional schematic of the AlGaN/GaN MOSHEMT fabricated for the detrapping transient current measurement.

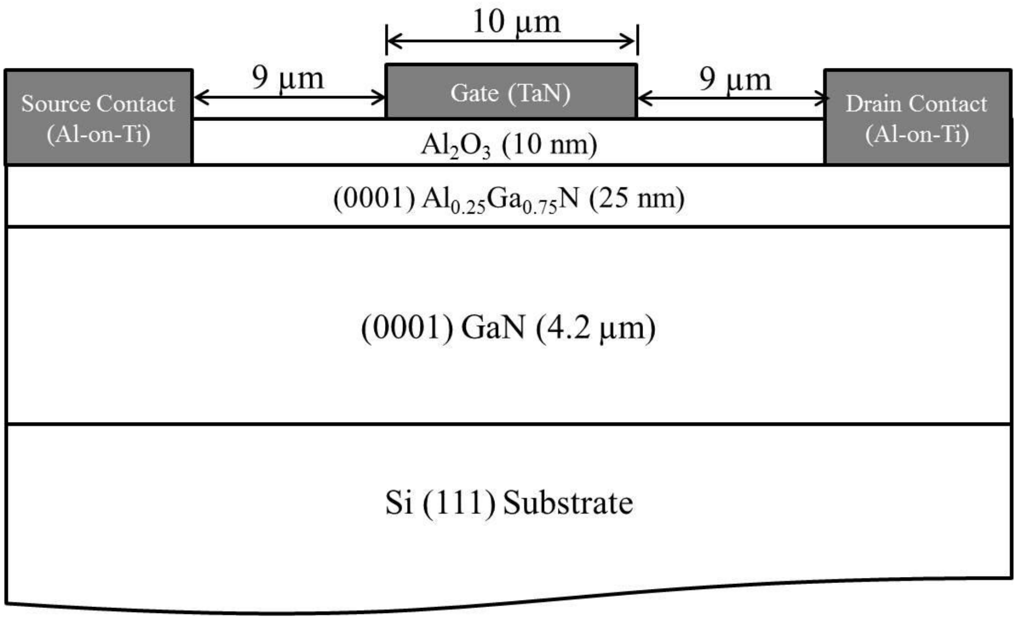

Figure 4.1: Cross-sectional schematic of AlGaN/GaN MOSHEMT fabricated for detrapping measurement.

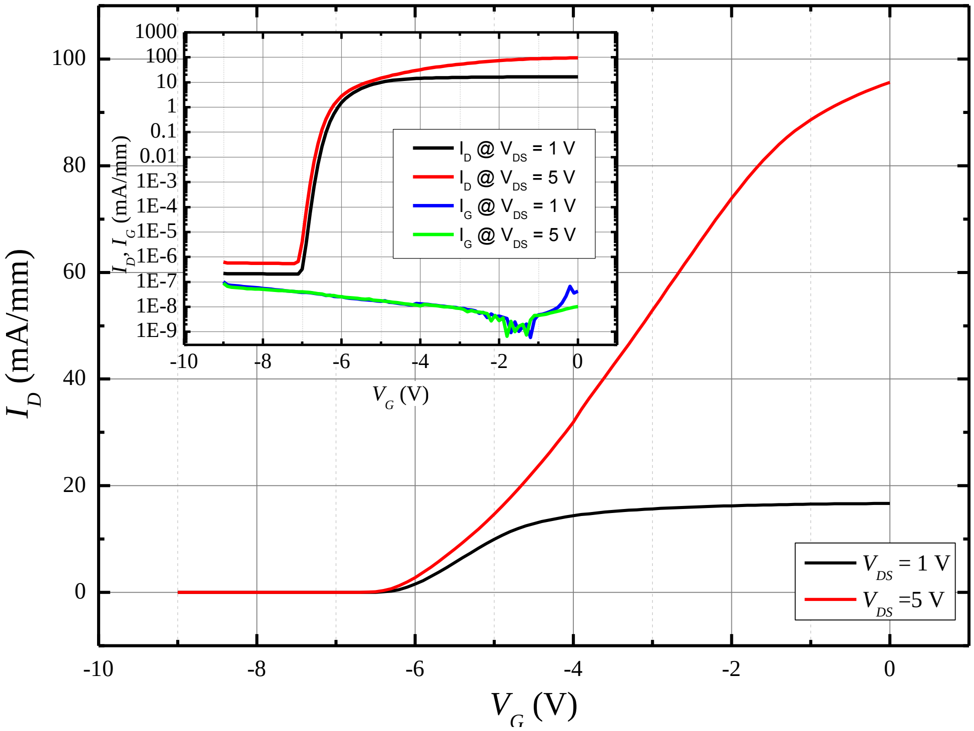

Figure 4.2: I_D-V_{GS} plot of AlGaN/GaN MOSHEMT in linear and I_D-V_{GS} and I_G-V_{GS} semi-log (inset) scales for V_{DS} = 1 V and 5 V at T = 300K.

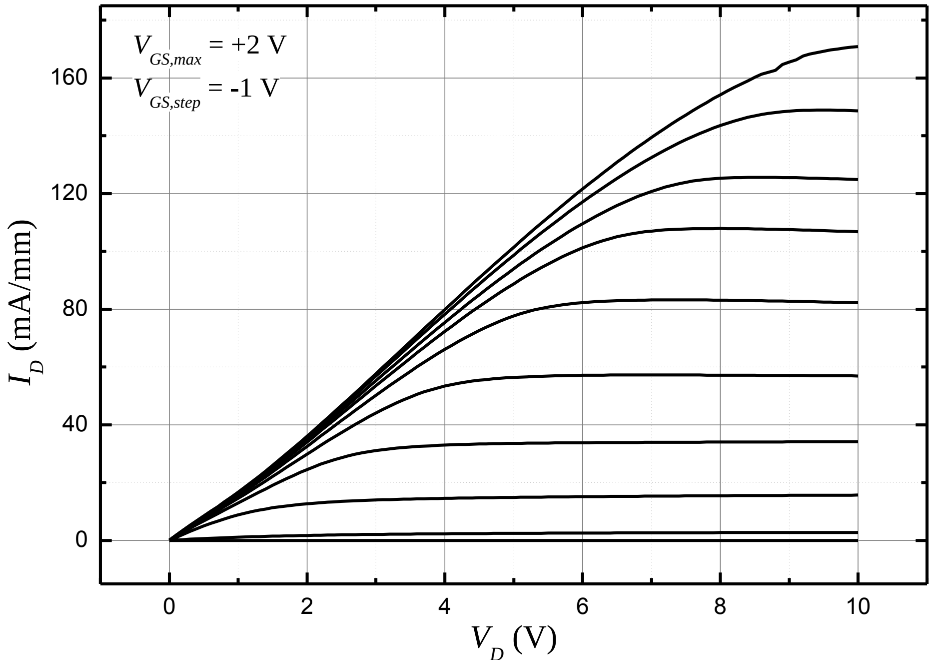

Figure 4.3: I_D-V_{DS} plot of AlGaN/GaN MOSHEMT with $V_{GS,max}$ = 2 V and $V_{GS,step}$ = -1 V at T = 300 K.

Figure 4.2 shows the measured I_D-V_{GS} characteristics of the AlGaN/GaN MOSHEMTs in linear and semi-log scales for V_{DS} = 1 V and 5 V. The DC characteristics of the device were threshold voltage (V_{th}) of -6.1 V, sub-threshold swing (SS) of 82.4 mV/dec, maximum transconductance ($g_{m,max}$) of 21.4 mS/mm, and drain current On/Off ratio of 1.7×10^8. Figure 4.3 shows the I_D-V_{DS} characteristics of the measured AlGaN/GaN MOSHEMTs. The maximum drain current ($I_{D,max}$) was 170 mA/mm at V_{GS} = 2 V.

4.2.2 Measurement Procedure

The transient currents were measured on the device using a Keithley 4200 Semiconductor Characterization System together with a MMR K-20 Programmable Temperature Controller. A gate bias stress of V_{GS} = -20 V and V_{DS}

= 0 V was applied for 50 s. After the gate stress was removed, V_{GS} and V_{DS} were switched to 1 V and 0.5 V, respectively. The transient drain current $i_D(t)$ as a function of time t was then measured in the device's linear regime so as to minimize trapping of electrons during the detrapping measurement. The gate stress transient measurements were performed at temperatures (T) ranging from 340 K to 370 K in the absence of light. Figure 4.4 shows the V_{GS} and V_{DS} biases applied to the device during the gate stressing and transient measurement.

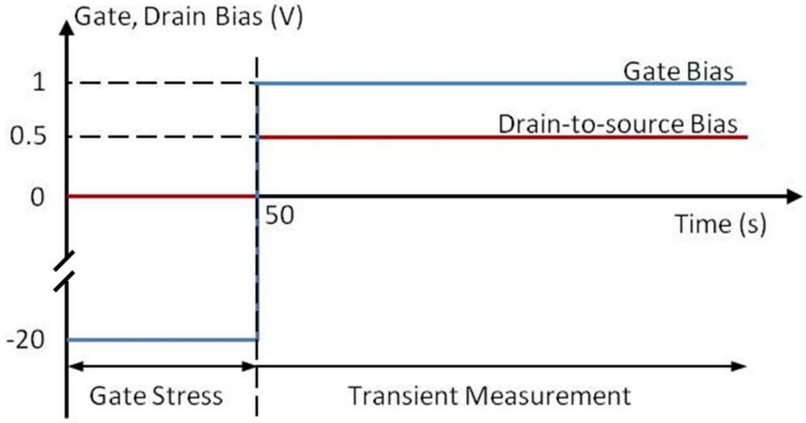

Figure 4.4: Gate and drain bias during gate stress and transient current measurement. The transient drain current was measured after 50 s drain stress.

4.2.3 Mathematical Fitting Model

The detrapping transient drain current $i_D(t)$ of the $Al_{0.25}Ga_{0.75}N/GaN$ MOSHEMT was studied using the methodology of Joh *et al*. [35]. This method takes into account that the measured $i_D(t)$ comprises of several independent detrapping processes, where electrons are emitted from the trap states. Emission of electrons from a particular trap state is assumed to have a unique time constant τ and is characterized by a decaying exponential function [69]-[90]. The sum of these exponential functions is used to fit the measured $i_D(t)$ in a least-mean-square fashion. The fitting equation was described by DasGupta *et al*. [70] as

$$\Delta i_{D,fitted}(t) = \sum_{i=1}^{n} \alpha_i \left(1 - e^{-t/\tau_i}\right) \tag{4.1}$$

$\Delta i_D(t)$ is defined as $i_D(t) - i_D(0)$, where $i_D(0)$ is the measured i_D at the onset of detrapping. The fitting parameter α_i represents the amplitude of each detrapping process, which is related to the density of electrons emitted from the trap state with time constant τ_i. The values of α_i's are extracted by minimizing $(\Delta i_{D,fitted} - \Delta i_{D,measured})^2$. In this study, forty-nine exponential functions ($n = 49$), with predefined τ_i's, distributed logarithmically in equal spacing, were used in the fitting equation. Good fittings of the $i_D(t)$ in both linear and semi-log scales were obtained, as shown in Figure 4.5.

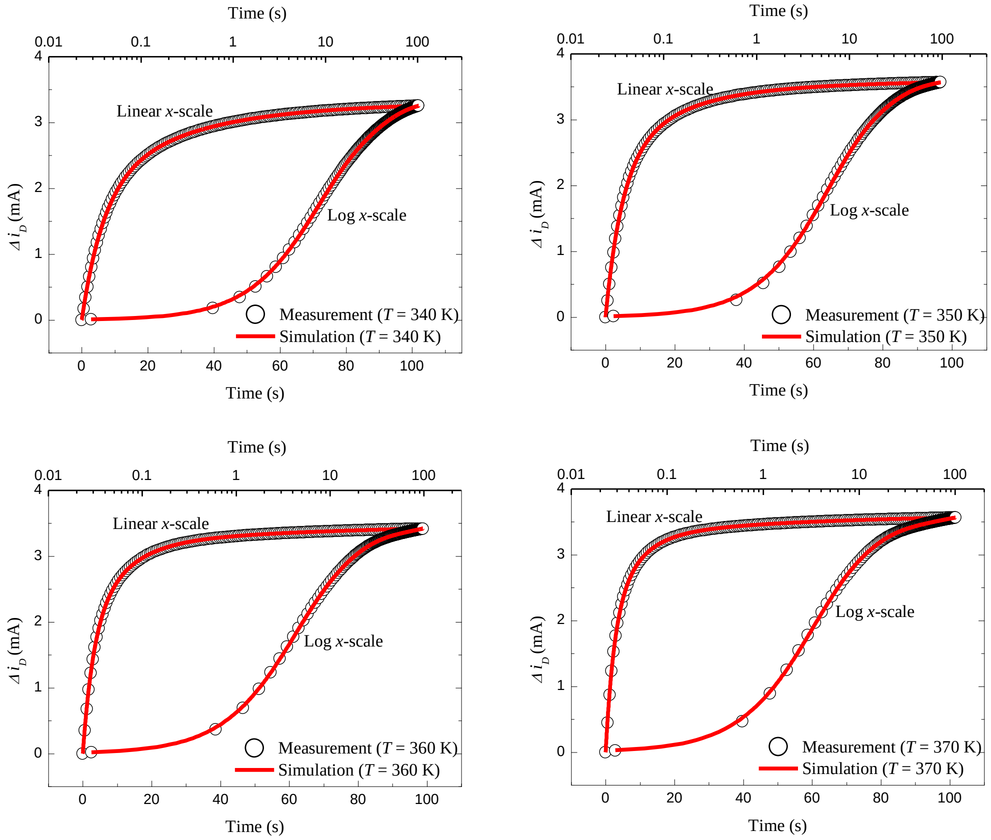

Figure 4.5: Transient drain current measurement and mathematical fitting at *T* = 340 - 370 K shows good fitting in linear and semi-log scales.

4.3 RESULTS AND DISCUSSION

4.3.1 Temperature-dependent Time Constant Spectra

The extracted α_i's were plotted with respect to τ_i's to form the time constant spectra as shown in Figure 4.6 for T = 340 K – 370 K. The time constant spectra clearly show two dominant detrapping processes (E1 and E2) at all the different temperatures. The reduction in the time constants of E1 and E2 with increasing temperature shows that E1 and E2 are sensitive to temperature.

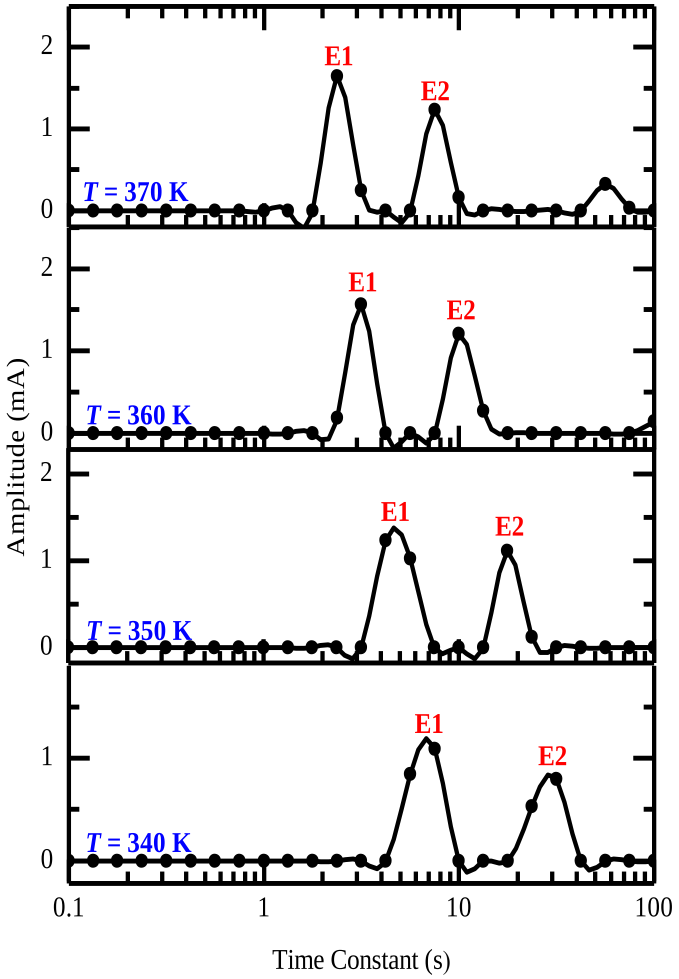

Figure 4.6: Temperature-dependent time constant spectra (α_i vs. τ_i) of the device measured at T = 340 K – 370 K. The two peaks (E1 and E2) represent dominant de-trapping processes in the device during the de-trapping measurements.

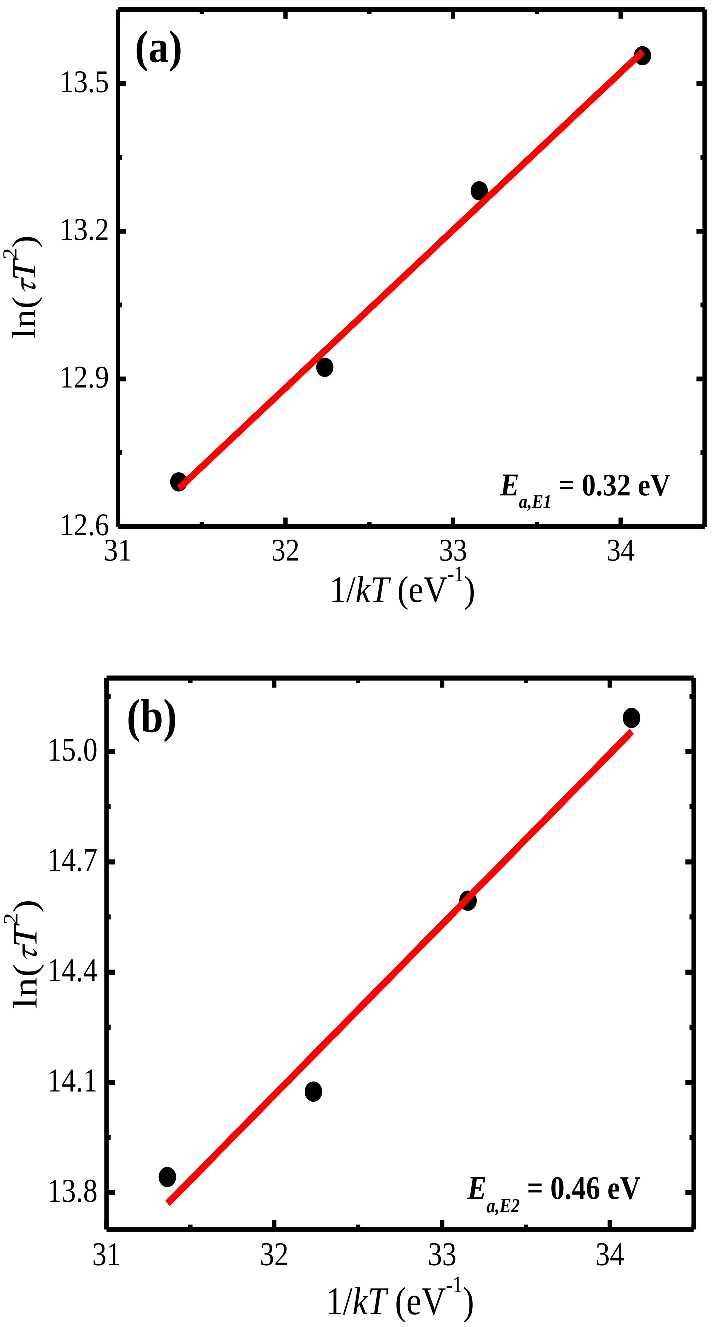

Figure 4.7: Linear fitting of the Arrhenius plots of the time constants of E1 and E2 show that (a) E1 has activation energy of 0.32 eV, and (b) E2 has activation energy of 0.46 eV.

$$\tau_e = \frac{exp\left((E_C - E_T)/kT\right)}{\gamma_n \sigma_n T^2} \tag{4.2}$$

The activation energies of E1 and E2 were extracted from linear fittings of Arrhenius plots using Equation 4.2, where τ_e is the emission time constant, E_C is the conduction band energy of AlGaN, E_T is the trap energy, k is Boltzmann's constant, T is temperature, σ_n is the electron capture cross-section and

$$\gamma_n = \left(\frac{v_{th}}{T^{1/2}}\right)\left(\frac{N_c}{T^{3/2}}\right) = 3.25 \times 10^{21}\left(\frac{m_n}{m_0}\right) cm^{-2}s^{-1}K^{-2}. \qquad (4.3)$$

where v_{th} is thermal velocity, N_c is the density of state, m_n is the electron density-of-states effective mass and m_0 is the free electron rest mass. Linear fittings of the Arrhenius plots, in Figure 4.7(a) and (b) show well defined activation energies (E_a) for E1 and E2 at 0.32 eV and 0.46 eV below the conduction band edge, E_C, of the AlGaN layer, respectively.

During the gate stress, V_{DS} was kept at 0 V. Therefore, it is expected that the trapping of electrons will be limited to the regions under and near the gate metal only. At V_{GS} = -20 V, the depletion region under the gate electrode will extend through the AlGaN layer and into the GaN layer. The gate leakage current through the Al_2O_3 and AlGaN layer can induce trapping of electrons in the AlGaN and GaN layers, as well as at the interfaces. When the gate bias V_{GS} is switched to +1 V, the depletion region will reduce instantaneously and the electrons trapped in the bulk materials will be emitted out of the trapped states quickly [71]. It is reported that the bulk traps are dominated by fast traps with fast time constants whereas extremely slow transients (τ > 1 s) are related to trapping in the surface states [72]-[94]. Since the time constants of E1 and E2 are 2.4 s and 7.5 s respectively at T = 370 K, E1 and E2 are highly likely to be present as interface trap states. In addition, the AlGaN surface could have been subjected to process related damages during the device fabrication [73] resulting in a higher density of defect states at the Al_2O_3/AlGaN interface compared to AlGaN/GaN interface. Therefore, we expect E1 and E2 to be predominantly located at the Al_2O_3/AlGaN interface.

Traps with ionization energies E_a close to 0.32 eV and 0.46 eV have been reported in the literature as donor-like traps in the AlGaN layer using other measurement techniques. Hasegawa *et al*. reported that the presence of deep donor-like traps, at E_a of 0.37 eV, is related to nitrogen vacancy in the AlGaN surface [60]. Ťapajna *et al*. proposed that traps, at the AlGaN subsurface, with E_a of 0.5 eV could have originated from oxygen related defect complexes [74].

4.3.2 Device Simulation using SILVACO ATLAS TCAD

In order to have a better understanding of the characteristics of the traps in the AlGaN/GaN MOSHEMT, device simulations using SILVACO ATLAS were carried out. Polarization-induced sheet charge densities at the Al_2O_3/AlGaN, AlGaN/GaN and GaN/substrate interface, were calculated using the theoretical calculations presented by O. Ambacher *et al*. [26] using equations (1.11 – 1.19 in Chapter 1) together with piezoelectric constants reported by Shimada *et al*. [75]. Figure 4.8 shows that the calculated polarization-induced sheet charge density in the Al_2O_3/AlGaN, AlGaN/GaN and GaN/substrate interface are -2.58×10^{13} cm^{-2}, 1.04×10^{13} cm^{-2} and 1.54×10^{13} cm^{-2}, respectively. Albrecht mobility [54] was used to model the electron mobility and Fowler-Nordheim tunnelling was used to model the OFF-state current in the simulation. Other models used in the simulation are discussed in Chapter 3 sub-section 3.5. Please refer to Appendix C for the code used in the simulation.

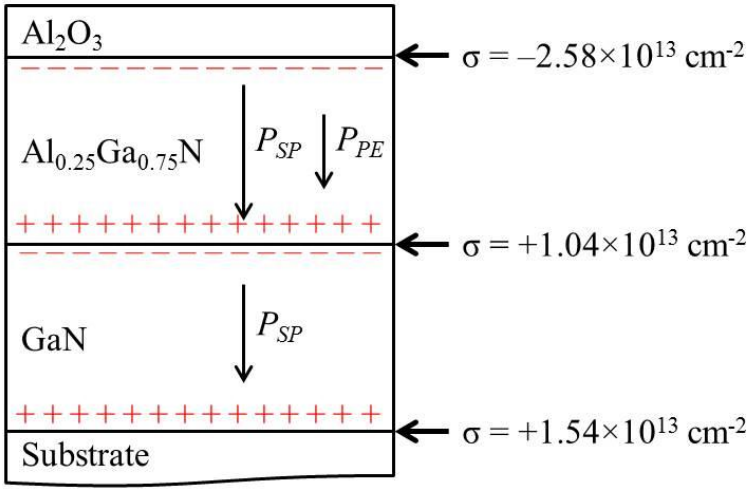

Figure 4.8: Calculated polarization-induced sheet charge densities at Al_2O_3/AlGaN, AlGaN/GaN and GaN/substrate interface were -2.58×10^{13} cm^{-2}, 1.04×10^{13} cm^{-2} and 1.54×10^{13} cm^{-2}, respectively.

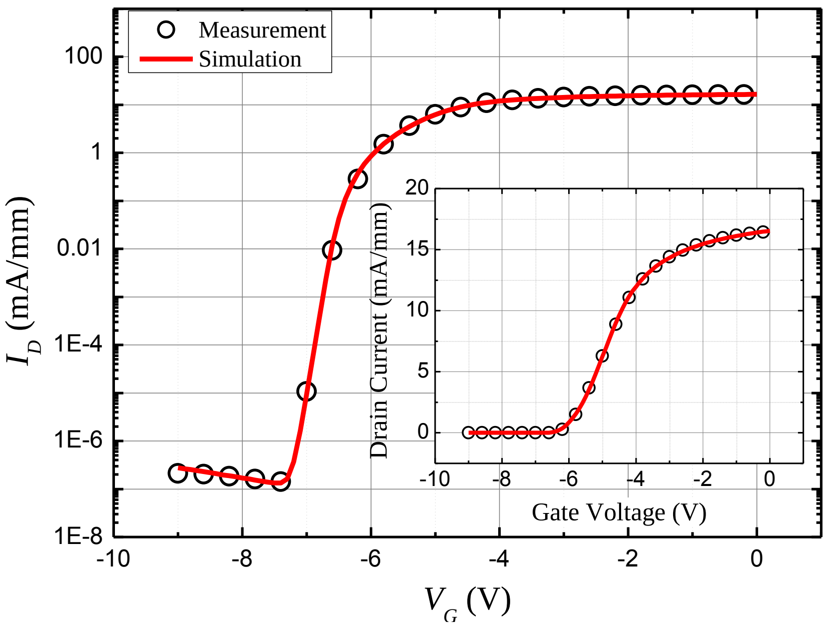

Figure 4.9: Simulation fittings of I_D-V_{GS} characteristics of the MOSHEMT at V_{DS} = 1 V measured at T = 370 K showing good fittings in semi-log and linear (inset) scales.

Trap energies and time constants of E1 and E2, obtained from sub-section 4.3.1, were used to define donor-like traps at the Al_2O_3/AlGaN interface. An example of simulation fitting of the measured I_D-V_{GS} characteristics for V_{DS} = 1 V at T = 370 K is shown in Figure 4.9. The densities of E1 and E2 were adjusted in the simulation to achieve good fitting to the measured I_D-V_{GS} data in both linear and semi-log scales. The donor-like trap densities of E1 and E2 used in the simulation fitting were 1.43×10^{13} cm^{-2} and 1.07×10^{13} cm^{-2} respectively. These values are reasonable since the density of surface states of AlGaN/GaN HEMTs greater than 1.5×10^{13} cm^{-2} were reported by others [34],[98].

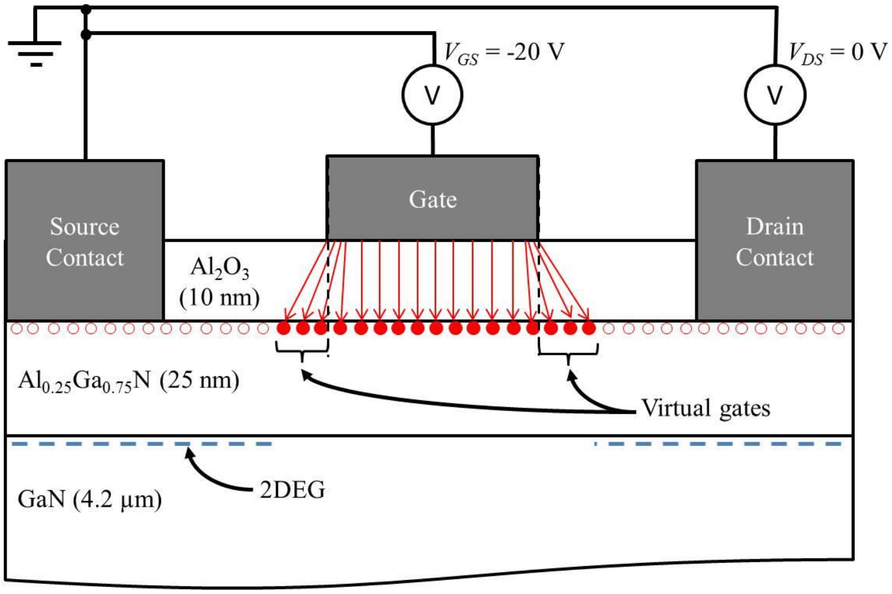

Figure 4.10: Cross-sectional schematic of the AlGaN/GaN MOSHEMT when the device was stressed at V_{GS} = -20 V and V_{DS} = 0 V. The red arrows show electrons from the gate electrode being captured by the trap states located at the Al_2O_3/AlGaN interface. The filled and empty red circles represent filled and empty trap states, respectively, at the Al_2O_3/GaN interface.

Figure 4.10 shows the cross-sectional schematic of the AlGaN/GaN MOSHEMT when the device was stressed at V_{GS} = -20 V and V_{DS} = 0 V. During this stress, the *2DEG* under the gate is depleted and the electrons from the gate leakage current can be captured at the trap states located at the Al_2O_3/AlGaN interface. This is shown using red arrows. The trapping of electrons in the L_{GS} and L_{GD} regions led to the formation of 'virtual gates', which affected the *2DEG* density at the AlGaN/GaN interface [29]. Since the drain and source were grounded, there was equal likelihood for the gate leakage current to flow towards the source and the drain. Therefore, the virtual gate should extend on both sides of the gate electrode [35]. Also, simulation study by Meneghesso *et al.* [76] showed the virtual gate to have a length of 2 µm. The filled and empty circles represent filled and empty trap states, respectively.

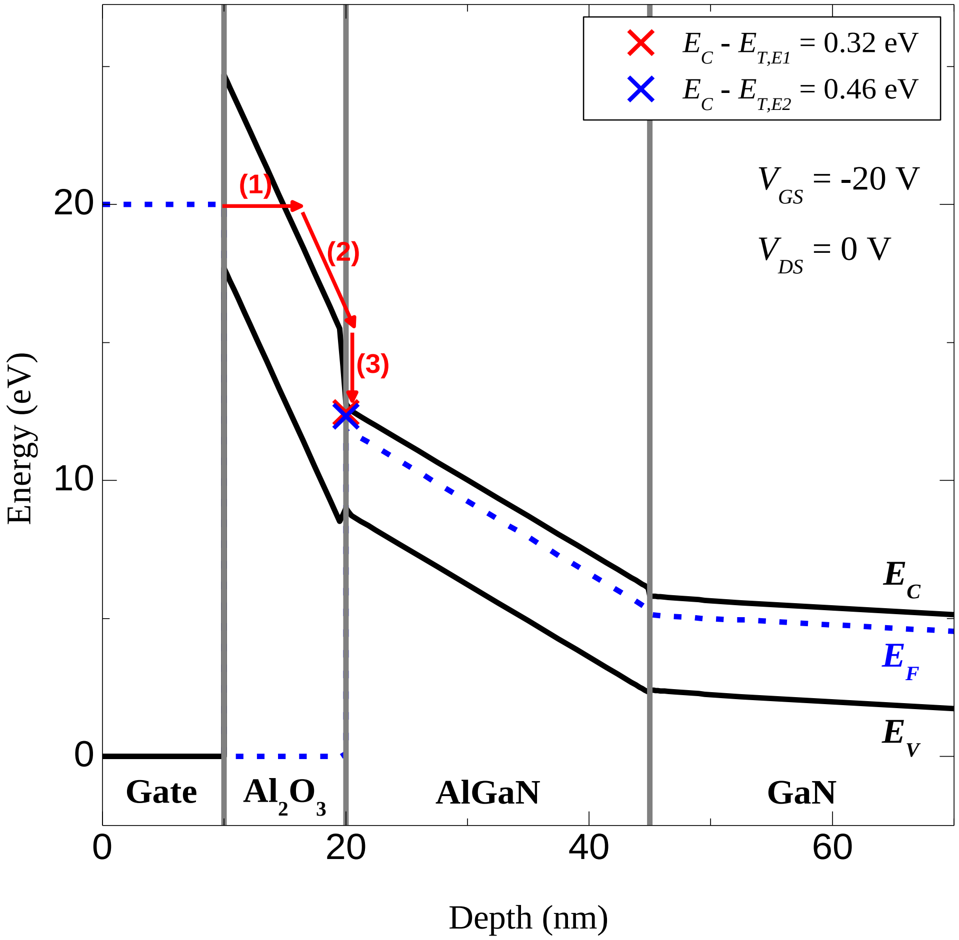

Figure 4.11: Energy band of AlGaN/GaN MOSHEMT, at T = 370 K, under the gate electrode at V_{GS} = -20 V and V_{DS} = 0 V, obtained from device simulation. The red colour arrows show a possible path of the gate injected current before getting captured by the trap states.

Figure 4.11 shows the energy band of the AlGaN/GaN MOSHEMT obtained from the device simulation, at T = 370 K under the gate electrode, when the device was stressed at V_{GS} = -20 V and V_{DS} = 0 V. From the device simulation, the vertical electric field through the Al_2O_3 layer is 9.8 MV/cm. At such high electric field, Fowler-Nordheim (FN) tunnelling is a dominant mechanism for gate leakage current [77]. The large negative gate bias caused the energy bands of

Al_2O_3 and AlGaN to be significantly pulled up. From the energy band point of view, it can be seen that the electrons will only need to tunnel through 5 nm of Al_2O_3 before reaching the conduction band of the Al_2O_3 and subsequently getting captured by the trap states in the Al_2O_3/AlGaN interface. The red arrows show a possible path taken by the gate electrons before getting captured. (1) Electrons from the gate electrode tunnel through the gate dielectric to reach the conduction band of Al_2O_3. (2) Electrons in the conduction band of Al_2O_3 'roll down' to the Al_2O_3/AlGaN interface due to the potential difference across the thickness of the Al_2O_3 layer. (3) Electrons are captured by the trap states at the Al_2O_3/AlGaN interface. The close proximity of the Fermi energy to the trap state energies, at the Al_2O_3/AlGaN interface, allows the capture states to be filled with electrons.

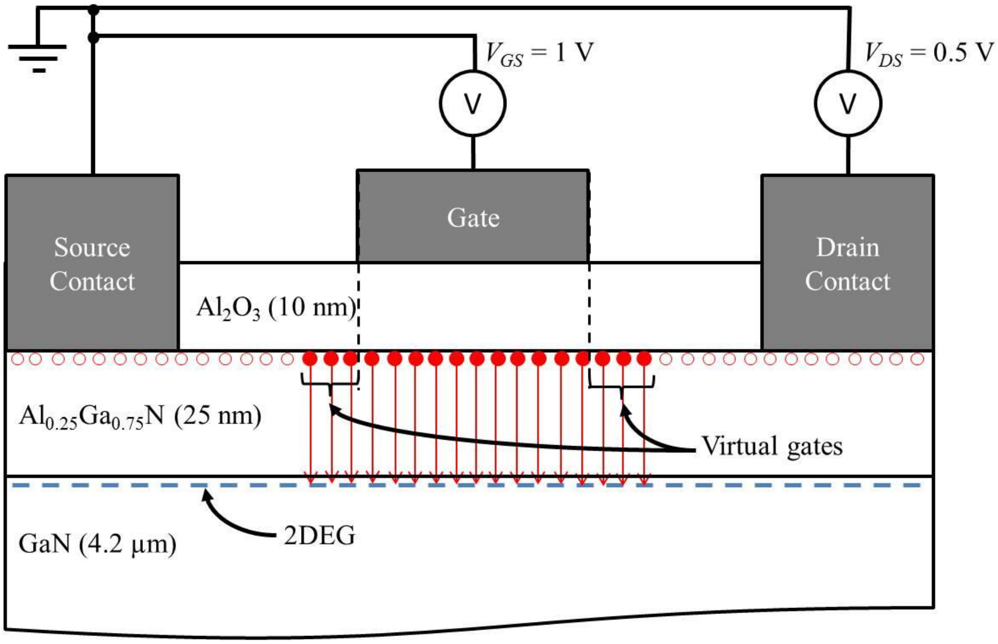

Figure 4.12: Cross-sectional schematic of the AlGaN/GaN MOSHEMT when the device was stressed at V_{GS} = 1 V and V_{DS} = 0.5 V. The red arrows show electrons being emitted from the trap states located at the Al_2O_3/AlGaN interface and flowing into the AlGaN/GaN interface.

Figure 4.12 shows the cross-sectional schematic of the AlGaN/GaN MOSHEMT during the transient measurement, at V_{GS} = 1 V and V_{DS} = 0.5 V. When V_{GS} is switched from -20 V to 1 V, the electrons captured at the trap states under the gate and 'virtual gates', at the Al_2O_3/AlGaN interface, begin to be thermally emitted (shown using filled red circles). This causes the *2DEG* to reappear at the AlGaN/GaN interface, under the gate and 'virtual gates'.

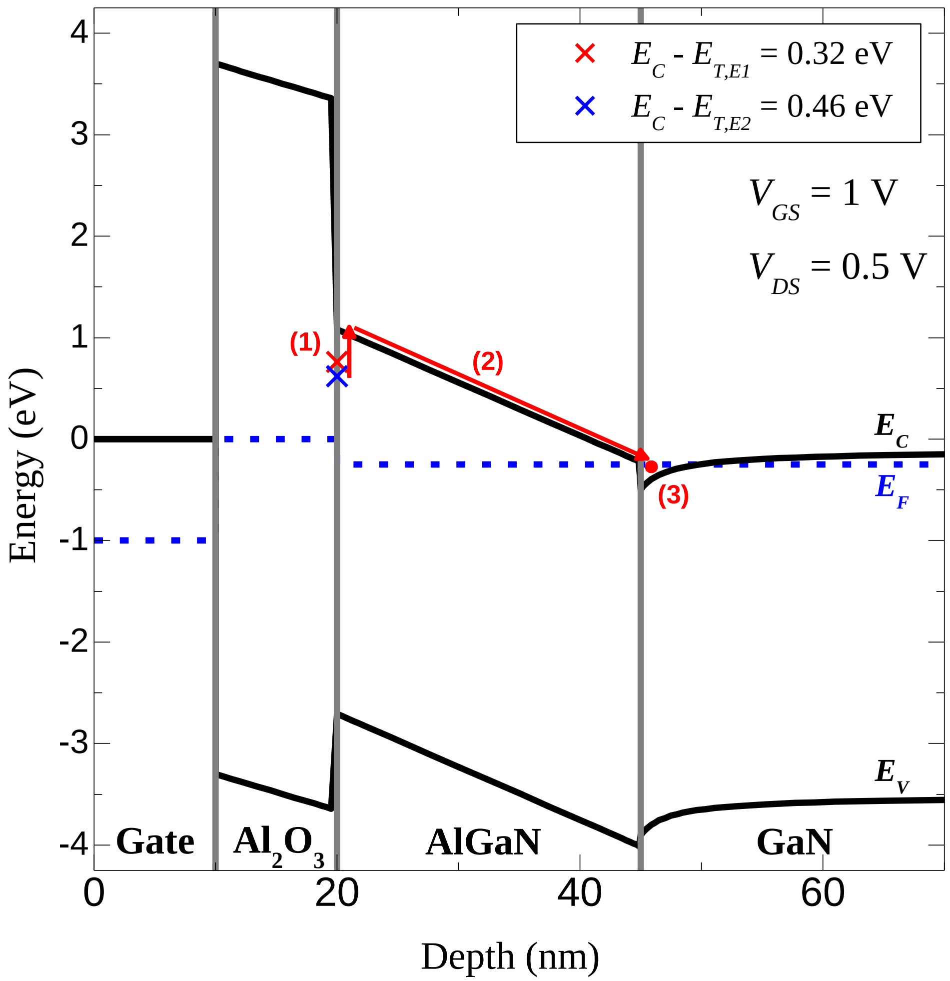

Figure 4.13: Energy band of AlGaN/GaN MOSHEMT under the gate electrode, at V_{GS} = 1 V and V_{DS} = 0.5 V, extracted from device simulation. The red colour arrows show a possible path taken by the electrons emitted from the trap states.

Figure 4.13 shows the energy band of the AlGaN/GaN MOSHEMT at T = 370 K, under the gate electrode, when the device was biased at V_{GS} = 1 V and V_{DS} = 0.5 V. When V_{GS} is switched from -20 V to 1 V, the captured electrons begin to be thermally emitted into AlGaN conduction band. The red arrows show a possible path of the thermally emitted electrons from the capture states: (1) Electrons emitted from trap states to the conduction band of the AlGaN layer, at the Al_2O_3/AlGaN interface; (2) Electrons at the AlGaN conduction band 'roll down' to the triangular quantum well at the AlGaN/GaN interface due to the potential difference across the thickness of the AlGaN layer; (3) Electrons are swept away laterally due to V_{DS}.

4.3.3 Temperature-dependent Time Constant Spectra with Modified Time Constants

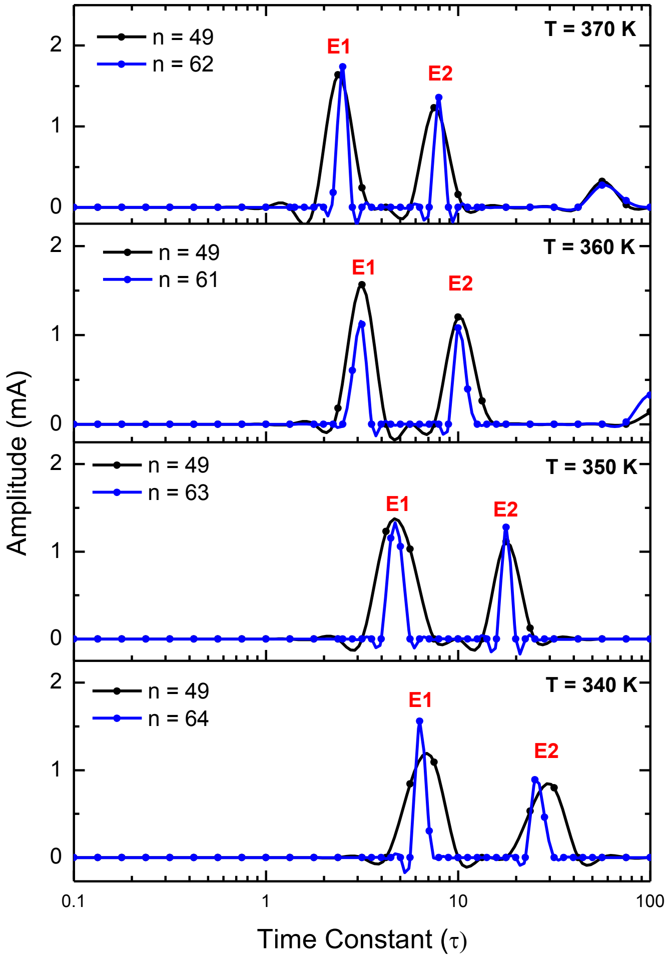

Figure 4.14: Comparison of temperature-dependent time constant spectra (α_i vs. τ_i) fittings with logarithmically equal time constant spacing and smaller spacing between time constants in the regions of the dominant peaks.

In order to check the accuracy of the fittings in obtaining the time constant spectra, it is recommended to use higher number of *n* in the regions of interest (eg. near the dominant peaks). Figure 4.14 shows the time constant spectra obtained using the fitting function with logarithmically equal time constant spacing (black line) and with higher density of time constant in the dominant peaks regions (blue line). As reported by Joh *et al.* [35], using higher number of n led to the widths of the dominant peaks to reduce. However, the time constants of the dominant peaks obtained from the new fittings did not change significantly with respect to the fittings obtained using n = 49. Therefore, n = 49 can be used to obtain accurate results and higher values of n is not necessary.

4.4 Conclusion

In summary, the detrapping characteristics at Al_2O_3/AlGaN interface of AlGaN/GaN MOSHEMT were investigated by combining gate-stress induced transient current measurement, mathematical fitting and device simulation. The measured drain current transient was measured and fitted using a fitting function. Good fittings were obtained in linear and semi-log scales. The α_i vs τ_i was used to plot the time constant spectra. Temperature dependent time constant spectra showed two dominant de-trapping processes (E1 and E2), which exhibited temperature dependence. The activation energies of E1 and E2 extracted from linear fittings of Arrhenius plots, gave 0.32 eV and 0.46 eV, respectively. The time constants of E1 and E2 at T = 370 K were 2.4 s and 7.5 s, respectively. Due to the slow time constant and the possibility of device fabrication-related process damages to the AlGaN surface, E1 and E2 are believed to be predominantly located at the Al_2O/AlGaN interface. Using device simulation, the two trap states were identified to be donor-like with densities of 1.43×10^{13} cm^{-2} and 1.07×10^{13} cm^{-2} respectively at T = 370 K.

Chapter 5: Characterization of Traps in AlGaN/GaN MOSHEMTs using Pulsed *I-V* Measurements and TCAD Device Simulation

5.1 Introduction

GaN-based metal oxide high electron mobility transistors (MOSHEMTs) are excellent candidates for high power [42], high frequency [44] and high temperature [64] applications with low gate leakage current [65]. Recent publication on AlGaN/GaN MOSHEMT has reported high drain current density larger than 1 A/mm [78]. However, a major issue that still needs to be addressed is the electron trapping process that leads to instability of threshold voltage (V_{th}) [31],[102], degradation of mobility [32], poor performance [79] and reliability [29],[104]-[105]. In particular, the drain current collapse, which is a recoverable process, that limits the performance of AlGaN/GaN HEMTs due to trapping charge in the AlGaN surface or GaN buffer layer [37],[106]. Investigation of drain current collapse using gate lag measurements revealed that the trapping of electrons at AlGaN surface states are responsible for the drain current collapse [80]. It was reported that the buildup of charges in the AlGaN surface due to lateral injection of electrons can cause the formation of parasitic virtual gates that degrades the device performance [81]-[109].

In order to understand the charge trapping process, it is important to employ pulsed current-voltage (*I*-*V*) measurement technique. This technique enables pulsing the drain and gate voltages of the AlGaN/GaN MOSHEMT at the same time. Therefore, the current collapse in the device can be quantitatively evaluated [82]-[110]. Compared to DC measurements, pulsed *I*-*V* measurements avoid the negative effects of joule-heating and transient effect of trapped charges [83]-[112].

In this chapter, the AlGaN/GaN MOSHEMT was fabricated and the impact of the traps located at the Al_2O_3/AlGaN interface was studied using a combination of pulsed *I*-*V* measurements with different quiescent gate bias ($V_{GS,Q}$) points and device simulation fittings using SILVACO ATLAS TCAD. By using this combination, the effect of electron trapping on the electrical characteristics of the device such as threshold voltage (V_{th}), two-dimensional electron gas (2DEG) sheet charge density (n_s), lateral electron mobility, density of ionized traps and nature of traps (i.e., donor-like or acceptor-like) at the Al_2O_3/AlGaN interface, can be well-investigated.

5.2 EXPERIMENT

5.2.1 Device Fabrication

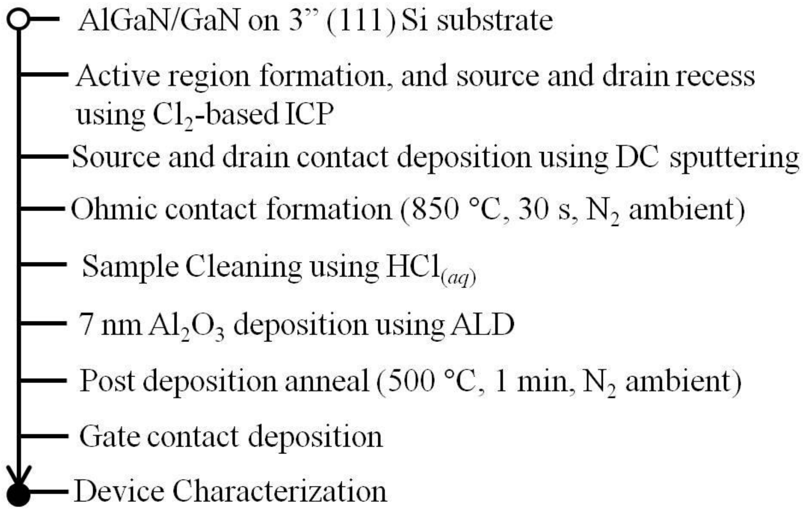

Figure 5.1: Summary of AlGaN/GaN MOSHEMT fabrication process flow for pulsed *I-V* measurement.

The Au-free $Al_{0.25}Ga_{0.75}N$(25 nm)/GaN MOSHEMTs were fabricated on Si(111) substrate. The AlGaN/GaN heterostructure of Si substrates were purchased from NTT-AT (Japan). The active region, and source and drain recess were defined using Cl_2 chemistry based (BCl_3 = 20 sccm and Cl_2 = 10 sccm) inductive coupled plasma reactive ion etching (ICP-RIE). During the etching, the power settings for the ICP and RIE were 400 W and 200 W, respectively, with chamber pressure of 10 mTorr. Metal stacks comprising of Ti(25 nm)\Al(100 nm)\Ni(30 nm)\W(50 nm) were successively deposited using DC sputtering at chamber pressure of 3.5 mTorr. The source and drain Ohmic contacts were formed by annealing at 850 °C for 30 s in N_2 ambient using rapid thermal annealing. The native oxide on the AlGaN surface was removed using dilute hydrochloric acid (HCl) ($HCl:H_2O$ = 1:1) solution prior to the dielectric deposition. A 7 nm thick Al_2O_3 layer was deposited as gate dielectric at 250 °C by atomic layer deposition (ALD), using $Al(CH_3)_3$ and H_2O as aluminum and oxygen precursors, respectively. This was followed by post deposition anneal (PDA) at 500 °C for 1 min. in N_2 ambient. The gate metal stack Ni(50 nm)\W(50 nm) was successively deposited using DC sputtering at chamber pressure of 3.5 mTorr. Dilute hydrofluoric acid (HF) solution ($HF:H_2O$ = 1:100) was used to remove the Al_2O_3 layer above the source and drain contacts. The device used in this study has a gate width of 70 µm, gate length (L_G) of 8 µm, and gate-to-source (L_{GS}) and gate-to drain (L_{GD}) separations of 10 µm each. Figure 5.1 shows the summary of the process flow and Figure 5.2 shows the cross-sectional schematic of the AlGaN/GaN MOSHEMT fabricated for the pulsed *I-V* measurement.

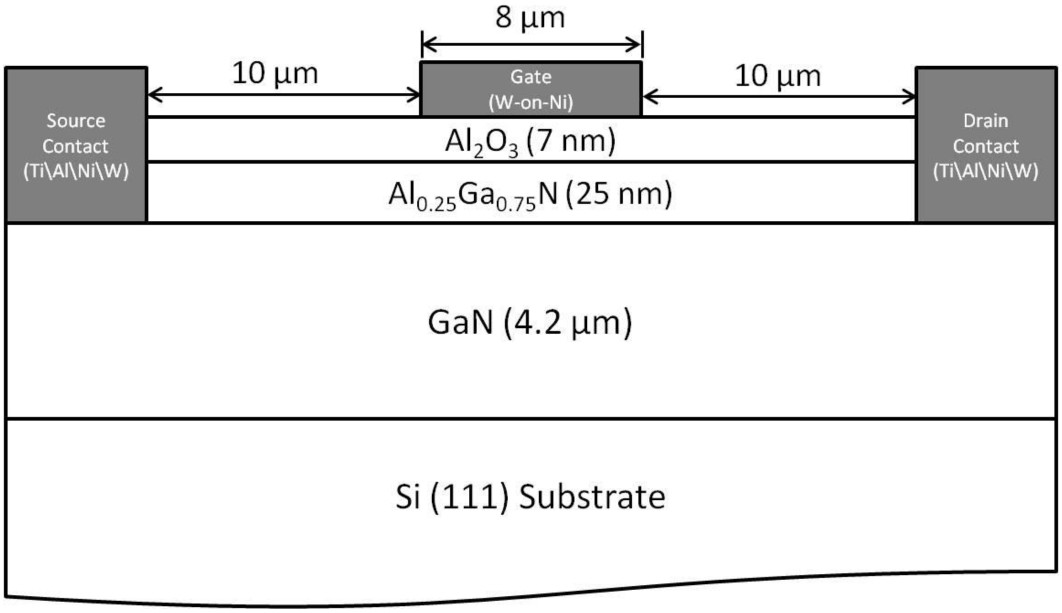

Figure 5.2: Cross-sectional schematic of the AlGaN/GaN MOSHEMT fabricated for pulsed *I-V* measurement.

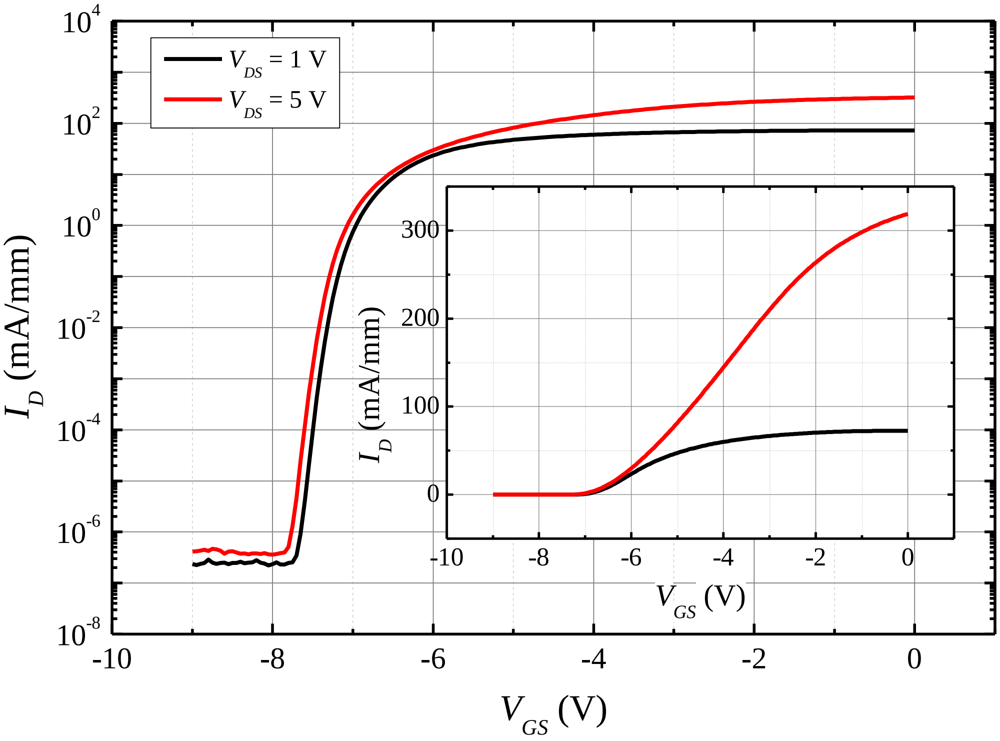

Figure 5.3: DC I_D-V_{GS} plot of AlGaN/GaN MOSHEMT in semi-log and linear (inset) scales for V_{DS} = 1 V and 5 V at T = 300 K.

Figure 5.3 shows the measured DC I_D-V_{GS} characteristics of the AlGaN/GaN MOSHEMT in the semi-log and linear (inset) scales for V_{DS} = 1 V and 5 V, at T = 300 K. The DC characteristics of the device were V_{th} of -6.4 V, sub-threshold swing (SS) of 73.3 mV/dec at V_{DS} = 5 V, maximum extrinsic transconductance ($g_{m,max}$) of 66.9 mS/mm at V_{DS} = 5 V and I_D On/Off ratio of 7.7×10^8 at V_{DS} = 5 V.

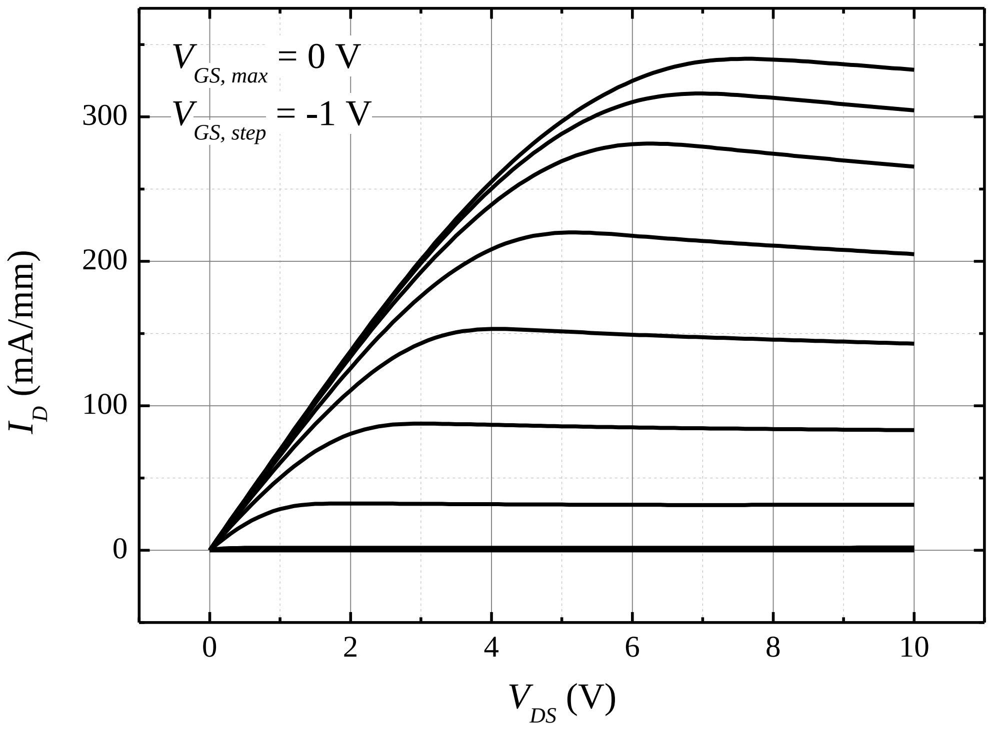

Figure 5.4: DC I_D-V_{DS} plot of AlGaN/GaN MOSHEMT with $V_{GS,max}$ = 0 V and $V_{GS,step}$ = -1 V, at T = 300 K.

Figure 5.4 shows the DC I_D-V_{DS} of the measured AlGaN/GaN MOSHEMT at T = 300 K. The maximum drain current ($I_{D,max}$) was 340 mA/mm at V_{GS} = 0 V. The contact resistance and specific contact resistivity approximated from the transmission line measurements (TLM) are 4.1 Ω.mm and 4.98×10^{-4} $\Omega.cm^2$ respectively.

Considering the large dimensions of the device such as L_G, L_{GS} and L_{GD}, the values of the DC characteristics are reasonable. B.-Y. Chou *et al*. [84] reported the DC characteristics of Al_2O_3/AlGaN/GaN MOSHEMT to have $g_{m,max}$ to be 140.6 mS/mm, *SS* to be 92.4 mV/decade and $I_{D,max}$ at V_{GS} = 0 V to be around 475 mA/mm [84].

5.2.2 Measurement Setup

The device was measured using a Keithley 4200 semiconductor characterization system with a pulse monitoring unit (4225-RPM). In the measurement setup, the pulse waveform's width, period, rise time and fall time were 0.5 μs, 50 μs, 0.1 μs and 0.1 μs, respectively. Figure 5.5 shows an example of a pulse waveform. The duty cycle of the pulse waveform was 1% in order to minimize the self-heating in the device [85] during the measurement.

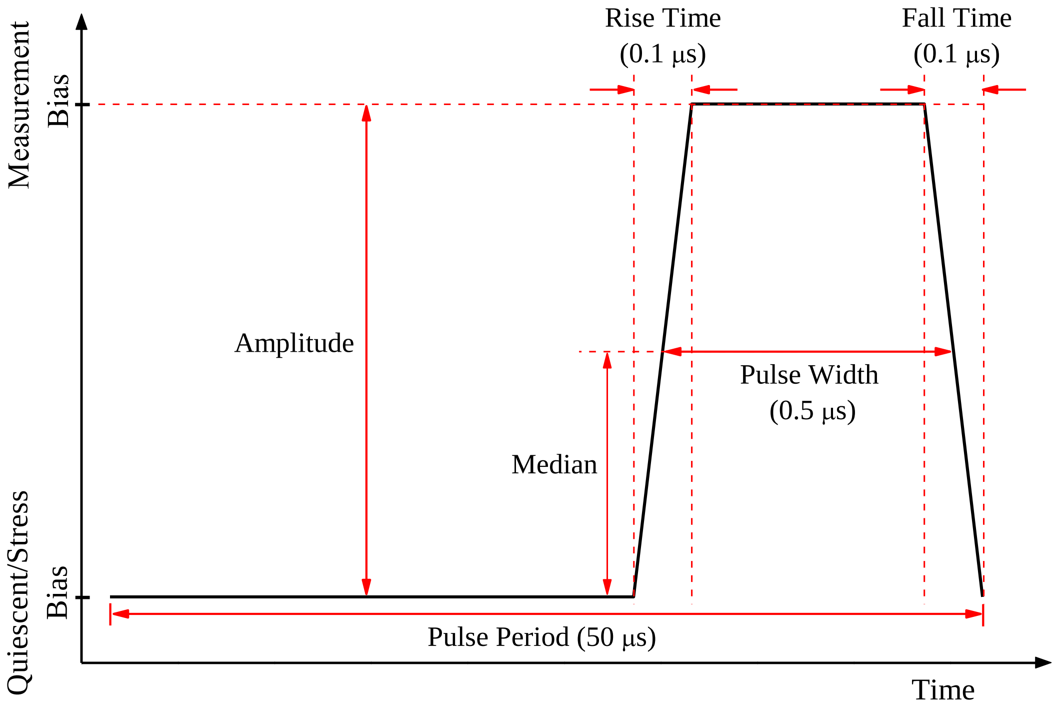

Figure 5.5: Example of pulse waveform (not drawn to scale) showing pulse period, pulse width, rise time and fall time were 50 μs, 0.5 μs, 0.1 μs and 0.1 μs, respectively. The duty cycle of the pulse waveform was 1 %.

The pulsed I_D-V_{GS} and I_D-V_{DS} curves (average of 10 consecutive current pulses) were measured at different gate-to-source quiescent bias ($V_{GS,Q}$) points, while the drain-to-source quiescent bias ($V_{DS,Q}$) point was kept constant. The quiescent biases refer to the stress biases applied to the device prior to the pulse width, where the drain current measurement is made. The pulsed I_D-V_{GS} measurements were measured from V_{GS} = -9 V to 0 V at V_{DS} = 1 V for ($V_{GS,Q}$, $V_{DS,Q}$) = (-15 V, 0 V), (0 V, 0 V), (0.5 V, 0 V), (1.0 V, 0 V) and (1.5 V, 0 V). Figure 5.6 shows an example of the V_{GS} and V_{DS} biases during the pulsed I_D-V_{GS} measurements. The different $V_{GS,Q}$ biases were applied to the device in order to induce trapping/detrapping of electrons under and near the gate metal, at the Al_2O_3/AlGaN interface. During the measurement, the stress was removed and instead the requisite gate bias was applied. However, since the measurement time was short, the captured electrons did not have sufficient time to be emitted from the traps. Hence, the effects of the trapped electrons on the *I-V* characteristic can be measured. Furthermore, since $V_{DS,Q}$ = 0 V during the stress, trapping of electrons in the channel region and in the buffer due to hot electrons can be neglected. Also, as mentioned earlier, during the pulsed *I-V* measurements, the negative effects of joule heating and transient trapping/detrapping during the measurement can be avoided, which are unavoidable in DC *I-V* measurements.

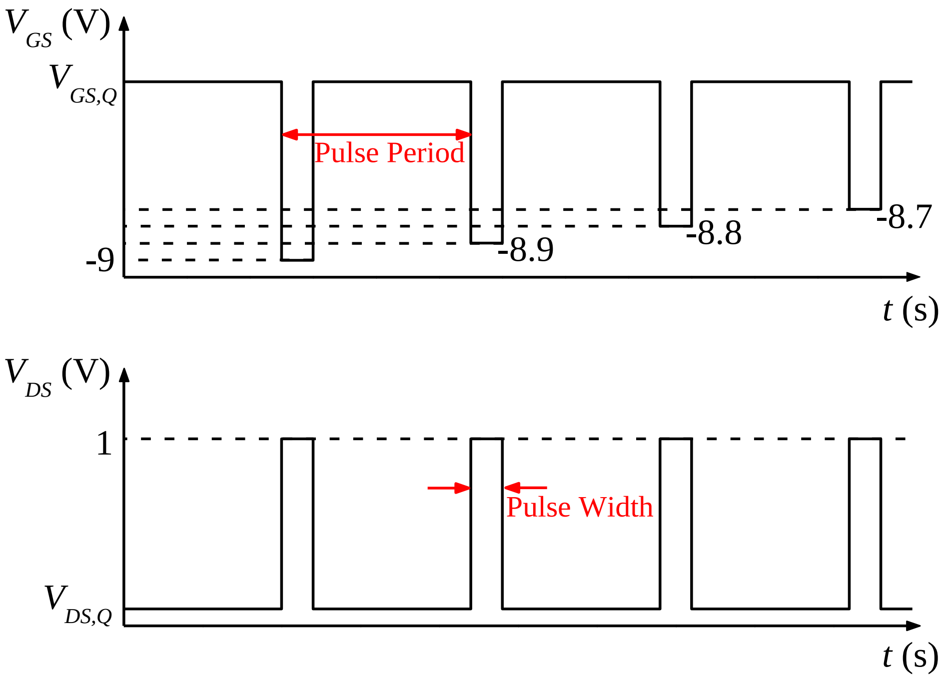

Figure 5.6: Example of V_{GS} (top) and V_{DS} (bottom) biases during I_D-V_{GS} measurement from V_{GS} = -9 to 0 V at V_{DS} = 1 V. The device was measured at various $V_{GS,Q}$ biases of -15 V, 0 V, 0.5 V, 1.0 V and 1.5 V, while $V_{DS,Q}$ was kept constant at 0 V.

5.3 RESULTS AND DISCUSSION

5.3.1 Pulsed *I-V* Characteristics

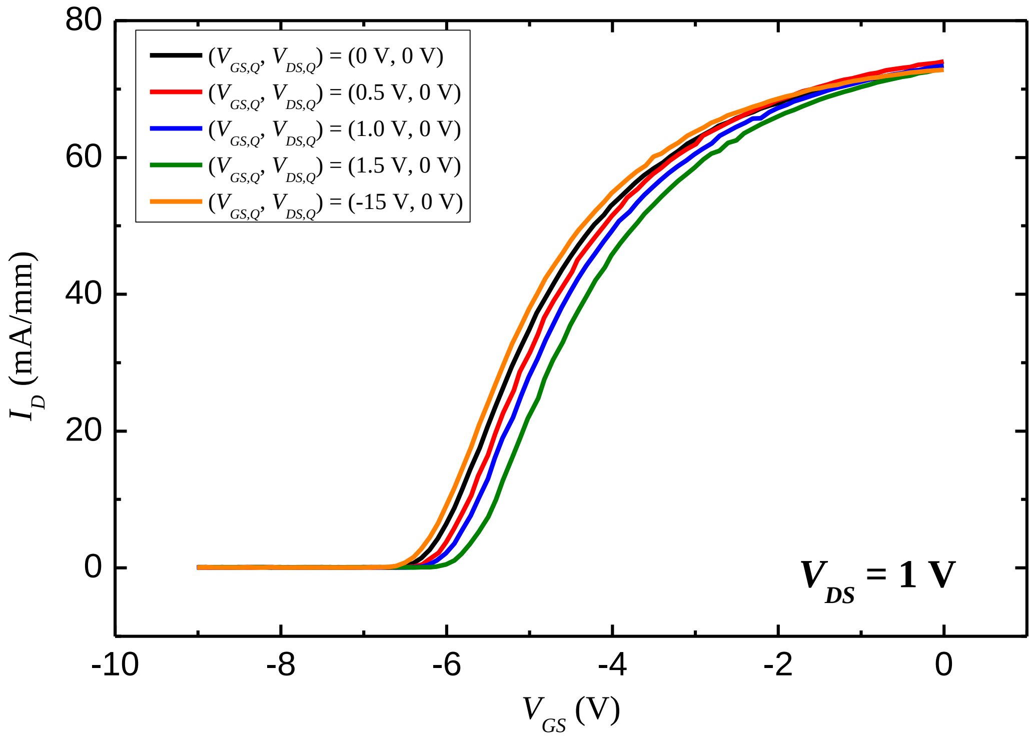

Figure 5.7: Pulsed I_D-V_{GS} measurement at V_{DS} = 1 V of AlGaN/GaN MOSHEMT for ($V_{GS,Q}$, $V_{DS,Q}$) = (-15 V, 0 V), (0 V, 0 V), (0.5 V, 0 V), (1.0 V, 0 V) and (1.5 V, 0 V).

Figure 5.7 shows the pulsed I_D-V_{GS} characteristics measured at V_{DS} = 1 V for ($V_{GS,Q}$, $V_{DS,Q}$) = (-15 V, 0 V), (0 V, 0 V), (0.5 V, 0 V), (1.0 V, 0V) and (1.5 V, 0 V). The shifts in V_{th} with respect to ($V_{GS,Q}$, $V_{DS,Q}$) = (0 V, 0 V) indicate that the $V_{GS,Q}$ biases were able to induce trapping/detrapping of electrons under the gate metal. Also, it can be inferred that the emission time constant of the trap must be slower than the pulse width (0.5 μs) in order to have an impact on the V_{th}. Pulsed I_D-V_{GS} measurement with ($V_{GS,Q}$, $V_{DS,Q}$) = (-15 V, 0 V) caused the V_{th} to shift to a more negative value, from -6.17 V to -6.27 V. This observation differs with literature studies on pulsed I-V measurements on AlGaN/GaN HEMTs, where a positive shift in the V_{th} was observed when a negative $V_{GS,Q}$ was applied to the devices. It is believed that the trapping of electrons at regions under and near the gate due to injection of electrons from the gate metal [86] caused the V_{th} to increase when negative $V_{GS,Q}$ was applied to the devices. In this experiment, 7 nm thick, high quality Al_2O_3 was deposited as gate dielectric using ALD. The low gate leakage current, in addition to the short $V_{GS,Q}$ bias duration of 49.4 µs $[Pulse\ Width - \frac{1}{2}(Rise\ Time + Fall\ time)]$ is believed to have low impact on the shift in V_{th}. Therefore, the phenomenon of positive shift of V_{th} due to negative $V_{GS,Q}$ bias was not observed on the sample.

On the other hand, positive $V_{GS,Q}$ causes the V_{th} to shift to increasingly positive values. The V_{th} of the device were -6.17 V, -6.03 V, -5.94 V and -5.77 V for ($V_{GS,Q}$, $V_{DS,Q}$) = (0 V, 0 V), (0.5 V, 0 V), (1.0 V, 0 V) and (1.5 V, 0 V), respectively.

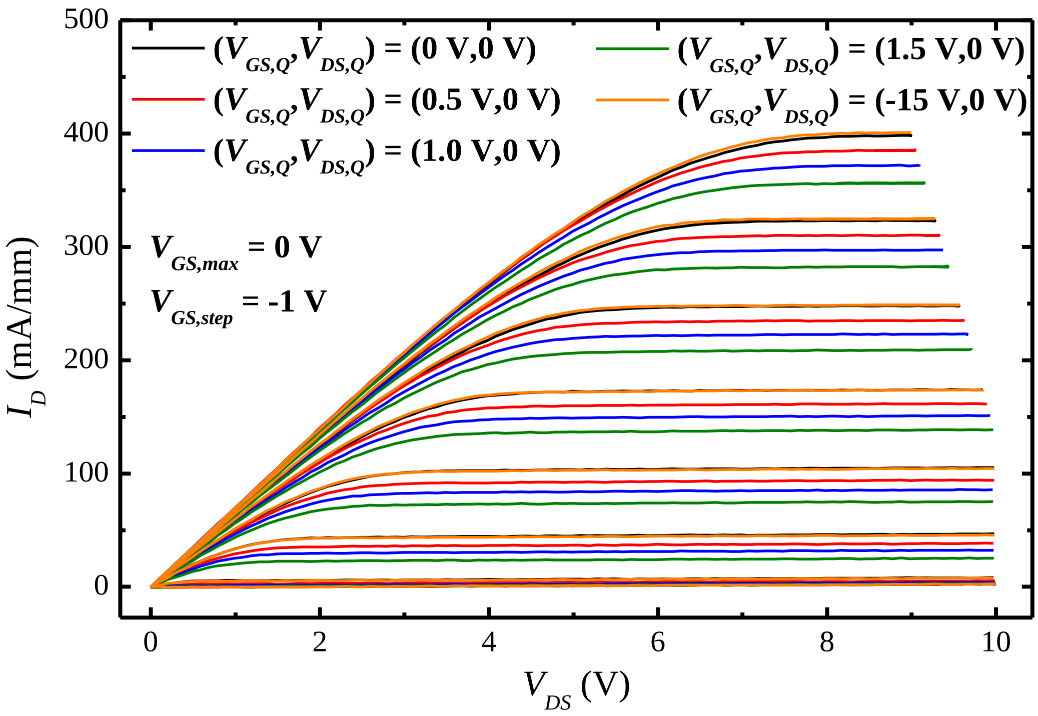

Figure 5.8: Pulsed I_D-V_{DS} measurements of AlGaN/GaN MOSHEMT for $V_{GS,max}$ = 0 V and $V_{GS,step}$ = -1 V at ($V_{GS,Q}$, $V_{DS,Q}$) = (-15 V, 0 V), (0 V, 0 V), (0.5 V, 0 V), (1.0 V, 0 V) and (1.5 V, 0 V).

Figure 5.8 shows the pulsed I_D-V_{DS} measurements for ($V_{GS,Q}$, $V_{DS,Q}$) = (-15 V, 0 V), (0 V, 0 V), (0.5 V, 0 V), (1.0 V, 0 V) and (1.5 V, 0 V). The pulsed I_D-V_{DS} measurements for ($V_{GS,Q}$, $V_{DS,Q}$) = (-15 V, 0 V) show slight increase in $I_{D,max}$ from 398 mA/mm to 400 mA/mm at V_{GS} = 0 V and negligible change in specific on-resistance (R_{ON}), compared to ($V_{GS,Q}$, $V_{DS,Q}$) = (0 V, 0 V). This observation also differs from studies in the literature, which reported decrease in maximum drain current and increase in dynamic on-resistance, also known as current collapse, in AlGaN/GaN HEMTs when negative $V_{GS,Q}$ was applied to the devices. Electrons trapping under and near the gate were reported to be a possible reason for the current collapse [87],[116]. Again, it is believed that the high quality gate dielectric and the short $V_{GS,Q}$ bias duration limited the gate leakage current during the negative $V_{GS,Q}$ bias. Thus, this observation was different from the ones reported in the literature for AlGaN/GaN HEMTs. Conversely, the $I_{D,max}$ for ($V_{GS,Q}$, $V_{DS,Q}$) = (0.5 V, 0 V), (1.0 V, 0V) and (1.5 V, 0 V) decreased to 385 mA/mm, 372 mA/mm and 356 mA/mm, respectively, from 398 mA/mm. The specific R_{ON} increased slightly from 4.04 mΩ.cm^2 to 4.07 mΩ.cm^2 for ($V_{GS,Q}$, $V_{DS,Q}$) = (1.5 V, 0 V) compared to (0 V, 0 V).

5.3.2 Device simulation using SILVACO ATLAS

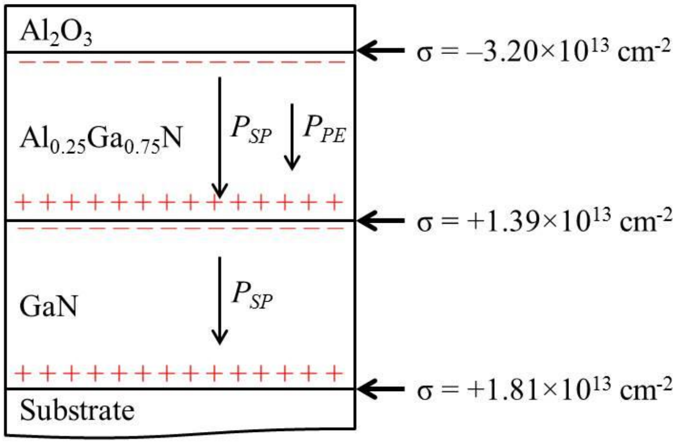

Figure 5.9: Polarization-induced sheet charge density (σ) at the Al_2O_3/AlGaN, AlGaN/GaN and GaN/substrate interfaces were -3.20 × 10^{13} cm^{-2}, 1.39 × 10^{13} cm^{-2} and 1.81 × 10^{13} cm^{-2}, respectively, from theoretical calculations [26].

In order to have a better understanding of the pulsed *I-V* results, two-dimensional TCAD simulations using SILVACO ATLAS were performed to fit the measured data. Owing to the short pulse width (0.5 µs) and $V_{DS,Q}$ = 0 V, we expect the joule heating in the device to be negligible during the measurement [88]. Therefore, the joule heating model in the simulations was not activated.

Polarization-induced sheet charge density (σ) at the Al_2O_3/AlGaN, AlGaN/GaN and GaN/substrate interfaces, obtained from theoretical calculations, using Equations (1.11 to 1.19 in Chapter 1) were -3.20×10^{13} cm^{-2}, 1.39×10^{13} cm^{-2} and 1.81×10^{13} cm^{-2}, respectively [26] (shown in Figure 5.9). In the simulation, Ibbetson *et al.*'s model of a single trap state at the AlGaN surface was adopted [34]. It is believed that the major traps that affect the device characteristics are predominantly located at the Al_2O_3/AlGaN interface due to the presence of dangling bonds and process related damages on the AlGaN surface [73]. Also, since the AlGaN/GaN heterostructure was grown *in situ* using metal-organic chemical vapor deposition (MOCVD) method, the bulk traps density is expected to be less dense compared to the Al_2O_3/AlGaN interface trap density. In the simulation, donor-like trap density with activation energy of 0.32 eV (from Chapter 4) and capture cross-section of 1×10^{-15} cm^2 [89] were used to define the trap states at Al_2O_3/AlGaN interface. The value of the trap energy used in the simulation is close to the trap energy reported by Hasegawa *et al.*, which was reported to have originated from nitrogen vacancies on the AlGaN surface [60]. Since $V_{DS,Q}$ = 0 V for all the pulsed *I-V* measurements, the extension of virtual gate by 2 µm on both sides of the gate metal was assumed [35],[99] (same as in Chapter 4). Lombardi mobility model was used to model the electron mobility in the simulation [90]-[120]. Other models used in the simulation were discussed in Chapter 3 sub-section 3.5. Please refer to the simulation codes in Appendix D – H.

5.3.2.1 Lombardi’s Constant Voltage and Temperature (CVT) Mobility Model

In Lombardi’s CVT model, the carrier mobility is approximated by a sum of three components using Matthissen’s rule [91]-[122]

$$\frac{1}{\mu} = \frac{1}{\mu_{ac}} + \frac{1}{\mu_b} + \frac{1}{\mu_{sr}} \tag{5.1}$$

where μ_{ac}, μ_b and μ_{sr} are the carrier mobility restricted by scattering with surface acoustic phonons, bulk carrier mobility and surface roughness scattering, respectively [90].

The first component (μ_{ac}) is the acoustic phonons related scattering that limits the surface mobility. The electron mobility for a nondegenerate surface and two-dimensional deformation potential theory of surface phonon scattering is given by [92]:

$$\mu_{ac} = \left(E_{\perp,},T\right) = B\frac{1}{E_\perp} + C\frac{1}{E_\perp^{1/3}}\frac{1}{T} \tag{5.2}$$

where *B* and *C* are fitting parameters, $E_\perp$ the electric field that is normal to the flow of current and T is the absolute temperature. *B* and *C* are fitting parameters defined as [93]-[129]

$$B = \frac{\hbar^3 \rho_{bulk} u_l^2}{m^* m_\mu Z_A^2}, \tag{5.3}$$

and

$$C = \frac{q\hbar^3 \rho_{bulk} u_l^2}{m^* m_\mu Z_A^2 k_B} \left(\frac{9\hbar^2}{4m^* q}\right)^{1/3} . \tag{5.4}$$

where q is the elementary charge, $\bar{h}$ is the Plank's constant, ρ_{bulk} is the bulk mass density, u_l is the velocity of sound, m^* is the effective mass, m_μ is the mobility mass, Z_A is the deformation potential, k_B is the Boltzmann's constant and T is the absolute temperature [91].

The second component (μ_b) is the bulk mobility related scattering due to optical/intervalley phonons. Stern *et al*. reported that the effective thickness of the inversion layer is dependent on the temperature [94]. The quantum-mechanical effects due to the electron confinement become less critical with increasing inversion layer effective thickness. Therefore, mobility of electron in the inversion layer becomes similar value to the bulk electron mobility, which is strongly dependent on several optical/intervalley scattering mechanisms at elevated temperature [95]. The bulk mobility can be described as

$$\mu_b(N,T) = \mu_0 + \frac{\mu_{max}(T)-\mu_0}{1+(N/C_r)^\alpha} - \frac{\mu_1}{1+(C_S/N)^\beta} , \tag{5.3}$$

where

$$\mu_{max}(T) = \mu_{max}\left(\frac{T}{300}\right)^{-\gamma} , \tag{5.4}$$

and *N* is the impurity density, μ_{max} is the Ohmic (pure lattice) electron mobility and *T* is the absolute temperature. The parameters μ_{max}, μ_0, C_r, α, μ_1, C_S, β and γ

can be determined from fitting to experimental data [96]-[129],[132]-[133]. The "min-max" behavior of μ_b can be obtained from the first two terms in Equation 5.3. The third term in Equation 5.3 accounts for decreasing μ_b at higher values of N [97]-[135].

The third component (μ_{sr}) is surface roughness related scattering. At high perpendicular electric field and low temperature, the surface mobility degradation is strongly dependent on the surface roughness scattering [98]-[139]. The electron mobility due to surface roughness scattering at high electric field can be described as

$$\mu_{sr}(E_\perp) = \frac{\delta}{E_\perp^2}\,. \tag{5.5}$$

where $E_\perp$ is the electric field normal to the flow of electrons and δ is a parameter to be extracted from fitting to measured data [96]-[129],[140].

5.3.3 Simulation results using SILVACO ATLAS TCAD

The simulated I_D-V_{GS} (line plots) in Figure 5.10 show good fittings with the measured data (scatter plot). In order to obtain the good fittings, only the density of the donor states at the Al_2O_3/AlGaN interface, under and near the gate, and electron mobility were adjusted in the simulation. From the simulation fittings, key parameters such as 2DEG sheet charge density (n_s) at the AlGaN/GaN interface, 2DEG lateral electron mobility and ionized trap density at the Al_2O_3/AlGaN interface were obtained and listed in Table 5.1.

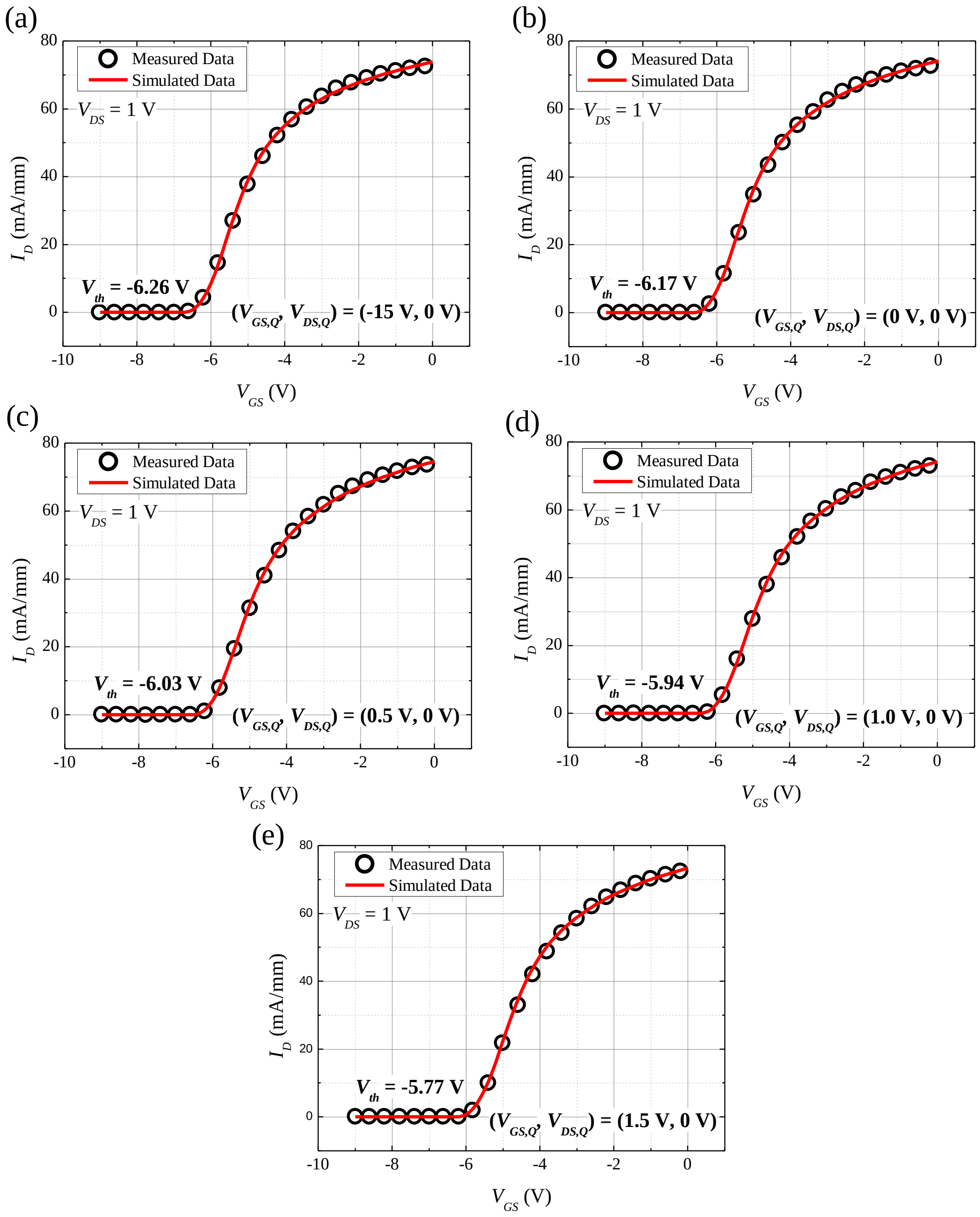

Figure 5.10: Simulation fittings (red line) superimposed on measured pulsed I_D-V_{GS} (scatter plots) for (a) ($V_{GS,Q}$, $V_{DS,Q}$) = (-15 V, 0 V), (b) ($V_{GS,Q}$, $V_{DS,Q}$) = (0 V, 0 V), (c) ($V_{GS,Q}$, $V_{DS,Q}$) = (0.5 V, 0 V), (d) ($V_{GS,Q}$, $V_{DS,Q}$) = (1.0 V, 0 V) and (e) ($V_{GS,Q}$, $V_{DS,Q}$) = (1.5 V, 0 V) shows good fittings.

Table 5.1: Key parameters obtained from the simulation fittings are lateral electron mobility of 2DEG at the AlGaN/GaN interface, 2DEG sheet charge density (n_s) at the AlGaN/GaN interface and ionized trap density at the Al_2O_3/AlGaN interface

$V_{GS,Q}$ (V)	V_{th} (V)	Mobility (cm^2/V.s)	n_s (cm^{-2})	Trap density (cm^{-2})
-15	-6.26	1599	9.60×10^{12}	3.15×10^{13}
0	-6.17	1627	9.39×10^{12}	3.05×10^{13}
0.5	-6.03	1664	9.22×10^{12}	2.97×10^{13}
1.0	-5.94	1690	9.00×10^{12}	2.86×10^{13}
1.5	-5.77	1735	8.66×10^{12}	2.70×10^{13}

The ionized trap density values obtained from the simulation are reasonable since the density of surface states of AlGaN/GaN could be greater than 1.5×10^{13} cm^{-2} [99]. The dynamics of the detrapping phenomenon is illustrated using the band diagram obtained from the simulations. Figure 5.11 shows the simulated conduction band (E_C), valance band (E_V) and electron quasi electron Fermi energy (E_{FN}) for $V_{GS,Q}$ = -15 V. At $V_{GS,Q}$ = -15 V, the partially ionized donor states at 0.32 eV below the AlGaN layer's E_C are able to emit their captured electrons [100] due to the strong electric field of 3.67 MV/cm, as obtained from the simulation. The emitted electrons are then swept into the 2DEG at the AlGaN/GaN interface due to the vertical electric field in the AlGaN layer. It is believed the increase in ionized donor-like trap density at the Al_2O_3/AlGaN interface due to the emission of electron led to an increased 2DEG density at the AlGaN/GaN interface (from 9.39×10^{12} cm^{-2} to 9.60×10^{12} cm^{-2}). Thus, the V_{th} shifts to a more negative value (from -6.17 V to -6.26 V) when the device was subjected from $V_{GS,Q}$ = 0 V to -15 V. An alternative explanation can be that the reduction in ionized acceptor-like trap density at the Al_2O_3/AlGaN interface due to the electron emission can also increase the 2DEG density [34] at the AlGaN/GaN interface and cause the V_{th} to become more negative.

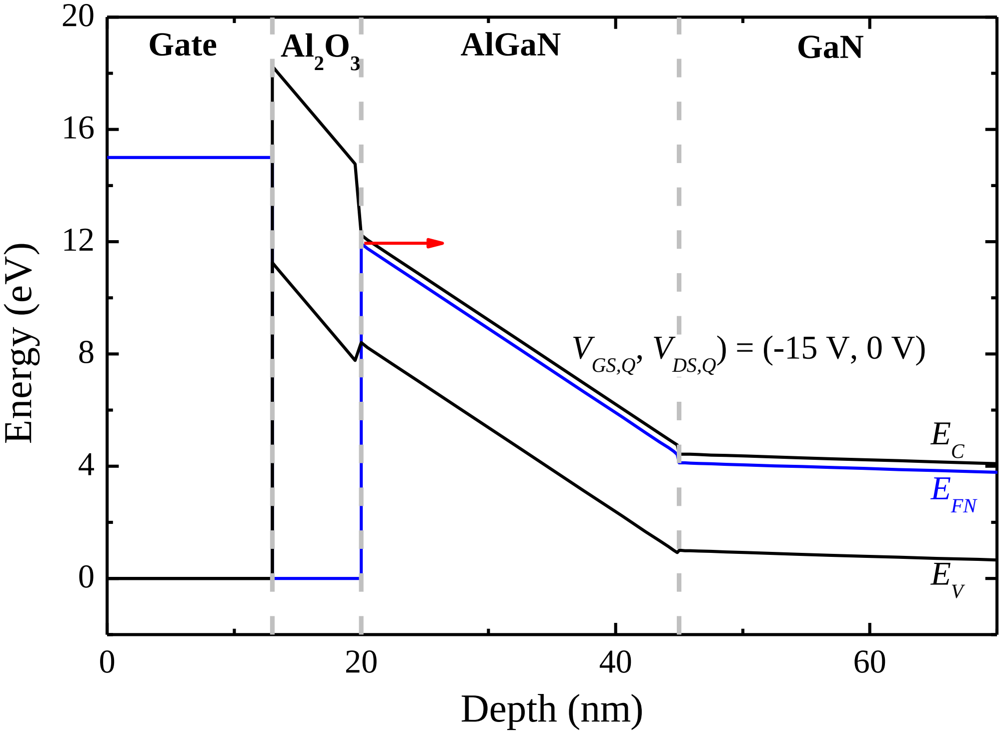

Figure 5.11: Energy band of AlGaN/GaN MOSHEMT at ($V_{GS,Q}$, $V_{DS,Q}$) = (-15 V, 0 V). The red arrow illustrates the emission of electrons from the interface states at the Al_2O_3/AlGaN interface.

The dynamics of the trapping phenomenon is illustrated using simulated band diagram shown in Figure 5.12. With increasing positive $V_{GS,Q}$ bias (from 0 V to 1.5 V), the E_C of the Al_2O_3 and AlGaN layers, near the gate metal, decreases. Due to lowering of the AlGaN barrier, there is higher probability for electrons in the 2DEG to be transferred to the interface states at the Al_2O_3/AlGaN interface. The trapping of the electrons neutralizes the donor states at the Al_2O_3/AlGaN interface [100]. Comparing the $V_{GS,Q}$ = 0 V and 1.5 V, the reduction in the ionized donor states at the Al_2O_3/AlGaN interface led to decrease in the 2DEG density at the AlGaN/GaN interface (from 9.39 × 10^{12} cm^{-2} to 8.66 × 10^{12} cm^{-2}) and increase in V_{th} (from -6.17 V to -5.77 V). Conversely, it is also possible for the positive $V_{GS,Q}$ biases to cause trapping of electrons in acceptor states at the Al_2O_3/AlGaN interface. This can also lead to reduction in 2DEG density and increase in V_{th}.

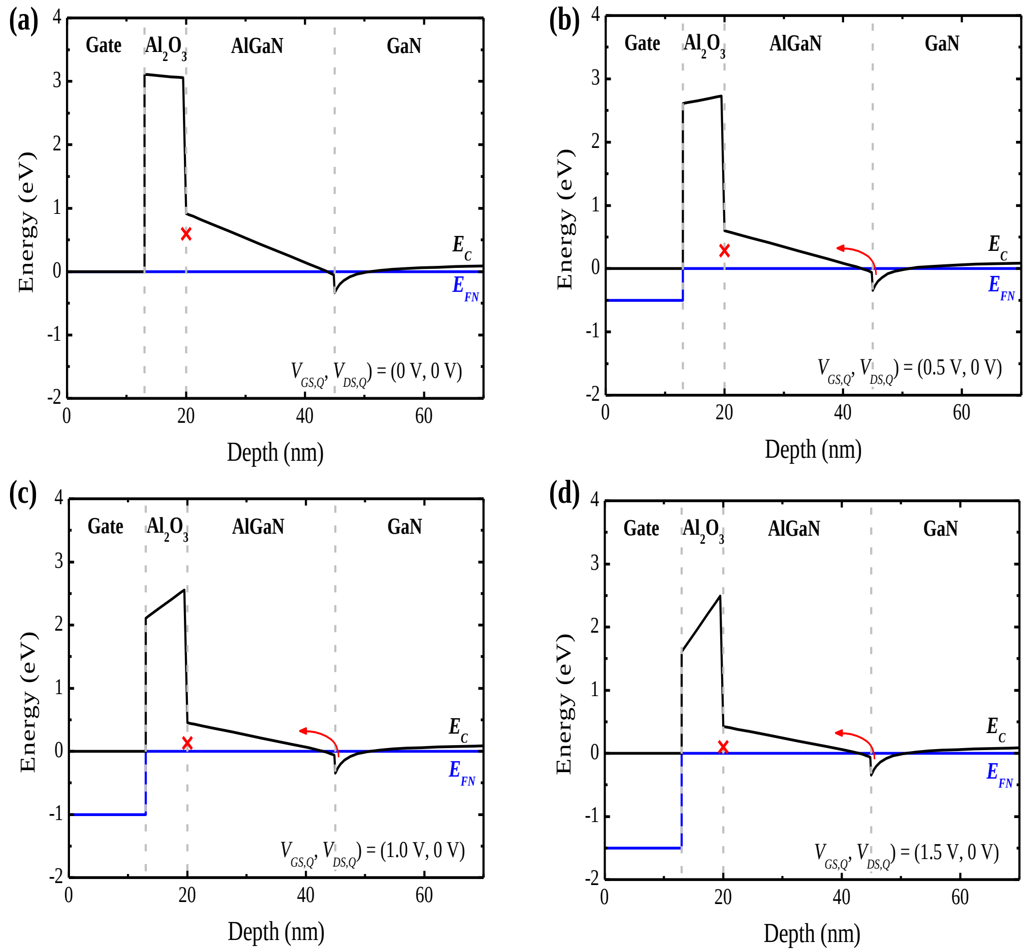

Figure 5.12: Energy band of AlGaN/GaN MOSHEMT for (a) ($V_{GS,Q}$, $V_{DS,Q}$) = (0 V, 0 V), (b) ($V_{GS,Q}$, $V_{DS,Q}$) = (0.5 V, 0 V), (c) ($V_{GS,Q}$, $V_{DS,Q}$) = (1.0 V, 0 V) and (d) ($V_{GS,Q}$, $V_{DS,Q}$) = (1.5 V, 0 V). E_C of the Al_2O_3 and AlGaN, near the gate metal, decreases with increasing $V_{GS,Q}$. The red arrow depicts the transfer of electrons from the 2DEG to the Al_2O_3/AlGaN interface. The red cross shows the trap energy level at $E_C - E_C$ = 0.32 eV.

The simulation fittings show that the lateral electron mobility in the 2DEG decreased from 1627 $cm^2V^{-1}s^{-1}$ to 1599 $cm^2V^{-1}s^{-1}$ when the device was subjected to $V_{GS,Q}$ = -15 V with respect to $V_{GS,Q}$ = 0 V. It is believed that the increase in positively charged donor states at the Al_2O_3/AlGaN interface caused scattering of electrons in the 2DEG. This led to the decrease in electron mobility. On the other hand, the lateral electron mobility increased from 1627 $cm^2V^{-1}s^{-1}$ to 1735 $cm^2V^{-1}s^{-1}$ when the device was subjected to $V_{GS,Q}$ = 1.5 V compared to $V_{GS,Q}$ = 0 V. It is believed that the reduction of positively charged donor states at the Al_2O_3/AlGaN interface, due to the electron trapping, reduced the electron scattering in the 2DEG. Thus, the electron mobility increased. This mechanism of impact on the 2DEG mobility due to trapping/detrapping of electrons at the AlGaN surface is possible since Liu *et al*. has also reported that a change in the density of ionized states on the AlGaN surface can affect the 2DEG mobility [48].

It was mentioned earlier that the shift in V_{th} could also be due to the trapping of electrons in acceptor-like states at the Al_2O_3/AlGaN interface [101]. If the positive $V_{GS,Q}$ biases caused trapping of electrons in acceptor states at the Al_2O_3/AlGaN interface, the increase in negative charge should increase the electron scattering. Thus, the electron mobility in the 2DEG will be reduced. Similarly, if the negative $V_{GS,Q}$ bias causes emission of electrons from ionized acceptor states, the 2DEG mobility should have increased due to decrease in negatively charged trap states. Therefore, it is highly plausible that the active trap states during the pulsed *I-V* measurements displayed donor-like characteristics instead of acceptor-like characteristics.

5.4 Conclusion

In summary, the characterization of traps in the Al_2O_3/AlGaN interface of AlGaN/GaN MIS-HEMT were investigated by performing pulsed *I*-*V* measurements with different $V_{GS,Q}$ and device simulation fittings using SILVACO ATLAS TCAD. With respect to ($V_{GS,Q}$, $V_{DS,Q}$) = (0 V, 0 V), the V_{th} and electron mobility for ($V_{GS,Q}$, $V_{DS,Q}$) = (-15 V, 0 V) decreased from –6.17 V to -6.27 V and from 1983 $cm^2V^{-1}s^{-1}$ to 1967 $cm^2V^{-1}s^{-1}$, respectively. On the other hand, ($V_{GS,Q}$, $V_{DS,Q}$) = (1.5 V, 0 V) caused the V_{th} to increase from -6.17 V to -5.77 V and the electron mobility increased from 1983 $cm^2V^{-1}s^{-1}$ to 2073 $cm^2V^{-1}s^{-1}$. The impact of the electron trapping on the AlGaN/GaN MOSHEMT analyzed using pulsed *I*-*V* measurements and device simulation provide plausible explanations that the active traps during the measurements show donor-like characteristics, instead of acceptor-like characteristics.

Chapter 6: Conclusion and Future Work

6.1 Summary of thesis work

Over the past four decades, the AlGaN/GaN high electron mobility transistor (HEMT) has become a promising candidate for high power [42], high breakdown voltage [41], high frequency [44] and high temperature [43] applications due the superior material properties of GaN [17]-[19],[51]-[52]. A metal oxide high electron mobility transistor (MOSHEMT) can be fabricated by depositing a gate dielectric between the gate metal and AlGaN layer in order to achieve low gate leakage current [65]. However, a major issue that still needs to be addressed is the electron trapping process that degrades the performance of the AlGaN/GaN MOSHEMT [29],[33]-[34],[102]-[105]. This thesis aims at studying the effects of Al_2O_3/AlGaN interface traps on the performance of the AlGaN/GaN MOSHEMTs. To explore and to have a good understanding of the traps, different methods of analysis were proposed and carried out, such as drain current transient measurement, pulsed *I-V* measurement and Technology Computer Aided Design (TCAD) device simulation. The key contributions of this thesis are listed in the next section.

6.2 Thesis contributions

This section summarizes the key contributions in AlGaN/GaN MOSHEMT research in this thesis.

6.2.1 TCAD investigation of AlGaN/GaN MOSHEMT passivation using SiH_4 treatment

Device simulations using SILVACO ATLAS TCAD were adopted to study the effects of SiH_4 passivation on the AlGaN/GaN MOSHEMT, reported by Liu *et al*. [48]. The SiH_4 treatment on the AlGaN/GaN MOSHEMT was reported to have decreased the threshold voltage (V_{th}), increased the on-state drain current ($I_{D,ON}$), reduced the off-state drain current ($I_{D,OFF}$), reduced the sub-threshold swing (SS), and increased the maximum extrinsic transconductance ($g_{m,max}$) [48]. In the simulation, donor-like trap ($E_C - E_{T,D} = 0.37$ eV) [60] and acceptor-like trap ($E_{T,A} - E_V = 1$ V) [62], and capture cross-sections of 1×10^{-15} cm^{-2} [89] were used to define the trap states at the HfAlO/AlGaN interface. Device simulation was used to fit the I_D-V_{GS} plots in linear and semi-log scales for the passivated and unpassivated devices. Good simulation fittings to the reported data revealed that the passivation led to the reduction of acceptor-like trap density by 6.0×10^{12} cm^{-2} in passivated samples. The density of the donor-like traps in both the passivated and unpassivated samples was 2.96×10^{13} cm^{-2}.

6.2.2 Trap Analysis of AlGaN/GaN MOSHEMTs using Gate Stress Induced Transient Current Methodology and TCAD Simulation

The properties of interface traps states at the Al_2O_3/AlGaN interface were studied using a combination of electrical measurements, numerical fitting and device simulations. A current transient method on AlGaN/GaN HEMTs reported by Joh *et al*. [35] was applied to study the traps in AlGaN/GaN MOSHEMTs for the first time. The presence of a dielectric layer between the gate metal and the AlGaN layer in the MOSHEMT allowed the study of the trap characteristics at the dielectric/AlGaN interface. The interface traps at the dielectric/AlGaN interface can affect the V_{th} and cause drain current collapse [102].

The current transient measurement consisted of two steps. The first step was a trap filling pulse (V_{DS} = 0 V and V_{GS} = -20 V for 50 s) immediately followed by the second step, which was the recovery drain current measurement at V_{DS} = 0.5 V and V_{GS} = 1 V. The measurements were made at T = 340 – 370 K. A fitting function was used to fit the transient data and two dominant detrapping processes (E1 and E2) were identified from the temperature-dependent time constant spectra. The time constants of E1 and E2 at T = 370 K were 2.4s and 7.5s, respectively. The activation energies of E1 and E2 were 0.32 eV and 0.46 eV, respectively, obtained from linear fittings to Arrhenius plots. Device simulation was used to fit the measured I_D-V_{GS} plots at T = 370 K. From the good simulation fitting, the density of the E1 and E2 were determined to be 1.43×10^{13} cm^{-2} and 1.07×10^{13} cm^{-2}, respectively.

6.2.3 Characterization of Traps in AlGaN/GaN MOSHEMTs using Pulsed *I-V* Measurements and TCAD Device Simulation

The impacts of traps located at the Al_2O_3/AlGaN interface were studied using a combination of pulsed *I-V* measurements and device simulation. The pulsed *I-V* measurements were performed at ($V_{GS,Q}$, $V_{DS,Q}$) = (-15 V, 0 V), (0 V, 0 V), (0.5 V, 0 V), (1.0 V, 0 V) and (1.5 V, 0 V). Compared to ($V_{GS,Q}$, $V_{DS,Q}$) = (0 V, 0 V), the V_{th} shifted to a more negative value from -6.17 V to -6.27 V at ($V_{GS,Q}$, $V_{DS,Q}$) = (-15 V, 0 V). This observation was different from results reported in the literature on AlGaN/GaN HEMTs. In the literature, it was reported that negative $V_{GS,Q}$ increased the R_{ON} and reduced $I_{D,sat}$. However, in this work, it is believed that the Al_2O_3 layer suppressed the trapping of electrons at the Al_2O_3/AlGaN interface due to lower gate leakage current, when the device was stressed at $V_{GS,Q}$ = -15 V. Instead, it is believed that the negative $V_{GS,Q}$ led to the emission of electrons from the traps at the Al_2O_3/AlGaN interface. Simulation fittings to the measured pulsed I_D-V_{GS} data showed that the 2DEG mobility decreased from 1627 cm^2/V.s. to 1599 cm^2/V.s, 2DEG n_s increased from 9.39×10^{12} cm^{-2} to 9.60×10^{12} cm^{-2} and the ionized trap density at the Al_2O_3/AlGaN interface increased from 3.05×10^{13} cm^{-2} to 3.15×10^{13} cm^{-2}. On the other hand, ($V_{GS,Q}$, $V_{DS,Q}$) = (0.5 V, 0 V), (1.0 V, 0 V) and (1.5 V, 0 V) caused the V_{th} to shift from -6.17 V to -6.03 V, -5.94 V and -5.77 V, respectively. Simulation fittings showed that the 2DEG mobility increased from 1627 cm^2/V.s to 1664 cm^2/V.s, 1690 cm^2/V.s and 1735 cm^2/V.s, respectively. 2DEG n_s decreased from 9.39×10^{12} cm^{-2} to 9.22×10^{12} cm^{-2}, 9.00×10^{12} cm^{-2} and 8.66×10^{12} cm^{-2}, respectively. Ionized trap density at the Al_2O_3/AlGaN interface decreased from 3.05×10^{13} cm^{-2} to 2.97×10^{13} cm^{-2}, 2.86×10^{13} cm^{-2} and 2.70×10^{13} cm^{-2}, respectively. The impact of the electron trapping in the AlGaN/GaN MOSHEMT analyzed using pulsed *I-V* measurements provide plausible explanations that the active traps during the measurements displayed donor-like characteristics, instead of acceptor-like characteristics.

6.3 Future Work

This thesis presented several techniques used to analyse the trapping effects in AlGaN/GaN MOSHEMTs. These techniques may serve as a basis for several other studies regarding trapping effects in AlGaN/GaN MOSHEMTs and other III-V material systems. Some suggestions for future analysis are listed below.

6.3.1 TCAD study of *I-V* measurements of AlGaN/GaN MOSHEMTs with other surface passivation

In Chapter 3, TCAD simulation study of SiH_4 passivation of AlGaN/GaN MOSHEMT was investigated. The device simulation of the AlGaN/GaN MOSHEMT including the mesh design and the various model used to replicate the physical device in simulation was demonstrated. In the literature, other passivation techniques such as MgO [45]-[58] and Sc_2O_3 [103]-[144], Si_3N_4 [104],[107],[145], SiO_2 [105]-[147], NH_3 [106], PH_3 [107], etc, have been reported to improve the performance of AlGaN/GaN MOSHEMTs. This TCAD device simulation method can be harnessed to obtain deep understanding on the effect of various passivation techniques on the trap states at the dielectric/AlGaN interface.

6.3.2 Current transient measurement to analyse the effect of traps with surface passivation

The technique of V_{DS} = 0 V state detrapping current transient was used to study the trap activation energy and time constant in Chapter 4. This technique eliminates the effect of self-heating in the device that can interfere with the measurement results. Using a fitting function, the time constant spectrum can be extracted from the measured drain current transient. If the dominant detrapping processes are sensitive to temperature, the activation energies of the traps can also be extracted. This method can be used to study the impact of the AlGaN/GaN MOSHEMT passivation on the dominant traps present in the device [70]. This technique can also be applied to study the dominant traps in other *III-V* material systems.

6.3.3 Pulsed current-voltage (*I-V*) analysis of passivated AlGaN/GaN MOSHEMTs

Pulsed *I-V* technique was explored to study the characteristic of traps in AlGaN/GaN MOSHEMT in Chapter 5. This technique minimizes the effect of self-heating and trapping transient during the measurement. Various gate-to-source quiescent ($V_{GS,Q}$) biases were employed to study the effects of trapping/detrapping in the device. This technique can be applied to investigate the impact of drain current collapse in AlGaN/GaN MOSHEMTs [88],[150], due to various passivation methods. This method can also be applied to study the effects of drain current collapse in other *III-V* material systems [108]-[152].

References

[1] J. I. Pankove, E. A. Miller, D. Richman and J. E. Berkeyheiser, "Electroluminescence in GaN," *J. Lumin*, vol. 4, pp. 63-66, 1971.

[2] P. Boguslawski, E. L. Briggs and J. Bernholc, "Native defects in gallium nitride," *Physical Rev. B*, vol. 51, no. 23, p. 17255, 1995.

[3] H. Amano, N. Sawaki, I. Akasaki and Y. Toyoda, "Metalorganic vapor phase epitaxial growth of a high quality GaN film using an AlN buffer layer," *Appl. Phys. Lett.*, vol. 48, pp. 353-355, 1986.

[4] S. Nakamura, "GaN Growth Using GaN Buffer Layer," *Jpn. J. Appl. Phys.*, vol. 30, no. 10A, pp. L1705-L1707, 1991.

[5] H. Amano, M. Kito, K. Hiramatsu and I. Akasaki, "P-Type Conduction in Mg-Doped GaN Treated with Low-Energy Electron Beam Irradiation (LEEBI)," *Jpn. J. Appl. Phys.*, vol. 28, no. 12, pp. L2112-L2114, 1989.

[6] M. A. Khan, J. M. V. Hove, J. N. Kuznia and D. T. Olson, "High electron mobility GaN/Al x Ga1−x N heterostructures grown by low-pressure metalorganic chemical vapor deposition," *Appl. Phys. Lett.*, vol. 58, p. 2408, 1991.

[7] S. Nakamura, T. Mukai, M. Senoh and N. Iwasa, "Thermal Annealing Effects on P-Type Mg-Doped GaN Films," *Jpn. J. Appl. Phys.,* vol. 31, pp. L139-L142, 1992.

[8] M. A. Khan, A. Bhattarai, J. N. Kuznia and D. T. Olson, "High electron mobility transistor based on a GaN-Al x Ga1−x N heterojunction," *Appl. Phys. Lett.,* vol. 63, pp. 1214-1215, 1993.

[9] S. Nakamura, T. Mukai and M. Senoh, "Candela-class high-brightness InGaN/AlGaN double-heterostructure blue-light-emitting diodes," *Appl. Phys. Lett.,* vol. 64, p. 1687, 1994.

[10] S. Nakamura, M. Senoh, S. Nagahama, N. Iwasa, T. Yamada, T. Matsushita, H. Kiyoku and Y. Sugimoto, "InGaN-Based Multi-Quantum-Well-Structure Laser Diodes," *Jpn. J. Appl. Phys.,* vol. 35, pp. L74-L76, 1996.

[11] "GaN Power Devices," Panasonic Corporation, 2015. [Online]. Available: http://www.semicon.panasonic.co.jp/en/products/powerics/ganpower/. [Accessed 14 July 2015].

[12] H. P. Maruska and J. J. Tietjen, "The preparation and Properties of Vapor-deposited Single-crystal-line GaN," *Appl. Phys. Lett.,* vol. 15, no. 10, pp. 327-329, 1969.

[13] J. M. Barker, R. Akis, D. K. Ferry, S. M. Goodnick, T. J. Thornton, D. D. Koleske, A. E. Wickenden and R. L. Henry, "High-field transport studies of GaN," *Physica B,* vol. 314, pp. 39-41, 2002.

[14] L. Lindsay, D. A. Broido and T. L. Reinecke, "Thermal Conductivity and Large Isotope Effect in GaN from First Principles," *Phys. Rev. Lett.,* vol. 109, p. 095901, 2012.

[15] R. S. Pengelly, S. M. Wood, J. W. Milligan, S. T. Sheppard and W. L. Pribble, "A Review of GaN on SiC High Electron-Mobility Power Transistors and MMICs," *IEEE Trans. Microw. Theory Techn.,* vol. 60, no. 6, pp. 1764-1783, 2012.

[16] I. B. Rowena, S. L. Selvaraj and T. Egawa, "Buffer Thickness Contribution to Suppress Vertical Leakage Current With High Breakdown Field (2.3 MV/cm) for GaN on Si," *IEEE Electron Dev. Lett.,* vol. 32, pp. 1534-1536, 2011.

[17] Y. Wu, B. P. Keller, S. Keller, D. Kapolnek, P. Kozodoy, S. P. Denbaars and U. K. Mishra, "Very high breakdown voltage and large transconductance realized on GaN heterojunction field effect transistors," *Appl. Phys. Lett.,* vol. 69, pp. 1438-1440, 1996.

[18] H. Tokuda, T. Kojima and M. Kuzuhara, "Over 3000 cm2V-1s-1 room temperature two-dimensional electron gas mobility by annealing Ni/Al

deposited on AlGaN/GaN heterostructures," *Appl. Phys. Express*, vol. 7, p. 041001, 2014.

[19] U. V. Bhapkar and M. S. Shur, "Monte Carlo calculation of celocity-field characteristics of wurzite GaN," *J. Appl. Phys.*, vol. 82, pp. 1649-1655, 1997.

[20] P. Srivastava, J. Das, D. Visalli, M. V. Hove, P. E. Malinowski, D. Marcon, S. Lenci, K. Geens, K. Cheng, M. Leys, S. Decoutere, R. P. Mertens and G. Borghs, "Record Breakdown Voltage (2200 V) of GaN DHFETs on Si With 2-um Buffer Thickness by Local Substrate Removal," *IEEE Electron Dev. Lett.*, vol. 32, pp. 30-32, 2011.

[21] F. Bernardini, V. Fiorentini and D. Vanderbilt, "Spontaneous polarization and piezoelectric constants of III-V nitrides," *Phys. Rev. B*, vol. 56, p. R10024, 1997.

[22] O. Ambacher, J. Smart, J. R.Shealy, N. G. Weimann, K. Chu, M. Murphy, W. J. Schaff, L. F. Eastman, R. Dimitrov, L. Wittmer, M. Stutzmann, W. Rieger and J. Hilsenbeck, "Two-dimensional electron gases induced by spontaneous and piezoelectric polarization charges in N- and Ga-face AlGaN/GaN heterostructures," *J. Appl. Phys.*, vol. 85, no. 6, pp. 3222-3233, 1999.

[23] R. Butte and N. Grandjean, "Effects of Polarization in Optoelectronic

Quantum Structures," in *Polarization Effects in Semiconductors: From Ab InitioTheory to Device Applications*, New York, Springer, 2008, p. 469.

[24] A. Zoroddu, F. Bernardini, P. Ruggerone and V. Fiorentini, "First-principles prediction of structure, energetics, formation enthalpy, elastic constants, polarization, and piezoelectric constants of AlN, GaN, and InN: Comparison of local and gradient-corrected density-functional theory," *Phys. Rev. B,* vol. 64, p. 045208, 2001.

[25] O. Ambacher and V. Cimalla, "Polarization Induced Effects in GaN-based Heterostructures and Novel Sensors," in *Polarization Effects in Semiconductors: From Ab InitioTheory to Device Applications*, New York, Springer, 2008, pp. 27-109.

[26] O. Ambacher, B. Foutz, J. Smart, J. R. Shealy, N. G. Weimann, K. Chu, M. Murphy, A. J. Sierakowski, W. J. Schaff, L. F. Eastman, R. Dimitrov, A. Mitchell and M. Stutzmann, "Two dimensional electron gases induced by spontaneous and piezoelectric polarization in undoped and doped AlGaN/GaN heterostructures," *J. Appl. Phys.*, vol. 87, no. 1, pp. 334-344, 2000.

[27] O. Ambacher, J. Smart, J. R. Shealy, N. G. Weimann, K. Chu, M. Murphy, W. J. Schaff, L. F. Eastman, R. Dimitrov, L. Wittmer, M. Stutzmann, W. Rieger and J. Hilsenbeck, "J. Appl. Phys.," *Two-dimensional electron gases induced by spontaneous and piezoelectric polarization charges in N- and*

Ga-face AlGaN/GaN heterostructures, vol. 85, p. 3222, 1999.

[28] P. M. Asbeck, E. T. Yu, S. S. Lau, G. J. Sullivan, J. V. Hove and J. M. Redwing, "Piezoelectric charge densities in AIGaN/GaN HFETs," *Electron. Lett.,* vol. 33, p. 1230, 1997.

[29] R. Vetury, N. Q. Zhang, S. Keller and U. K. Mishra, "The Impact of Surface States on the DC and RF Characteristics of AlGaN/GaN HFETs," *IEEE Trans. Electron Device,* vol. 48, no. 3, pp. 560-566, 2001.

[30] B. Luo, R. Mehandru, J. Kim, *. B. P. G. F. Rena, A. H. Onstine, C. R. Abernathy, S. J. Pearton, R. Fitch, J. Gillespie, T. Jenkins, J. Sewell, D. Via, A. Crespo and Y. Irokawa, "Comparison of Surface Passivation Films for Reduction of Current Collapse in AlGaN/GaN High Electron Mobility Transistors," *J. Electrochem. Soc,* vol. 149, no. 11, pp. G613-G619, 2002.

[31] C. D. Young, Y. Zhao, D. Heh, R. Choi, B. H. Lee and G. Bersuker, "Pulsed Id–Vg Methodology and Its Application to Electron-Trapping Characterization and Defect Density Profiling," *IEEE Trans. Electron Devices,* vol. 56, no. 6, pp. 1322-1329, 2009.

[32] O. I. Saadat, J. W. Chung, E. L. Piner and T. Palacios, "Gate-First AlGaN/GaN HEMT Technology for High-Frequency Applications," *IEEE Electron Device Lett.,* vol. 30, no. 12, pp. 1254-1256, 2009.

[33] J. M. Tirado, J. L. Snchez-Rojas and J. I. Izpura, "Trapping Effects in the Transient Response of AlGaN/GaN HEMT Devices," *IEEE Trans. Electron Devices,* vol. 54, no. 3, pp. 410-417, 2007.

[34] J. P. Ibbetson, P. T. Fini, K. D. Ness, S. P. DenBaars, J. S. Speck and U. K. Mishra, "Polarization effects, surface states, and the source of electrons in AlGaN/GaN heterostructure field effect transistors," *Appl. Phys. Lett.,* vol. 77, p. 250, 2000.

[35] J. Joh and J. d. Alamo, "A Current-Transient Methodology for Trap Analysis for GaN High Electron Mobility Transistors," *IEEE,* vol. 58, no. 1, pp. 132-140, 2011.

[36] S. Keller, Y.-F. Wu, G. Parish, N. Ziang, J. J. Xu, S. P. D. B. P. Keller and U. K. Mishra, "Gallium Nitride Based High Power Heterojunction Field Effect Transistors: Process Development and Present Status at UCSB," *IEEE Trans Electron Device,* vol. 48, no. 3, pp. 552-559, 2001.

[37] S. C. Binari, P. B. Klein and T. E. Kazior, "Trapping effects in GaN and SiC microwave FETs," *Proc. IEEE,* vol. 90, no. 6, pp. 1048-1058, 2002.

[38] G. Koley, V. Tilak, L. F. Eastman and M. G. Spencer, "Slow transients observed in AlGaN/GaN HFETs: Effects of SiNx passivation and UV illumination," *IEEE Trans. Electron Devices,* vol. 50, no. 4, pp. 886-893, 2003.

[39] J. Piprek, Nitride Semiconductor Devices: Principles and Simulation, WILEY-VCH, 2007.

[40] R. Oberhuber, G. Zandler and P. Vogl, "Mobility of two-dimensional electrons in AlGaN/GaN modulation-doped field-effect transistors," *Appl. Phys. Lett.,* vol. 73, p. 818, 1998.

[41] W. Saito, Y. Takada, M. Kuraguchi, K. Tsuda, I. Omura, T. Ogura and H. Ohashi, "High breakdown voltage AlGaN-GaN power-HEMT design and high current density switching behavior," *Trans. Electron Dev.,* vol. 50, p. 2528, 2003.

[42] Y.-F. Wu, D. Kapolnek, J. P. Ibbetson, P. Parikh, B. P. Keller and U. K. Mishra, "Very-High Power Density AlGaN/GaN HEMTs," *IEEE Trans. Electron Devices,* vol. 48, no. 3, pp. 586-590, 2001.

[43] N. Maeda, T. Saitoh, K. Tsubaki, T. Nishida and N. Kobayashi, "Superior Pinch-Off Characteristics at 400degC in AlGaN/GaN Heterostructure Field Effect Transistors," *Jpn. J. Appl. Phys.,* vol. 38, p. L987, 1999.

[44] T. Palacios, A. Chakraborty, S. Heikman, S. Keller, S. P. DenBaars and U. K. Mishra, "AlGaN/GaN High Electron Mobility Transistors With InGaN Back-Barriers," *IEEE Electron Dev. Lett.,* vol. 27, p. 13, 2006.

[45] B. Luo, J. W. Johnson, B. P. Gila, A. Onstine, C. R. Abernathy, F. Ren, S. J. Pearton, A. G. Baca, A. M. Dabiran, A. M. Wowchack and P. P. Chow,

"Surface passivation of AlGaN/GaN HEMTs using MBE-grown MgO or Sc2O3," *Solid-State Electron,* vol. 46, p. 467, 2002.

[46] B. Luo, J. W. Johnson, J. Kim, R. M. Mehandru, F. Ren, B. P. Gila, A. H. Onstine, C. R. Abernathy, S. J. Pearton, A. G. Baca, R. D. Briggs, R. J. Shul, C. Monier and J. Han, "Influence of MgO and Sc 2 O 3 passivation on AlGaN/GaN high-electron-mobility transistors," *Appl. Phys. Lett.,* vol. 80, p. 1661, 2002.

[47] W. Lu, V. Kumar, R. Schwindt, E. Piner and I. Adesida, "A comparative study of surface passivation on AlGaN/GaN HEMTs," *Solid-State Electron,* vol. 46, p. 1441, 2002.

[48] X. Liu, E. K. F. Low, J. Pan, W. Liu, K. L. Teo, L. S. Tan and Y. C. Yeo, "Impact of In situ vacuum anneal and SiH4 treatment on electrical characteristics of AlGaN/GaN metal-oxide-semiconductor high-electron mobility transistors," *Appl. Phys. Lett.,* vol. 99, p. 093504, 2011.

[49] SILVACO, "ATLAS User's Manual," 2011.

[50] A. Fontserè, A. Pérez-Tomás, M. Placidi, P. Fernández-Martínez, N. Baron, S. Chenot, Y. Cordier, J. C. Moreno, P. M. Gammond and M. Jennings, "Temperature dependence of Al/Ti-based Ohmic contact to GaN devices: HEMT and MOSFET," *Microelectron. Eng.,* vol. 88, p. 3140, 2011.

[51] Y. Gotoh, H. Tsuji and J. Ishikawa, "Measurement of work function of transition metal nitride and carbide thin films," *J. Vac. Sci. Technol. B,* vol. 21, p. 1607, 2003.

[52] S. J. Moon, J. C. Byung, C. Y. Chia, D. H. C. Siu, J. W. Sung, M. Shajan, L. K. Bera, N. Balasubramanian and D. L. Kwong, "Formation of Hafnium–Aluminum–Oxide Gate Dielectric Using Single Cocktail Liquid Source in MOCVD Process," *IEEE Trans. Electron Dev.,* vol. 50, p. 2088, 2003.

[53] H. J. Oh, J. Q. Lin, S. J. Lee, G. K. Dalapati, A. Sridhara, D. Z. Chi, S. J. Chua, G. Q. Lo and D. L. Kwong, "Study on interfacial properties of InGaAs and GaAs integrated with chemical-vapor-deposited high-k gate dielectrics using x-ray photoelectron spectroscopy," *Appl. Phys. Lett.,* vol. 93, p. 062107, 2008.

[54] J. D. Albrecht, R. P. Wang, P. P. Ruden, M. Farahmand and K. F. Brennan, "Electron transport characteristics of GaN for high temperature device modeling," *J. Appl. Phys,* vol. 83, p. 4777, 1998.

[55] M. Farahmand, C. Garetto, E. Bellotti, K. F. Brennan, M. Goana, E. Ghillino, G. Ghione, J. D. Albrecht and P. P. Ruden, "Monte Carlo Simulation of Electron Transport in the III-Nitride Wurtzite Phase Materials System: Binaries and Ternaries," *IEEE Trans. Electron Dev.,* vol. 48, p. 535, 2001.

[56] M. Lenzlinger and E. H. Snow, "Fowler-Nordheim Tunneling into Thermally Grown SiO2," *J. Applied Physics,* vol. 40, no. 1, p. 278, 1969.

[57] S. Keeney, F. Piccinini, M. Morelli, A. Mathewson, C. Lombardi, R. Bez, L. Ravazzi and D. Cantarelli, "Complete transient simulation of flash EEPROM devices," *IEDM Tech. Dig.,* pp. 201-204, 1990.

[58] J. A. Garrido, A. JimeÂnez, J. L. SaÂnchez-Rojas, E. MunÄoz, F. OmneÁs and P. Gibart, "Polarization Field Determination in AlGaN/GaN HFETs," *Phys. Status Solidi A,* vol. 176, p. 195, 1999.

[59] S. R. Kurtz, A. A. Allerman, D. D. Koleske, A. G. Baca and R. D. Briggs, "Electronic properties of the AlGaNÕGaN heterostructure and two-dimensional electron gas observed by electroreflectance," *J. Appl. Phys.,* vol. 95, p. 1888, 2004.

[60] H. Hasegawa, T. Inagaki, S. Ootomo and T. Hashizume, "Mechanisms of current collapse and gate leakage currents in AlGaN/GaN heterostructure field effect transistors," *J. Vac. Sci. Technol. B,* vol. 21, p. 1844, 2003.

[61] J. Neugebauer and C. G. V. d. Walle, "Gallium vacancies and the yellow luminescence in GaN," *Appl. Phys. Lett.,* vol. 69, p. 503, 1996.

[62] M. Miczek, C. Mizue, T. Hashizume and B. Adamowicz, "Effects of interface states and temperature on the C-V behavior of metal/insulator/AlGaN/GaN heterostructure capacitors," *J. Appl. Phys.,* vol.

103, p. 104510, 2008.

[63] J. K. Kaushik, V. R. Balakrishnan, B. S. Panwar and R. Muralidharan, "Inverse temperature dependence of reverse gate leakage current in AlGaN/GaN HEMT," *Semicond. Sci. Technol,* vol. 28, p. 015206, 2013.

[64] Y. Cai, Z. Cheng, Z. Yang, C. W. Tang, K. M. Lau and K. J. Chen, "High-Temperature Operation of AlGaN/GaN HEMTs Direct-Coupled FET Logic (DCFL) Integrated Circuits," *IEEE Electron Device Lett.,* vol. 28, no. 5, pp. 328-331, 2007.

[65] S. Ootomo, T. Hashizume and H. Hasegawa, "A Novel Thin Al2O3 Gate Dielectric by ECR-Plasma Oxidation of Al for AlGaN/GaN Insulated Gate Heterostructure Field-Effect Transistors," *Phys. Stat. Sol. (c),* vol. 0, no. 1, pp. 90-94, 2002.

[66] R. Magno, R. Shelby and W. T. Anderson, "A deep-level transient spectroscopy study of high electron mobility transistors subjected to lifetime stress tests," *J. Appl. Phys.,* vol. 66, no. 11, pp. 5613-5617, 1989.

[67] W. Mickanin, P. Canfield, E. Finchem and B. Odekirk, "Frequency-dependent transients in GaAs MESFETs: Process, geometry, and material effects," *Proc. IEEE GaAs IC Symp,* pp. 211-214, 1989.

[68] R. Yeats, D. C. D’Avanzo, K. Chan, N. Fernandez, T. W. Taylor and C. Vogel, "Gate slow transients in GaAs MESFETs-causes, cures, and impact

on circuits," *Proc. Int. Electron Device Meeting,* pp. 842-845, 1988.

[69] C. T. Sah, "Bulk and Interface Imprefections in Semiconductors," *Solid-State Electron.,* vol. 19, pp. 975-990, 1976.

[70] S. DasGupta, M. Sun, A. Armstrong, R. J. Kaplar, M. J. Marinella, J. B. Stanley, S. Atcitty and T. Palacios, "Slow Detrapping Transients due to Gate and Drain Bias Stress in High Breakdown Voltage AlGaN/GaN HEMTs," *IEEE Trans. Electron Devices,* vol. 59, no. 8, pp. 2115-2122, 2012.

[71] T. Mizutani, T. Okino, K. Kawada, Y. Ohno, S. Kishimoto and K. Maezawa, "Drain current DLTS of AlGaN/GaN HEMTs," *Phys. Status Solidi A,* vol. 200, no. 1, pp. 195-198, 2003.

[72] R. Stoklas, D. Gregušová, J. Novák, A. Vescan and P. Kordoš, "Investigation of trapping effects in AlGaN/GaN/Si field-effect transistors by frequency dependent capacitance and conductance analysis," *Appl. Phys. Lett.,* vol. 93, p. 124103, 2008.

[73] W. Saito, M. Kuraguchi, Y. Takada, K. Tsuda, I. Omura and T. Ogura, "Influence of Surface Defect Charge at AlGaN–GaN-HEMT Upon Schottky Gate Leakage Current and Breakdown Voltage," *IEEE Trans. Electron Devices,* vol. 52, no. 2, pp. 159-164, 2005.

[74] M. Ťapajna, U. K. Mishra and M. Kuball, "Importance of impurity diffusion for early stage degradation in AlGaN/GaN high electron mobility transistors upon electrical stress," *Appl. Phys. Lett.*, vol. 97, p. 023503, 2010.

[75] K. Shimada, T. Sota and K. Suzuki, "First-principles study on electronic and elastic properties of BN, AlN, and GaN," *J. Appl. Phys.*, vol. 84, no. 9, pp. 4951-4958, 1998.

[76] G. Meneghesso, G. Verzellesi, R. Pierobon, F. Rampazzo, A. Chini, U. K. Mishra, C. Canali and E. Zanoni, "Surface-Related Drain Current Dispersion Effects in AlGaN-GaN HEMTs," *IEEE Trans. Electron Device*, vol. 51, no. 10, pp. 1554-1561, 2004.

[77] Z. H. Liu, G. I. Ng, S. Arulkumaran, Y. K. T. Maung and H. Zhou, "Temperature-dependent forward gate current transport in atomic-layer-deposited Al2O3/AlGaN/GaN metal-insulator-semiconductor high electron mobility transistor," *Appl. Phys. Lett.*, vol. 98, p. 163501, 2011.

[78] J. J. Zhu, X. H. Ma, Y. Xie, B. Hou, W. W. Chen, J. C. Zhang and Y. Hao, "Improved Interface and Transport Properties of AlGaN/GaN MIS-HEMTs with PEALD-Grown AlN Gate Dielectric," *IEEE Trans. Electron Devices*, 2015.

[79] M.Tapajna, S. W. Kaun, M. H. Wong, F. Gao, T. Palacios, U. K. Mishra, J. S. Speck and M. Kuball, "Influence of threading dislocation density on

early degradation in AlGaN/GaN high electron mobility transistors," *Appl. Phys. Lett.,* vol. 99, p. 223501, 2011.

[80] S. C. Binari, K. Ikossi, J. A. Roussos, W. Kruppa, D. Park, H. B. Dietrich, D. D. Koleske, A. E. Wickenden and R. L. Henry, "Trapping Effects and Microwave Power Performance in AlGaN/GaN HEMTs," *IEEE Trans. Electron Devices*, vol. 48, no. 3, pp. 465-471, 2001.

[81] I. Daumiller, D. Theron, C. Gaquiere, A. Vescan, R. Dietrich, A. Wieszt, H. Leier, R. Vetury, U. Mishra, I. Smorchkova, S. Keller, C. Nguyen and E. Kohn, "Current instabilities in GaN-based devices," *IEEE Electron Dev. Lett.,* vol. 22, no. 2, pp. 62-64, 2001.

[82] G. Meneghesso, G. Verzellesi, F. Danesin, F. Rampazzo, F. Zanon, A. Tazzoli, M. Meneghini and E. Zanoni, "Reliability of GaN high-electron-mobility transistors: State of the art and perspectives," *IEEE Trans. Device Mater. Rel.,* vol. 8, no. 2, pp. 332-343, 2008.

[83] K. A. Jenkins and J. Y.-C. Sun, "Measurement of I-V Curves of Silicon-on-Insulator (SOI) MOSFET's Without Self-Heating," *IEEE Electron Device Lett.,* vol. 16, no. 4, pp. 145-147, 1995.

[84] B.-Y. Chou, W.-C. Hsu, H.-Y. Liu, C.-S. Lee, Y.-S. Wu, W.-C. Sun, S.-Y. Wei, S.-M. Yu and M.-H. Chiang, "Investigations of AlGaN/GaN MOS-HEMT with Al2O3 deposition by ultrasonic spray pyrolysis method,"

Semicond. Sci. Technol., vol. 30, p. 015009, 2015.

[85] J. Sun, H. Fatima, A. Koudymov, A. Chitnis, X.Hu, H.-M. Wang, J. Zhang, G. Simin, J. Yang and M. A. Khan, "Thermal Management of AlGaN–GaN HFETs on Sapphire Using Flip-Chip Bonding With Epoxy Underfill," *IEEE Electron Device Lett.,* vol. 24, no. 6, pp. 375-377, 2003.

[86] M. Meneghini, D. Bisi, D. Marcon, S. Stoffels, M. V. Hove, T.-L. Wu, S. Decoutere, G. Meneghesso and E. Zanoni, "Trapping and Reliability Assessment in D-Mode GaN-Based MIS-HEMTs for Power Applications," *IEEE Trans. Power Electron.,* vol. 29, no. 5, pp. 2199-2206, 2014.

[87] M. Meneghini, N. Ronchi, A. Stocco, G. Meneghesso, U. K. Mishra, Y. Pei and E. Zanoni, "Investigation of Trapping and Hot-Electron Effects in GaN HEMTs by Means of a Combined Electrooptical Method," *IEEE Trans. Electron Devices,* vol. 58, no. 9, pp. 2996-3003, 2011.

[88] P. Nakkala, A. Martin, M. Campovecchio, S. Laurent, P. Bouysse, E. Bergeault, R. Quéré, O. Jardel and S. Piotrowicz, "Pulsed characterisation of trapping dynamics in AlGaN/GaN HEMTs," *Electron. Lett.,* vol. 49, no. 22, pp. 1406-1407, 2013.

[89] Y. Fu, Z. Li, W. T. Ng and J. K. O. Sin, in *Integrated Power Devices and TCAD Simulation*, Boca Raton, CRC Press Taylor & Francis Group, 2014, p. 114.

[90] *Device Simulator Atlas Ver.5.16.3.R Atlas User's Manual,* Silvaco Inc., July 2011.

[91] C. Lombardi, S. Manzini, A. Saporito and M. Vanzi, "A physically based mobility model for numerical simulation of nonpolar devices," *IEEE Trans. Computer-Aided Design,* vol. 7, no. 11, pp. 1164-1171, 1988.

[92] C. T. Sah, T. H. Ning and L. L. Tschopp, "The scattering of electrons by surface oxide charges and by lattice vibrations at the silicon-silicon dioxide interface," *Surface Sci.,* vol. 32, pp. 561-575, 1972.

[93] S. A. Schwarz and S. E. Russek, "Semi-emphirical equations for electron velocity in silicon: part II - MOS inversion layer," *IEEE Trans. Electron Devices,* vol. 30, pp. 1634-1639, 1983.

[94] F. Stern, "Self-consistent results for n-type Si inversion layers," *Phys. Rev. B,* vol. 5, no. 12, pp. 4891-4899, 1972.

[95] V. I. Fistul, Heavily doped semiconductors, New York: Plenum, 1969.

[96] J. Du, H. Yan, C. Yin, Z. Feng, S. Dun and Q. Yu, "Simulation and characterization of millimeter-wave InAlN/GaN high electron mobility transistors using Lombardi mobility model," *J. Appl. Phys.,* vol. 115, p. 164510, 2014.

[97] G. Masetti, M. Severi and S. Solmi, "Modeling of carrier mobility against

carrier concentration in arsenic-, phosphorous- and boron-doped silicon," *IEEE Trans. Electron Devices,* Vols. ED-30, pp. 764-769, 1983.

[98] F. F. Fang and A. B. Fowler, "Transport properties of electrons in inverted silicon surfaces," *Phys. Rev. B,* vol. 169, no. 3, pp. 619-631, 1968.

[99] T. Palacios and U. K. Mishra, "AlGaN/GaN High Electron Mobility Transistors," in *Nitride Semiconductor Devices: Principles and Simulation*, Weinheim, WILEY-VCH Verlag GmbH & Co. KGaA, 2007, pp. 222-224.

[100] T.-L. Wua, D. Marcon, N. Ronchi, B. Bakeroot, S. You, S. Stoffels, M. V. Hove, D. Bisi, M. Meneghini, G. Groeseneken and S. Decoutere, "Analysis of slow de-trapping phenomena after a positive gate bias on AlGaN/GaN MIS-HEMTs with in-situ Si3N4/Al2O3 bilayer gate dielectrics," *Solid-State Electron,* vol. 103, pp. 127-130, 2015.

[101] S. Huang, S. Yang, J. Roberts and K. J. Chen, "Threshold Voltage Instability in Al2O3/GaN/AlGaN/GaN Metal–Insulator–Semiconductor High-Electron Mobility Transistors," *Jpn. J. Appl. Phys.,* vol. 50, p. 110202, 2011.

[102] M. Lachab, M. Sultana, H. Fatima, V. Adivarahan, Q. Fareed and M. A. Khan, "Direct current performance and current collapse in AlGaN/GaN insulated gate high-electron mobility transistors on Si (1 1 1) substrate with very thin SiO2 gate dielectric," *Semicond. Sci. Technol.,* vol. 27, p. 125001,

2012.

[103] R. Mehandru, B. Luo, J. Kim, F. Ren, B. P. Gila, A. H. Onstine, C. R. Abernathy, S. J. Pearton, D. Gotthold, R. Birkhahn, B. Peres, R. Fitch, J. Gillespie, T. Jenkins, J. Sewell, D. Via and A. Crespo, "AlGaN/GaN metal-oxide-semiconductor high electron mobility transistors using Sc2O3 as the gate oxide and surface passivation," *Appl. Phys. Lett.*, vol. 82, no. 15, pp. 2530-2532, 2003.

[104] H. Kim, R. M. Thompson, V. Tilak, T. R. Prunty, J. R. Shealy and L. Eastman, "Effects of SiN passivation and high-electric field on AlGaN-GaN HFET degradation," *IEEE Electron Device Lett.*, vol. 24, no. 7, pp. 421-423, 2003.

[105] S. Arulkumaran, T. Egawa, H. Ishikawa, T. Jimbo and Y. Sano, "Surface passivation effects on AlGaN/GaN high-electron-mobility transistors with SiO2, Si3N4 and silicon oxynitride," *Appl. Phys. Lett.*, vol. 84, no. 4, pp. 613-615, 2004.

[106] A. P. Edwards, J. A. Mittereder, S. C. Binari, D. S. Katzer, D. F. Storm and J. A. Roussos, "Improved reliability of AlGaN-GaN HEMTs using an NH3 plasma treatment prior to SiN passivation," *IEEE Electron Device Lett.*, vol. 26, no. 4, pp. 225-227, 2005.

[107] C. Zhang, Y. Hao and Q. Feng, "Effective surface passivation of

AlGaN/GaN heterostructures by using PH3 plasma treatment and HfO2 dielectric," *Phys. Status Solidi C*, vol. 9, no. 3-4, pp. 934-937, 2012.

[108] R. Wang, G. Li, O. Laboutin, Y. Cao, W. Johnson, G. Snider, P. Fay, D. Jena and H. Xing, "210-GHz InAlN/GaN HEMTs With Dielectric-Free Passivation," *IEEE Electron Device Lett.*, vol. 32, no. 7, pp. 892-894, 2011.

[109] O. Ambacher, J. Smart, J. R. Shealy, N. G. Weimann, K. Chu, M. Murphy, W. J. Schaff, L. F. Eastman, R. Dimitrov, L. Wittmer, M. Stutzmann, W. Rieger and J. Hilsenbeck, "Two-dimensional electron gases induced by spontaneous and piezoelectric polarization charges in N- and Ga-face AlGaN/GaN heterostructures," *J. Appl. Phys.*, vol. 85, no. 6, pp. 3222-3233, 1999.

[110] I. P. Smorchkova, C. R. Elsass, J. P. Ibbetson, R. Vetury, B. Heying, P. Fini, E. Haus, S. P. DenBaars, J. S. Speck and U. K. Mishra, "Polarization-induced charge and electron mobility in AlGaN/GaN heterostructures grown by plasma-assisted molecular-beam epitaxy," *J. Appl. Phys.*, vol. 86, pp. 4520-4526, 1999.

[111] J. Joh and J. A. d. Alamo, "Mechanisms for electrical degradation of GaN high-electron mobility transistors," *IEDM Tech. Dig.*, pp. 415-418, 2006.

[112] J. Joh, J. A. d. Alamo and J. Jimenez, "A simple current collapse measurement technique for GaN high-electron mobility transistors," *IEEE*

Electron Device Lett., vol. 29, no. 7, pp. 665-667, 2008.

[113] J. A. Mittereder, S. C. Binari, P. B. Klein, J. A. Roussos, D. S. Katzer, D. F. Storm, D. D. Koleske, A. E. Wickenden and R. L. Henry, "Current collapse induced in AlGaN/GaN high-electron-mobility transistors by bias stress," *Appl. Phys. Lett.*, vol. 83, no. 8, pp. 1650-1652, 2003.

[114] T. Mizutani, Y. Ohno, M. Akita, S. Kishimoto and K. Maezawa, "A study on current collapse in AlGaN/GaN HEMTs induced by bias stress," *IEEE Trans. Electron Devices*, vol. 50, no. 10, pp. 2015-2020, 2003.

[115] A. P. Zhang, E. B. Kaminsky, A. F. Allen, J. W. Hedrick, A. Vertiatchikh and L. F. Eastman, "Stability of AlGaN/GaN high-power HEMTs under DC and RF stresses," *Electron Lett.*, vol. 40, no. 19, pp. 1229-1230, 2004.

[116] J. A. d. Alamo and J. Joh, "GaN HEMT reliability," *Microelectron. Reliab.*, vol. 49, no. 5, pp. 1200-1206, 2009.

[117] D. Brunner, H. Angerer, E. Bustarret, F. Freudenberg, R. Hopler, R. Dimitrov, O. Ambacher and M. Stutzmann, "polarization in undoped and doped AlGaN/GaN heterostructures," *J. Appl. Phys.*, vol. 82, p. 5090, 1997.

[118] F. V. Fiorentini and O. Ambacher, "Evidence for nonlinear macroscopic polarization in III–V nitride alloy heterostructures," *Appl. Phys. Lett.*, vol. 80, p. 1204, 2002.

[119] T. Hashizume, S. Ootomo and H. Hasegawa, "Suppression of current collapse in insulated gate AlGaN/GaN heterostructure field-effect transistors using ultrathin Al2O3 dielectric," *Appl. Phys. Lett.*, vol. 83, no. 14, pp. 2952-2954, 2003.

[120] W. D. Hu, X. S. Chen, F. Yin, J. B. Zhang and W. Lu, "Two-dimensional transient simulations of drain lag and current collapse in GaN-based high-electron-mobility transistors," *J. Appl. Phys.*, vol. 105, p. 084502, 2009.

[121] J. R. Shealy, V. Kaper, V. Tilak, T. Prunty, J. A. Smart, B. Green and L. F. Eastman, "An AlGaN/GaN high-electron-mobility transistor with an AlN sub-buffer layer," *J. Phys. Condens. Matter*, vol. 14, pp. 3499-3509, 2002.

[122] D. Ducatteau, A. Minko, V. Hoel, E. Morvan, E. Delos, B. Grimbert, H. Lahreche, P. Bove, C. Gaquiere, J. De Jaeger and S. Delage, "Output power density of 5.1/mm at 18 GHz with an AlGaN/GaN HEMT on Si substrate," *IEEE Electron Device Lett.*, vol. 27, no. 1, pp. 7-9, 2006.

[123] K. Horio, A. Nakajima and K. Itagaki, "Analysis of field-plate effects on buffer-related lag phenomena and current collapse in GaN MESFETs and AlGaN/GaN HEMTs," *Semicond. Sci. Technol.*, vol. 24, no. 8, p. 085022, 2009.

[124] S.-H. Lo and C.-P. Lee, "Analysis of surface state effect on gate lag phenomena in GaAs MESFET's," *IEEE Trans. Electron Devices*, vol. 41,

pp. 1504-1511, 1994.

[125] W. Tan, M. Uren, P. Houston, R. Green, R. Balmer and T. Martin, "Surface leakage currents in SiNx passivated AlGaN/GaN HFETs," *IEEE Electron Device Lett.*, vol. 27, no. 1, pp. 1-3, 2006.

[126] O. Mitrofanov and M. Manfra, "Dynamics of trapped charge in GaN/AlGaN/GaN high electron mobility transistors grown by plasma-assisted molecular beam epitaxy," *Appl. Phys. Lett.*, vol. 84, no. 3, pp. 422-424, 2004.

[127] P. Kordoš, R. Stoklas, D. Gregušová and J. Novák, "Characterization of AlGaN/GaN metal-oxide-semiconductor field-effect transistors by frequency dependent conductance analysis," *Appl. Phys. Lett.*, vol. 94, p. 223512, 2009.

[128] S. Zafar, A. Kumar, E. Gusev and E. Cartier, "Threshold voltage instabilites in high-k gate dielectric stacks," *IEEE Trans. Device Mater. Rel.*, vol. 5, no. 1, pp. 45-64, 2005.

[129] B. H. Lee, R. Choi, J. H. Sim, S. A. Krishnan, J. J. Peterson, G. A. Brown and G. Bersuker, "Validity of constant voltage stress based reliability assessment of high-k devices," *IEEE Trans. Device Mater. Rel.*, vol. 5, no. 1, pp. 20-25, 2005.

[130] G. Ribes, J. Mitard, M. Denais, S. Bruyere, F. Monsieur, C. Parthasarathy, E. Vincent and G. Ghibaudo, "Review on high-k dielectrics reliability issues," *IEEE Trans. Device Mater. Rel.*, vol. 5, no. 1, pp. 5-19, 2005.

[131] A. P. Zhang, L. B. Rowland, E. B. Kaminsky, V. Tilak, J. C. Grande, J. Teetsov, A. Vertiatchikh and L. F. Eastman, "Correlation of Device Performance and Defects in AlGaN/GaN High-Electron Mobility Transistors," *J. Electron. Mater.*, vol. 32, no. 5, pp. 388-394, 2003.

[132] M. J. Uren, J. Möreke and M. Kuball, "Buffer Design to Minimize Current Collapse in GaN/AlGaN HFETs," *IEEE Trans. Electron Devices*, vol. 59, no. 12, pp. 3327-3333, 2012.

[133] C. D. Young, Y. Zhao, M. Pendley, B. H. Lee, K. Matthews, J. H. Sim, R. Choi, G. A. Brown, R. W. Murto and G. Bersuker, "Ultra-Short Pulse Current–Voltage Characterization of the Intrinsic Characteristics of High-κ Devices," *Jpn. J. Appl. Phys.*, vol. 44, no. 4B, pp. 2437-2440, 2005.

[134] D. Bisi, M. Meneghini, C. d. Santi, A. Chini, M. Dammann, P. Brückner, M. Mikulla, G. Meneghesso and E. Zanoni, "Deep-Level Characterization in GaN HEMTs-Part I: Advantages and Limitations of Drain Current Transient Measurements," *IEEE Trans. Electron Devices*, vol. 60, no. 10, pp. 3166-3175, 2013.

[135] P. P. Debye and E. M. Conwell, "Electrical properties of n-type

germanium," *Phys. Rev.*, vol. 93, pp. 693-706, 1954.

[136] A. G. Sabnis and J. T. Clemens, "Characterization of electron mobility in the inverted (100) Si surface," *IEDM Tech, Dig.*, pp. 18-21, 1979.

[137] S. C. Sun and J. D. Plummer, "Electron mobility in inversion and accumulation layers on thermally oxidised silicon surfaces," *IEEE Trans. Electron Devices*, vol. 27, pp. 1497-1508, 1980.

[138] K. Yamaguchi, "Field-dependent mobility model for two-dimensional numerical analysis MOSFETs," *IEEE Trans. Electron Devices,* vol. 26, pp. 1068-1074, 1979.

[139] G. Baccarini, A. M. Mazzoni and C. Morandi, "The diffuse scattering model of effective mobility in the strongly inverted layer of MOS transistors," *Solid-State Electron,* vol. 17, p. 785, 1974.

[140] A. Pérez-Tomás, M. Placidi, X. Perpiñà, A. Constant, P. Godignon, X. Jordà, P. Brosselard and J. Millán, "GaN metal-oxide-semiconductor field-effect transistor inversion channel mobility modeling," *J. Appl. Phys.,* vol. 105, p. 114510, 2009.

[141] D. M. Caughey and R. E. Thomas, "Carrier mobility in silicon empirically related to doping and field," *Proc. IEEE*, vol. 55, pp. 2192-2193, 1967.

[142] G. Baccarani and P. Ostoja, "Electron mobility empirically related to the

phosphorus concentration," *Solid-State Electron*, vol. 18, no. 6, pp. 579-580, 1975.

[143] C. Jacoboni, C. Canali, G. Ottaviani and A. A. Quaranta, "A review of some charge transport properties of silicon," *Solid-State Electronics*, vol. 20, pp. 77-89, 1977.

[144] A. Hartstein, T. H. Ning and A. B. Fowler, "Electron scattering in silicon inversion layers by oxide and surface roughness," *Surface Sci.*, vol. 58, pp. 178-181, 1976.

[145] S. M. Goodnick, R. G. Gann, D. K. Ferry, C. W. Wilmsen and O. L. Krivanek, "Surface roughness induced scattering and band tailing," *Surface Sci.*, vol. 113, pp. 233-238, 1982.

[146] A. Hartstein, A. B. Fowler and M. Albert, "Temperature dependence of scattering in the inversion layer," *Surface Sci.*, vol. 98, pp. 181-190, 1980.

[147] D. S. Jeon and D. E. Burk, "MOSFET electron inversion layer mobilities - a physically based semi-empirical model for a wide temperature range," *IEEE Trans. Electron Devices*, vol. 36, no. 8, pp. 1456-1463, 1989.

[148] J. Gillespie, R. Fitch, J. Sewell, R. Dettmer, G. Via, A. Crespo, T. Jenkins, B. Luo, R. Mehandru, J. Kim, F. Ren, B. Gila, A. Onstine, C. Abernathy and S. Pearton, "Effects of Sc2O3 and MgO passivation layers on the output power of AlGaN/GaN HEMTs," *IEEE Electron Device Lett.*, vol. 23, no. 9,

pp. 505-507, 2002.

[149] B. M. Green, K. K. Chu, E. M. Chumbes, J. Smart, J. Shealy and L. Eastman, "The Effect of Surface Passivation on the Microwave Characteristics of Undoped AlGaN/GaN HEMT's," *IEEE Electron Device Lett.,* vol. 21, no. 6, pp. 268-270, 2000.

[150] J. Bernát, P. Javorka, A. Fox, M. Marso, H. Lüth and P. Kordoš, "Effect of surface passivation on performance of AlGaN/GaN/Si HEMTs," *Solid-State Electron.,* vol. 47, pp. 2097-2103, 2003.

[151] A. Chini, M. Esposto, G. Meneghesso and E. Zanoni, "Evaluation of GaN HEMT degradation by means of pulsed I-V, leakage and DLTS measurements," *Electron. Lett.,* vol. 45, no. 8, pp. 426-427, 2009.

[152] M.-Y. Kao, K. H. G. Duh, P. Ho and P.-C. Chao, "An extremely low-noise InP-based HEMT with silicon nitride passivation," *IEDM Tech. Dig.,* pp. 907-910, 1994.

[153] A. T. Winzer, R. Goldhahn, G. Gobsch, A. Link, M. Eickhoff, U. Rossow and A. Hangleiter, "Determination of the polarization discontinuity at the AlGaN/GaN interface by electroreflectance spectroscopy," *Appl. Phys. Lett.,* vol. 86, p. 181912, 2005.

Appendix A: TCAD simulation fitting code for unpassivated device (Chapter 3)

```
go atlas simflag="-v 5.16.3.r"
mesh auto width=1000
set thickness=0.007

x.m l=0    s=0.2
x.m l=0.5  s=0.1
x.m l=1    s=0.1
x.m l=13.  s=0.1
x.m l=14   s=0.2

y.m l=-0.02   s=0.05
y.m l=-0.0075 s=0.005
y.m l=-0.007  s=0.00025
y.m l=-0.0035 s=0.002
y.m l=0.0     s=0.00025
y.m l=0.0125  s=0.005
y.m l=0.02    s=0.0001
y.m l=0.0275  s=0.001
y.m l=0.03    s=0.01
y.m l=0.05    s=0.05
y.m l=0.1     s=0.1
y.m l=0.2     s=0.2
y.m l=0.5     s=0.5
y.m l=1       s=0.2
y.m l=2       s=0.2
y.m l=2.9995  s=0.2
y.m l=3       s=0.00025
y.m l=3.0005  s=1
y.m l=4       s=1
eliminate columns x.min=0 x.max=14 y.min=0.1

region num=1 x.min=0 x.max=14 y.min=0 y.max=0.02 mat=algan x.comp=0.25 donor=1e15
region num=2 x.min=0 x.max=14 y.min=-0.02 y.max=0 mat=sio2 insulator
region num=3 x.min=0 x.max=14 y.min=-$thickness y.max=0 material=hfo2
region num=4 x.min=0 x.max=14 y.min=0.02 y.max=1 mat=gan donors=1e15
region num=5 x.min=0 x.max=14 y.min=1 y.max=3 mat=gan acceptor=3e17
region num=6 x.min=0 x.max=14 y.min=3 y.max=4 mat=sapphire insulator

elec num=1 name=source x.min=0 x.max=1 y.min=-0.02 y.max=0.03
elec num=2 name=drain x.min=13 x.max=14 y.min=-0.02 y.max=0.03
elec num=3 name=gate x.min=6 x.max=8 y.min=-0.02 y.max=-$thickness
elec num=4 substrate

interface charge=1.04008e13 y.min=0.02 y.max=0.0205 s.s
interface charge=-2.57861e13 y.min=0 y.max=0.0005 s.i
interface charge=1.53853e13 y.min=2.9995 y.max=3 s.i
```

```
inttrap donor e.level=3.54 density=2.96e13 degen=1 sign=1e-15 sigp=1e-15 y.min=-0.0005 y.max=0.01 s.i
inttrap acceptor e.level=2.91 density=6.0e12 degen=1 sign=1e-15 sigp=1e-15 y.min=-0.0005 y.max=0.01 s.i

material mat=algan align=0.75 eg300=3.91
material mat=sio2 affinity=1.0
material mat=hfo2 eg300=6.4 permittivity=19 affinity=2.1
models prpmob albrct fermi print srh hei fnord fnholes nearflg f.ae=5e-6 f.be=4.2e6
mobility albrct.n an.albrct=3e-3 bn.albrct=3e-4 cn.albrct=3.6e-2 vsatn=3e7
contact name=gate workfunction=4.8
output con.band val.band charge band.par qss e.mobility
method trap autonr newton maxtrap=100 tol.relax=100
mobility gansat.n

solve
save outf=is_85pol_c12_mob.str

solve init
solve vgate=0
solve vdrain=0

log outfile=ramp_vd.log
solve vdrain=0 vfinal=5 vstep=0.05 name=drain
save outf=ramp_vd.str
log off

log outfile=ramp_vg.log
solve vgate=0 vfinal=0 vstep=0.05 name=gate
log off

log outf=idvg_vd5_85pol_c12c5a.log
solve vgate=0 vfinal=-10 vstep=-0.05 name=gate
save outf=idvg_vd5_85pol_c12c5a.str
log off

quit
```

Appendix B: TCAD simulation fitting code for passivated device (Chapter 3)

```
go atlas simflag="-v 5.16.3.r"
mesh auto width=1000
set thickness=0.007

x.m l=0    s=0.2
x.m l=0.5  s=0.1
x.m l=1    s=0.1
x.m l=13.  s=0.1
x.m l=14   s=0.2

y.m l=-0.02   s=0.05
y.m l=-0.0075 s=0.005
y.m l=-0.007  s=0.00025
y.m l=-0.0035 s=0.002
y.m l=0.0     s=0.00025
y.m l=0.0125  s=0.005
y.m l=0.02    s=0.0001
y.m l=0.0275  s=0.001
y.m l=0.03    s=0.001
y.m l=0.05    s=0.01
y.m l=0.1     s=0.1
y.m l=0.2     s=0.2
y.m l=0.5     s=0.5
y.m l=1       s=0.2
y.m l=2       s=0.2
y.m l=2.9995  s=0.2
y.m l=3       s=0.00025
y.m l=3.0005  s=1
y.m l=4       s=1
eliminate columns x.min=0 x.max=14 y.min=0.1

region num=1 x.min=0 x.max=14 y.min=0 y.max=0.02 mat=algan x.comp=0.25 donor=1e15
region num=2 x.min=0 x.max=14 y.min=-0.02 y.max=0 mat=sio2 insulator
region num=3 x.min=0 x.max=14 y.min=-$thickness y.max=0 material=hfo2
region num=4 x.min=0 x.max=14 y.min=0.02 y.max=1 mat=gan donors=1e15
region num=5 x.min=0 x.max=14 y.min=1 y.max=3 mat=gan acceptor=3e17
region num=6 x.min=0 x.max=14 y.min=3 y.max=4 mat=sapphire insulator

elec num=1 name=source x.min=0 x.max=1 y.min=-0.02 y.max=0.03
elec num=2 name=drain x.min=13 x.max=14 y.min=-0.02 y.max=0.03
elec num=3 name=gate x.min=6 x.max=8 y.min=-0.02 y.max=-$thickness
elec num=4 substrate


interface charge=1.04008e13 y.min=0.02 y.max=0.0205 s.s
interface charge=-2.57861e13 y.min=0 y.max=0.0005 s.i
interface charge=1.53853e13 y.min=2.9995 y.max=3 s.i
```

```
inttrap donor e.level=3.54 density=2.96e13 degen=1 sign=1e-15 sigp=1e-15 y.min=-0.0005 y.max=0.01 s.i

material mat=algan align=0.75 eg300=3.91
material mat=sio2 affinity=1.0
material mat=hfo2 eg300=6.4 permittivity=19 affinity=2.1
models prpmob albrct fermi print srh hei fnord fnholes nearflg f.ae=1e-7 f.be=1.78e7
mobility albrct.n an.albrct=3e-3 bn.albrct=3e-4 cn.albrct=1.95e-2 vsatn=3e7
contact name=gate workfunction=4.8
output con.band val.band charge band.par qss e.mobility
method trap autonr newton maxtrap=100 tol.relax=100
mobility gansat.n

solve
save outf=is_85pol_pass_mob.str

solve init
solve vgate=0
solve vdrain=0

log outfile=ramp_vd.log
solve vdrain=0 vfinal=5 vstep=0.05 name=drain
log off

log outfile=ramp_vg.log
solve vgate=0 vfinal=0 vstep=0.05 name=gate
log off

log outf=idvg_vd5_85pol_pass3.log
solve vgate=0 vfinal=-10 vstep=-0.05 name=gate
save outf=idvg_vd5_85pol_pass3.str
log off

quit
```

Appendix C: TCAD simulation fitting of I_D-V_{GS} at T = 370 K (Chapter 4)

```
go atlas simflag="-v 5.16.3.r"
mesh auto width=1000
set thickness=0.01

x.m l=0    s=0.4
x.m l=0.5  s=0.4
x.m l=10    s=0.4
x.m l=20    s=0.4
x.m l=29.5  s=0.4
x.m l=30   s=0.4

y.m l=-0.02   s=0.05
y.m l=-0.0105 s=0.005
y.m l=-0.01   s=0.0005
y.m l=-0.0045 s=0.002
y.m l=0.0     s=0.0005
y.m l=0.0125  s=0.005
y.m l=0.025   s=0.0002
y.m l=0.0275  s=0.001
#y.m l=0.0325  s=0.005
y.m l=0.05    s=0.005
y.m l=0.1     s=0.01
y.m l=1       s=0.1
y.m l=4.215   s=0.1
y.m l=4.22    s=0.0005
y.m l=4.225   s=1
y.m l=5.225   s=1

eliminate columns x.min=0 x.max=30 y.min=0.1

region num=1 x.min=0 x.max=30 y.min=0 y.max=0.025 mat=algan x.comp=0.25 donor=1e15
region num=2 x.min=0 x.max=30 y.min=-0.02 y.max=0 mat=air
region num=3 x.min=0 x.max=30 y.min=-$thickness y.max=0 material=al2o3
region num=4 x.min=0 x.max=30 y.min=0.025 y.max=0.325 mat=gan donor=8e16
region num=5 x.min=0 x.max=30 y.min=0.325 y.max=4.225 mat=gan acceptor=5e19
region num=6 x.min=0 x.max=30 y.min=4.225 y.max=5.225 mat=si insulator

elec num=1 name=source x.min=0 x.max=1 y.min=-0.02 y.max=0.03
elec num=2 name=drain x.min=29 x.max=30 y.min=-0.02 y.max=0.03
elec num=3 name=gate x.min=10 x.max=20 y.min=-0.02 y.max=-$thickness
elec num=4 substrate

interface charge=1.04008e13 y.min=0.025 y.max=0.0255 s.s
interface charge=-2.57861e13 y.min=-0.0005 y.max=0 s.s
interface charge=1.53853e13 y.min=4.222 y.max=4.23 s.i

inttrap donor e.level=3.468 density=1.43e13 degen=1 taun=2.4 sigp=1e-15 y.min=-0.0005
y.max=0.01 s.s
```

```
inttrap donor e.level=3.328 density=1.07e13 degen=1 taun=7.5 sigp=1e-15 y.min=-0.0005 y.max=0.01 s.s

#t=370k
material mat=gan eg300=3.405
material mat=algan eg300=3.788
material mat=al2o3 permittivity=9 eg300=7
models albrct print srh hei fnord fnholes nearflg fermi joule.heat temp=370 f.ae=2.5e-7 f.be=5.72e7
contact name=gate workfunction=4.7
contact name=source con.resist=1.95e-4
contact name=drain con.resist=1.95e-4
output con.band val.band charge band.par qss e.mobility
mobility  an.albrct=2.61e-4 bn.albrct=2.9e-4 cn.albrct=1e-4
method trap autonr newton maxtrap=100 tol.relax=100

solve
save outf=hemt_370k_1d2a.str

solve init
solve vgate=0
solve vdrain=0

log outfile=ramp_vd.log
solve vdrain=0 vfinal=1 vstep=0.05 name=drain
save outf=ramp_vd.str
log off

log outf=idvg_vd1_370k_1d2a.log
solve vgate=0 vfinal=-9 vstep=-0.1 name=gate
save outf=idvg_vd1_370k_1d2a.str
log off

quit
```

Appendix D: TCAD simulation fitting of pulsed I_D-V_{GS} at ($V_{GS,Q}$, $V_{DS,Q}$) = (0 V, 0 V) (Chapter 5)

```
go atlas simflag="-v 5.16.3.r"
mesh auto width=1000
set thickness=0.007

x.m l=0    s=0.25
x.m l=1    s=0.25
x.m l=2    s=0.25
x.m l=4    s=0.25
x.m l=6    s=0.25
x.m l=14   s=0.25
x.m l=19   s=0.25
x.m l=20   s=0.25
x.m l=29   s=0.25
x.m l=30   s=0.25

y.m l=-0.02   s=0.01
y.m l=-0.0075 s=0.005
y.m l=-0.007   s=0.0005
y.m l=-0.0045 s=0.002
y.m l=0.0     s=0.0005
y.m l=0.0125  s=0.005
y.m l=0.025   s=0.0002
y.m l=0.0275  s=0.001
y.m l=0.0325  s=0.002
y.m l=0.06    s=0.004
y.m l=0.1     s=0.1
y.m l=4.215   s=0.1
y.m l=4.22    s=0.0005
y.m l=4.225   s=1
y.m l=5.225   s=1

eliminate columns x.min=0 x.max=30 y.min=0.1

region num=1 x.min=0 x.max=30 y.min=0 y.max=0.025 mat=algan x.comp=0.25 donor=1e15
region num=2 x.min=0 x.max=30 y.min=-0.02 y.max=0 mat=air
region num=3 x.min=0 x.max=30 y.min=-$thickness y.max=0 material=al2o3
region num=4 x.min=0 x.max=30 y.min=0.025 y.max=0.325 mat=gan donor=4e16
region num=5 x.min=0 x.max=30 y.min=0.325 y.max=4.225 mat=gan acceptor=5e16
region num=6 x.min=0 x.max=30 y.min=4.225 y.max=5.225 mat=si insulator

elec num=1 name=source x.min=0 x.max=1 y.min=-0.02 y.max=0.03
elec num=2 name=drain x.min=29 x.max=30 y.min=-0.02 y.max=0.03
elec num=3 name=gate x.min=11 x.max=19 y.min=-0.02 y.max=-$thickness
elec num=4 substrate
```

```
interface charge=1.3854e13 y.min=0.025 y.max=0.0255 s.s
interface charge=-3.1954e13 y.min=-0.0005 y.max=0 s.s
interface charge=1.81e13 y.min=4.222 y.max=4.23 s.i

inttrap donor e.level=3.46 density=3.05e13 degen=1 sign=1e-15 sigp=1e-15 y.min=-0.0005 y.max=0.01 s.s

material mat=gan eg300=3.437
material mat=algan eg300=3.83
material mat=al2o3 permittivity=9 eg300=7
models print srh hei fnord fnholes nearflg fermi f.ae=7e-7 f.be=7e7 cvt
contact name=gate workfunction=5.01
output con.band val.band charge band.par qss e.mobility
mobility mu0n.cvt=100 crn.cvt=3e17 mumaxn.cvt=2850 gamn.cvt=3 alphn.cvt=0.7 bn.cvt=9e7 cn.cvt=3.23e6 deln.cvt=2.1e17 kn.cvt=2.3
method trap autonr newton maxtrap=100 tol.relax=100

solve
save outf=hemt_p0_cvt_g1.str

solve init
solve vgate=0
solve vdrain=0

log outfile=ramp_vd.log
solve vdrain=0 vfinal=1 vstep=0.05 name=drain
save outf=ramp_vd.str
log off

log outf=pulse_p0_g1.log
solve vgate=0 vfinal=-9 vstep=-0.05 name=gate
save outf=pulse_p0_g1.str
log off

quit
```

Appendix E: TCAD simulation fitting of pulsed I_D-V_{GS} at ($V_{GS,Q}$, $V_{DS,Q}$) = (0.5 V, 0 V) (Chapter 5)

```
go atlas simflag="-v 5.16.3.r"
mesh auto width=1000
set thickness=0.007

x.m l=0    s=0.25
x.m l=1    s=0.25
x.m l=2    s=0.25
x.m l=4    s=0.25
x.m l=6    s=0.25
x.m l=14   s=0.25
x.m l=19   s=0.25
x.m l=20   s=0.25
x.m l=29   s=0.25
x.m l=30   s=0.25

y.m l=-0.02   s=0.01
y.m l=-0.0075 s=0.005
y.m l=-0.007   s=0.0005
y.m l=-0.0045 s=0.002
y.m l=0.0     s=0.0005
y.m l=0.0125  s=0.005
y.m l=0.025   s=0.0002
y.m l=0.0275  s=0.001
y.m l=0.0325  s=0.002
y.m l=0.06    s=0.004
y.m l=0.1     s=0.1
y.m l=4.215   s=0.1
y.m l=4.22    s=0.0005
y.m l=4.225   s=1
y.m l=5.225   s=1

eliminate columns x.min=0 x.max=30 y.min=0.1

region num=1 x.min=0 x.max=30 y.min=0 y.max=0.025 mat=algan x.comp=0.25 donor=1e15
region num=2 x.min=0 x.max=30 y.min=-0.02 y.max=0 mat=air
region num=3 x.min=0 x.max=30 y.min=-$thickness y.max=0 material=al2o3
region num=4 x.min=0 x.max=30 y.min=0.025 y.max=0.325 mat=gan donor=4e16
region num=5 x.min=0 x.max=30 y.min=0.325 y.max=4.225 mat=gan acceptor=5e16
region num=6 x.min=0 x.max=30 y.min=4.225 y.max=5.225 mat=si insulator

elec num=1 name=source x.min=0 x.max=1 y.min=-0.02 y.max=0.03
elec num=2 name=drain x.min=29 x.max=30 y.min=-0.02 y.max=0.03
elec num=3 name=gate x.min=11 x.max=19 y.min=-0.02 y.max=-$thickness
elec num=4 substrate
```

```
interface charge=1.3854e13 y.min=0.025 y.max=0.0255 s.s
interface charge=-3.1954e13 y.min=-0.0005 y.max=0 s.s
interface charge=1.81e13 y.min=4.222 y.max=4.23 s.i

inttrap donor e.level=3.46 density=3.05e13 degen=1 sign=1e-15 sigp=1e-15 x.min=0 x.max=9
y.min=-0.0005 y.max=0.01 s.s

inttrap donor e.level=3.46 density=2.97e13 degen=1 sign=1e-15 sigp=1e-15 x.min=9 x.max=21
y.min=-0.0005 y.max=0.01 s.s

inttrap donor e.level=3.46 density=3.05e13 degen=1 sign=1e-15 sigp=1e-15 x.min=21 x.max=30
y.min=-0.0005 y.max=0.01 s.s

material mat=gan eg300=3.437
material mat=algan eg300=3.83
material mat=al2o3 permittivity=9 eg300=7
models print srh hei fnord fnholes nearflg fermi joule.heat f.ae=7e-7 f.be=7e7 cvt
contact name=gate workfunction=5.01
output con.band val.band charge band.par qss e.mobility
mobility mu0n.cvt=100 crn.cvt=3e17 mumaxn.cvt=2920 gamn.cvt=3 alphn.cvt=0.7 bn.cvt=9e7
cn.cvt=3.23e6 deln.cvt=2.1e17 kn.cvt=2.3
method trap autonr newton maxtrap=100 tol.relax=100

solve
save outf=hemt_p0.5_cvt_g1.str

solve init
solve vgate=0
solve vdrain=0

log outfile=ramp_vd.log
solve vdrain=0 vfinal=1 vstep=0.05 name=drain
save outf=ramp_vd.str
log off

log outf=pulse_p0.5_g1.log
solve vgate=0 vfinal=-9 vstep=-0.1 name=gate
save outf=pulse_p0.5_g1.str
log off

quit
```

Appendix F: TCAD simulation fitting of pulsed I_D-V_{GS} at ($V_{GS,Q}$, $V_{DS,Q}$) = (1.0 V, 0 V) (Chapter 5)

```
go atlas simflag="-v 5.16.3.r"
mesh auto width=1000
set thickness=0.007

x.m l=0    s=0.25
x.m l=1    s=0.25
x.m l=2    s=0.25
x.m l=4    s=0.25
x.m l=6    s=0.25
x.m l=14   s=0.25
x.m l=19   s=0.25
x.m l=20   s=0.25
x.m l=29   s=0.25
x.m l=30   s=0.25

y.m l=-0.02   s=0.01
y.m l=-0.0075 s=0.005
y.m l=-0.007   s=0.0005
y.m l=-0.0045 s=0.002
y.m l=0.0      s=0.0005
y.m l=0.0125  s=0.005
y.m l=0.025   s=0.0002
y.m l=0.0275  s=0.001
y.m l=0.0325  s=0.002
y.m l=0.06    s=0.004
y.m l=0.1      s=0.1
y.m l=4.215   s=0.1
y.m l=4.22    s=0.0005
y.m l=4.225   s=1
y.m l=5.225   s=1

eliminate columns x.min=0 x.max=30 y.min=0.1

region num=1 x.min=0 x.max=30 y.min=0 y.max=0.025 mat=algan x.comp=0.25 donor=1e15
region num=2 x.min=0 x.max=30 y.min=-0.02 y.max=0 mat=air
region num=3 x.min=0 x.max=30 y.min=-$thickness y.max=0 material=al2o3
region num=4 x.min=0 x.max=30 y.min=0.025 y.max=0.325 mat=gan donor=4e16
region num=5 x.min=0 x.max=30 y.min=0.325 y.max=4.225 mat=gan acceptor=5e16
region num=6 x.min=0 x.max=30 y.min=4.225 y.max=5.225 mat=si insulator

elec num=1 name=source x.min=0 x.max=1 y.min=-0.02 y.max=0.03
elec num=2 name=drain x.min=29 x.max=30 y.min=-0.02 y.max=0.03
elec num=3 name=gate x.min=11 x.max=19 y.min=-0.02 y.max=-$thickness
elec num=4 substrate
```

```
interface charge=1.3854e13 y.min=0.025 y.max=0.0255 s.s
interface charge=-3.1954e13 y.min=-0.0005 y.max=0 s.s
interface charge=1.81e13 y.min=4.222 y.max=4.23 s.i

inttrap donor e.level=3.46 density=3.05e13 degen=1 sign=1e-15 sigp=1e-15 x.min=0 x.max=9 y.min=-0.0005 y.max=0.01 s.s

inttrap donor e.level=3.46 density=2.86e13 degen=1 sign=1e-15 sigp=1e-15 x.min=9 x.max=21 y.min=-0.0005 y.max=0.01 s.s

inttrap donor e.level=3.46 density=3.05e13 degen=1 sign=1e-15 sigp=1e-15 x.min=21 x.max=30 y.min=-0.0005 y.max=0.01 s.s

material mat=gan eg300=3.437
material mat=algan eg300=3.83
material mat=al2o3 permittivity=9 eg300=7
models print srh hei fnord fnholes nearflg fermi joule.heat f.ae=7e-7 f.be=7e7 cvt
contact name=gate workfunction=5.01
output con.band val.band charge band.par qss e.mobility
mobility mu0n.cvt=100 crn.cvt=3e17 mumaxn.cvt=2950 gamn.cvt=3 alphn.cvt=0.7 bn.cvt=9e7 cn.cvt=3.23e6 deln.cvt=2.1e17 kn.cvt=2.3
method trap autonr newton maxtrap=100 tol.relax=100

solve
save outf=hemt_p1.0_cvt_g1.str
#tonyplot hemt_p1.0_cvt_g1.str

solve init
solve vgate=0
solve vdrain=0

log outfile=ramp_vd.log
solve vdrain=0 vfinal=1 vstep=0.05 name=drain
save outf=ramp_vd.str
log off

log outf=pulse_p1.0_g1.log
solve vgate=0 vfinal=-9 vstep=-0.05 name=gate
save outf=pulse_p1.0_g1.str
log off

quit
```

Appendix G: TCAD simulation fitting of pulsed I_D-V_{GS} at ($V_{GS,Q}$, $V_{DS,Q}$) = (1.5 V, 0 V) (Chapter 5)

```
go atlas simflag="-v 5.16.3.r"
mesh auto width=1000
set thickness=0.007

x.m l=0    s=0.25
x.m l=1    s=0.25
x.m l=2    s=0.25
x.m l=4    s=0.25
x.m l=6    s=0.25
x.m l=14   s=0.25
x.m l=19   s=0.25
x.m l=20   s=0.25
x.m l=29   s=0.25
x.m l=30   s=0.25

y.m l=-0.02   s=0.01
y.m l=-0.0075 s=0.005
y.m l=-0.007   s=0.0005
y.m l=-0.0045 s=0.002
y.m l=0.0     s=0.0005
y.m l=0.0125  s=0.005
y.m l=0.025   s=0.0002
y.m l=0.0275  s=0.001
y.m l=0.0325  s=0.002
y.m l=0.06    s=0.004
y.m l=0.1     s=0.1
y.m l=4.215   s=0.1
y.m l=4.22    s=0.0005
y.m l=4.225   s=1
y.m l=5.225   s=1

eliminate columns x.min=0 x.max=30 y.min=0.1

region num=1 x.min=0 x.max=30 y.min=0 y.max=0.025 mat=algan x.comp=0.25 donor=1e15
region num=2 x.min=0 x.max=30 y.min=-0.02 y.max=0 mat=air
region num=3 x.min=0 x.max=30 y.min=-$thickness y.max=0 material=al2o3
region num=4 x.min=0 x.max=30 y.min=0.025 y.max=0.325 mat=gan donor=4e16
region num=5 x.min=0 x.max=30 y.min=0.325 y.max=4.225 mat=gan acceptor=5e16
region num=6 x.min=0 x.max=30 y.min=4.225 y.max=5.225 mat=si insulator

elec num=1 name=source x.min=0 x.max=1 y.min=-0.02 y.max=0.03
elec num=2 name=drain x.min=29 x.max=30 y.min=-0.02 y.max=0.03
elec num=3 name=gate x.min=11 x.max=19 y.min=-0.02 y.max=-$thickness
elec num=4 substrate
```

```
interface charge=1.3854e13 y.min=0.025 y.max=0.0255 s.s
interface charge=-3.1954e13 y.min=-0.0005 y.max=0 s.s
interface charge=1.81e13 y.min=4.222 y.max=4.23 s.i

inttrap donor e.level=3.46 density=3.05e13 degen=1 sign=1e-15 sigp=1e-15 x.min=0 x.max=9
y.min=-0.0005 y.max=0.01 s.s

inttrap donor e.level=3.46 density=2.7e13 degen=1 sign=1e-15 sigp=1e-15 x.min=9 x.max=21
y.min=-0.0005 y.max=0.01 s.s

inttrap donor e.level=3.46 density=3.05e13 degen=1 sign=1e-15 sigp=1e-15 x.min=21 x.max=30
y.min=-0.0005 y.max=0.01 s.s

material mat=gan eg300=3.437
material mat=algan eg300=3.83
material mat=al2o3 permittivity=9 eg300=7
models print srh hei fnord fnholes nearflg fermi joule.heat f.ae=7e-7 f.be=7e7 cvt
contact name=gate workfunction=5.01
output con.band val.band charge band.par qss e.mobility
mobility mu0n.cvt=100 crn.cvt=3e17 mumaxn.cvt=3010 gamn.cvt=3 alphn.cvt=0.7 bn.cvt=9e7
cn.cvt=3.23e6 deln.cvt=2.1e17 kn.cvt=2.3
method trap autonr newton maxtrap=100 tol.relax=100

solve
save outf=hemt_p1.5_cvt_g1.str

solve init
solve vgate=0
solve vdrain=0

log outfile=ramp_vd.log
solve vdrain=0 vfinal=1 vstep=0.05 name=drain
save outf=ramp_vd.str
log off

log outf=pulse_p1.5_g1.log
solve vgate=0 vfinal=-9 vstep=-0.05 name=gate
save outf=pulse_p1.5_g1.str
log off

quit
```

Appendix H: TCAD simulation fitting of pulsed I_D-V_{GS} at ($V_{GS,Q}$, $V_{DS,Q}$) = (-15 V, 0 V) (Chapter 5)

```
go atlas simflag="-v 5.16.3.r"
mesh auto width=1000
set thickness=0.007

x.m l=0    s=0.25
x.m l=1    s=0.25
x.m l=2    s=0.25
x.m l=4    s=0.25
x.m l=6    s=0.25
x.m l=14   s=0.25
x.m l=19   s=0.25
x.m l=20   s=0.25
x.m l=29   s=0.25
x.m l=30   s=0.25

y.m l=-0.02   s=0.01
y.m l=-0.0075 s=0.005
y.m l=-0.007   s=0.0005
y.m l=-0.0045 s=0.002
y.m l=0.0     s=0.0005
y.m l=0.0125  s=0.005
y.m l=0.025   s=0.0002
y.m l=0.0275  s=0.001
y.m l=0.0325  s=0.002
y.m l=0.06    s=0.004
y.m l=0.1     s=0.1
y.m l=4.215   s=0.1
y.m l=4.22    s=0.0005
y.m l=4.225   s=1
y.m l=5.225   s=1

eliminate columns x.min=0 x.max=30 y.min=0.1

region num=1 x.min=0 x.max=30 y.min=0 y.max=0.025 mat=algan x.comp=0.25 donor=1e15
region num=2 x.min=0 x.max=30 y.min=-0.02 y.max=0 mat=air
region num=3 x.min=0 x.max=30 y.min=-$thickness y.max=0 material=al2o3
region num=4 x.min=0 x.max=30 y.min=0.025 y.max=0.325 mat=gan donor=4e16
region num=5 x.min=0 x.max=30 y.min=0.325 y.max=4.225 mat=gan acceptor=5e16
region num=6 x.min=0 x.max=30 y.min=4.225 y.max=5.225 mat=si insulator

elec num=1 name=source x.min=0 x.max=1 y.min=-0.02 y.max=0.03
elec num=2 name=drain x.min=29 x.max=30 y.min=-0.02 y.max=0.03
elec num=3 name=gate x.min=11 x.max=19 y.min=-0.02 y.max=-$thickness
elec num=4 substrate
```

```
interface charge=1.3854e13 y.min=0.025 y.max=0.0255 s.s
interface charge=-3.1954e13 y.min=-0.0005 y.max=0 s.s
interface charge=1.81e13 y.min=4.222 y.max=4.23 s.i

inttrap donor e.level=3.46 density=3.05e13 degen=1 sign=1e-15 sigp=1e-15 x.min=0 x.max=9
y.min=-0.0005 y.max=0.01 s.s

inttrap donor e.level=3.46 density=3.15e13 degen=1 sign=1e-15 sigp=1e-15 x.min=9 x.max=21
y.min=-0.0005 y.max=0.01 s.s

inttrap donor e.level=3.46 density=3.05e13 degen=1 sign=1e-15 sigp=1e-15 x.min=21 x.max=30
y.min=-0.0005 y.max=0.01 s.s

material mat=gan eg300=3.437
material mat=algan eg300=3.83
material mat=al2o3 permittivity=9 eg300=7
models print srh hei fnord fnholes nearflg fermi joule.heat f.ae=7e-7 f.be=7e7 cvt
contact name=gate workfunction=5.01
output con.band val.band charge band.par qss e.mobility
mobility mu0n.cvt=100 crn.cvt=3e17 mumaxn.cvt=2810 gamn.cvt=3 alphn.cvt=0.7 bn.cvt=9e7
cn.cvt=3.23e6 deln.cvt=2.1e17 kn.cvt=2.3
method trap autonr newton maxtrap=100 tol.relax=100

solve
save outf=hemt_p-15_cvt_g1.str
#tonyplot hemt_p-15_cvt_g1.str

solve init
solve vgate=0
solve vdrain=0

log outfile=ramp_vd.log
solve vdrain=0 vfinal=1 vstep=0.05 name=drain
save outf=ramp_vd.str
log off

log outf=pulse_p-15_g1.log
solve vgate=0 vfinal=-9 vstep=-0.1 name=gate
save outf=pulse_p-15_g1.str
log off

quit
```

Appendix I: Publications and Conferences

List of Publications (First Author)

1. **S. S. Pannirselvam**, Gyanathan Ashvini, Yee-Chia Yeo and Leng Seow Tan, “Characterization of Traps in AlGaN/GaN MIS-HEMTs using Pulsed I-V Measurements and TCAD Device Simulation”, submitted to *Semicond. Sci. Technol.*

2. **S. S. Pannirselvam**, Xinke Liu, Kain Lu Low, Yee-Chia Yeo and Leng Seow Tan, “Trap Analysis of AlGaN/GaN MOS-HEMTs using Gate Stress Induced Transient Current Methodology and TCAD Simulation”, submitted to *Appl. Phys. Express.*

List of Conferences (First Author)

1. **S. S. Pannirselvam**, Liu. X, Y-.C. Yeo and L. S. Tan, “Effects of in situ Surface Passivation of AlGaN/GaN MOS-HEMT: A Simulation Study”, *International Conference on Solid State Devices and Material*, 2012.

Other Publications

1. X. Liu, M. A. Bhuiyan, **S. S. Pannirselvam**, C. B. Soh, Z. Liu, D. Z. Chi, W. Liu4, Y. Lu1, W. Yu, L. S. Tan and Y.-C. Yeo, “High voltage AlGaN/GaN metal–oxide–semiconductor high-electron mobility transistors with regrown $In_{0.14}Ga_{0.86}N$ contact using a CMOS compatible gold-free process”, *Appl. Phys. Express*, vol. **7**, pp. 126501 (2014).

2. J. D. Ye, **S. Pannirselvam**, S. T. Lim, J. F. Bi, X. W. Sun, G. Q. Lo and K. L. Teo, “Two-dimensional electron gas in Zn-polar ZnMgO/ZnO heterostructure grown by metal-organic vapour phase epitaxy”, *Appl. Phys. Lett*. vol. 97, pp. 111908 (2010).

Other Conference

J. D. Ye, S. T. Tan, **P. Somasuntharam**, S. L. Gu, N Tang, X. W. Sun. G. Q. Lo and K L Teo, “Modification of growth kinetics and suliace potential by arsenic surfactant on ZnO (0001) surface” *International Conference on the Physics of Semiconductors*, 25 - 30 Jul, 2010, COEX, SEOUL, South Korea.